Characterization of the Complexin - SNARE Protein Network in Different Synaptic Systems

Dissertation

for the award of the degree
"Doctor rerum naturalium" (Dr.rer.nat.)
of the Georg-August-Universität Göttingen

within the doctoral program
Cellular and Molecular Physiology of the Brain (CMPB)
of the Georg-August University School of Science (GAUSS)

submitted by

Jutta Margaretha Meyer
born in
Löningen, Germany

Göttingen, 2022

Members of the Thesis Advisory Committee

Prof. Dr. Nils Brose
Department of Molecular Neurobiology,
Max Planck Institute for Multidisciplinary Sciences, Göttingen

Prof. Dr. Blanche Schwappach
Dean of the Medical Faculty at the University Medical Center Hamburg-Eppendorf (UKE)
formerly Department of Molecular Biology, University Medical Center Göttingen (UMG)

Prof. Dr. Reinhard Jahn
Department of Neurobiology
Max Planck Institute for Multidisciplinary Sciences, Göttingen

Members of the Examination Board

Prof. Dr. Nils Brose (1st reviewer)
Department of Molecular Neurobiology,
Max Planck Institute for Multidisciplinary Sciences, Göttingen

Prof. Dr. Tiago Fleming Outeiro (2nd reviewer)
Experimental Neurodegeneration,
University Medical Center, Göttingen

Further members of the Examination Board

Prof. Dr. Blanche Schwappach
Dean of the Medical Faculty at the University Medical Center Hamburg-Eppendorf (UKE)
formerly Department of Molecular Biology, University Medical Center Göttingen (UMG)

Prof. Dr. Reinhard Jahn
Department of Neurobiology
Max Planck Institute for Multidisciplinary Sciences, Göttingen

Prof. Dr. Oliver Wirths
Department of Psychiatry, Division of Molecular Psychiatry
University Medical Center, Göttingen

Prof. Dr. Carolin Wichmann
Group Molecular Architecture of Synapses
Institute for Auditory Neuroscience & InnerEarLab
University Medical Center, Göttingen

Date of oral examination: May 2nd, 2022

Declaration

I hereby declare that this thesis entitled "Characterization of the Complexin - SNARE protein network in different synaptic systems" was written independently and with no other sources and aids than quoted.

Jutta Meyer
Göttingen, February 28th, 2022

Table of Contents

Abstract

At neuronal synapses, the exocytotic SNARE complex is formed by Syntaxin 1, SNAP25 and Synaptobrevin 2. Complexin (Cplx) regulates the SNARE function to achieve the high speed and spatial precision of synaptic vesicle fusion. All four known mammalian Cplxs share a short central α helix, which was shown to be necessary for SNARE complex binding of Cplx1. The high degree of conservation in this central domain suggests that probably all Cplxs exert their function via an interaction with SNARE complexes, raising the question whether different Cplxs act upon different SNARE complex types. Peptides representing this domain bind to reconstituted SNARE complexes with submicromolar affinities *in vitro*. An affinity purification approach was developed with short synthetic peptides covering the central α-helical SNARE-binding domain of Cplxs1 to 4. After incubation of the immobilized Cplx peptides with detergent extracts of mouse cortex or retina, multiple Cplx-binding proteins were detected using a quantitative mass spectrometry approach.

The detailed analysis of these proteins shows that basically there are differences in the Cplx interactomes. In the cortex samples, a variety of possible regulators and effectors were identified, among them different members of the of SNARE protein family including Syntaxin 1, SNAP25 and Synaptobrevin 2. Moreover, the samples also contained the complete set of SNAREs which are known to form complexes of the endosomal and lysosomal pathway, respectively. Surprisingly, these SNARE proteins were found to be Cplx isoform independent. A co-enrichment with neuronal SNARE proteins was excluded by repeating the affinity purification approach with HEK cells, which do not contain neuronal SNARE proteins. A functional effect of Cplx on non-exocytotic pathways was shown with a transferrin uptake assay.

Cplx1 and Cplx2 are expressed in conventional synapses of almost all neuron types of the brain, while Cplx3 and Cplx4 are preferentially expressed in ribbon synapses of retinal photoreceptors and bipolar cells. The different distribution pattern of the two Cplx subgroups raises the question whether Cplx3 and 4 contribute to the highly specialized mode of neurotransmitter release found in ribbon synapses. Therefore, analysis of proteins which were detected in the course of experiments using retina material was rather directed to the extended interaction network. Interestingly, RIBEYE and some Transducin subunits were identified as specific interactors of Cplx3 and 4.

The results of this work suggest that Cplx may be involved in processes beyond the regulation of synaptic exocytosis.

Zusammenfassung

In neuronalen Synapsen wird der exozytotische SNARE-Komplex aus Syntaxin 1, SNAP25 und Synaptobrevin 2 gebildet. Complexin (Cplx) reguliert die SNARE Funktion, was zum Erreichen einer hohen Geschwindigkeit und räumlichen Präzision der synaptischen Vesikelfusion beiträgt. Ein gemeinsames Merkmal der vier, bei Säugetieren beschriebenen Cplx ist die zentrale α-Helix, die essenziell für die SNARE-Komplexbindung von Cplx1 ist. Der hohe Konservierungsgrad dieser Domäne deutet darauf hin, dass alle Cplx ihre Funktion über eine Interaktion mit SNARE-Komplexen ausüben, was die Frage aufwirft, ob verschiedene Cplx mit verschiedenen SNARE-Komplex-Typen interagieren. Cplx-Peptide, die diese Domäne repräsentieren, binden mit submikromolaren Affinitäten an *in vitro* rekonstituierte SNARE-Komplexe. Diese Eigenschaft wurde zur Entwicklung eines Affinitätsreinigungsverfahren verwendet: kurze synthetischen Peptide, die die zentrale SNARE-Bindungsdomäne von Cplxs1 bis 4 abdecken, wurden immobilisiert und mit Detergenzextrakten aus Mäusekortex oder -retina inkubiert. Die so angereicherten Cplx-bindenden Proteine wurden durch quantitative Massenspektrometrie analysiert.

Die Auswertung der gesammelten Daten zeigte, dass es grundsätzlich Unterschiede in den Cplx-Interaktomen gibt. In den Cortex-Proben wurde eine Vielzahl möglicher Regulatoren und Effektoren identifiziert, darunter verschiedene Mitglieder der SNARE-Proteinfamilie, wie Syntaxin 1, SNAP25 und Synaptobrevin 2. Darüber hinaus enthielten die Proben komplette Sets an SNARE-Proteinen, die für den endosomalen bzw. lysosomalen Signalweg von Bedeutung sind. Überraschenderweise erwiesen sich diese SNARE-Proteine als unabhängig von der Cplx-Isoform. Eine Absicherung der Ergebnisse erfolgte *in vitro* durch Anreicherungs-Experimente unter Verwendung von Lysaten aus HEK-Zellen, die keine neuronalen SNARE-Proteine enthalten, sowie *in vivo* durch Transferrin-Aufnahme.

Cplx1 und Cplx2 werden in konventionellen Synapsen des zentralen Nervensystems exprimiert, während Cplx3 und Cplx4 überwiegend in den Bandsynapsen der retinalen Photorezeptoren und Bipolarzellen lokalisiert sind. Dieses unterschiedliche Verteilungsmuster wirft die Frage auf, ob Cplx3 und 4 zu der hochspezialisierten Art der Neurotransmitterfreisetzung in Bandsynapsen beitragen. Die Analyse der Proteine, die im Rahmen der Experimente mit Retina-Material nachgewiesen wurden, richtete sich daher eher auf das erweiterte Interaktionsnetzwerk. Interessanterweise wurden RIBEYE und einige Transducin-Untereinheiten als spezifische Interaktoren von Cplx3 und 4 identifiziert.

Die Ergebnisse dieser Arbeit legen nahe, dass Cplx an Prozessen beteiligt sein könnte, die über die Regulierung der synaptischen Exozytose hinausgehen.

List of Abbreviations

ABS	Ammonium bicarbonate
AH	Accessory α helix
APS	Ammonium persulfate
ATP	Adenosine-5'-triphosphate
AZ	Active zone
BSA	Bovine serum albumin
Ca^{2+}	Calcium, ionized
CO_2	Carbon dioxide
COPII	Coat protein complex II
Cplx	Complexin
CTD	Carboxy-terminal domain
DAVID	Database for annotation, visualization and integrated discovery
DKO	Double-knockout
DMEM	Dulbecco's modified eagle medium
DMSO	Dimethyl sulfoxide
DPBS	Dulbecco's phosphate buffer saline
DTT	Dithiothreitol
EDTA	Ethylendiaminetetraacetic acid
EGFP	Enhanced green fluorescent protein
EGTA	Ethylenglycoltetraacetic acid
ER	Endoplasmic reticulum
ERG	Electroretinogram
ERGIC	ER-Golgi intermediate comparts
FASP	Filter aided sample preparation
FBS	Fetal bovine serum
GAPDH	Glyceraldehyde-3-phosphate dehydrogenase
GO	Gene ontology
HCl	Hydrochloric acid
HEK	Human embryonic kidney
HEPES	4-(2-hydroxyethyl)-1-piperazineethanesulfonic acid
HPLC	High performance liquid chromatography
ICC	Immunocytochemistry
INL	Inner nuclear layer
IPL	Inner plexiform layer
ITC	Isothermal titration calorimetry
KCl	Potassium chloride

K_D	Dissociation constant
kDa	Kilodalton
KH_2PO_4	Potassium hydrogen phosphate
MgCl	Magnesium chloride
MS	Mass spectrometry
MVB	Multivesicular bodies
NaCl	Sodium chloride
NaOH	Sodium hydroxide
NFL	Nerve fiber layer
NSF	N-ethylmaleimide-sensitive factor
NTD	N-terminal domain
ONL	Outer nuclear layer
OPL	Outer plexiform layer
PAA	Polyacrylamide
PBS	Phosphate buffered saline
PFA	Paraformaldehyde
PMSF	Phenylmethylsulfonylfluoride
Q	Glutamine
R	Arginine
RBP	Ribbon-binding peptide
RIM	Rab-3-interacting molecule
rpm	Round per minute
SDS	Sodiumdodecylsulfate
SEM	Standard error of the mean
SNAP	Synaptosome associated protein
SNARE	Soluble N-ethylmaleimide-sensitive fusion protein attachment protein receptors
Stx	Syntaxin
TEMED	Tetramethylethylenediamine
TGN	Trans Golgi-network
TKO	Triple-knockout
TM	Transmembrane domain
Tris	Trizma-base
VAMP	Vesicle associated membrane protein
VPS	Vacuolar protein sorting-associated protein
WB	Western blot
WT	Wildtype

1 Introduction

1.1 Membrane fusion

In eukaryotic cells, intracellular organelles are separated by membranes. This allows reactions to proceed separately and minimizes the energy required to maintain large concentration differences. The communication between these compartments is often mediated by vesicles, which can be formed during several processes of the secretory and endocytic pathway. Therefore, cargo proteins are collected in buds arising from the membrane of one compartment and then delivered to the target compartment by fusion with its membrane. In this way soluble content is released and membrane proteins are incorporated into the target membrane (Bonifacino and Glick, 2004). Key molecules of membrane fusion processes are the SNAREs (soluble NSF attachment protein receptors, where NSF stands for N-ethyl-maleimide-sensitive fusion protein), which are conserved from yeast to man.

1.2 SNARE proteins

1.2.1 SNARE protein structure

The SNARE protein family includes 38 members in mammals and 24 members in yeast. All members contain a SNARE motif, which is evolutionary conserved and consists of 60-70 amino acids with a heptad repeat. Most of the proteins contain a transmembrane domain or alternatively hydrophobic post-translational modifications that mediate membrane anchorage. The N-terminal domain is the most individual part of this protein family (Figure 1) (Fasshauer, 2003; Burri and Lithgow, 2004; Brunger, 2005; Hong and Lev, 2014).

In the process of membrane fusion the SNARE motifs play a central role because they mediate the complex formation of SNARE proteins located on opposite membranes. Originally, SNAREs were divided into two groups, the target (t)- and the vesicle (v)-SNAREs. This classification was depending on the membranes, where the proteins were found on. However, in some cases, such as homotypic membrane fusions, it may be more appropriate to use a nomenclature based on the conserved structure of the complex (Jahn and Scheller, 2006). A complex generally comprises three Q-SNARE motifs (glutamine residue in the central position; Q_a, Q_b, Q_c) and one R-SNARE motif (arginine residue in the

central position) and has a high degree of conservation. The unstructured monomeric motifs associate spontaneously to a very stable complex of four intertwined parallel α helices, ordered as coiled coils. Thereby the membranes come closer, and the fusion will be initiated (Fasshauer et al., 2002; Fasshauer, 2003).

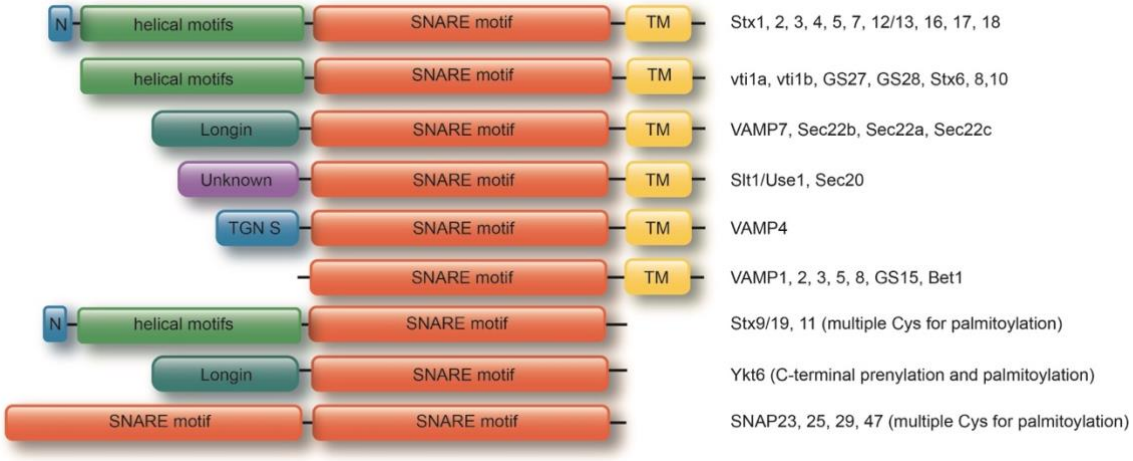

Figure 1: Domain organization of SNARE proteins. All members contain a SNARE motif (red) and many of them have a transmembrane domain (TM; yellow). Seven of these 35 SNARE proteins do not contain a TM-domain. They associate via various lipid interactions with the membrane, like palmitoylation or prenylation. The N-terminal domain is the most individual part, which can contain helical motifs (green), longin domains (blue) or additional SNARE motifs. Some structures are also individual for a special isoform, as e.g. the cytoplasmatic domain of VAMP4, which consists of a dileucine motif and acidic clusters, that mediate the recycling from endosome to the trans Golgi-network (TGN). Illustration modified from Hong and Lev, 2014. Abbreviations: Stx: Syntaxin, VAMP: vesicle associated membrane protein, SNAP: synaptosome associated protein.

1.2.2 SNARE protein localization and specificity

To ensure the specificity of the vesicle targeting, tethering factors recruited by small GTPases, called Rab proteins, and phosphoinositides are required (Di Paolo and De Camilli, 2006; Stenmark, 2009; Donaldson and Jackson, 2011), whereas the specificity of the fusion processes is regulated by unique sets of SNAREs (Jahn and Scheller, 2006). Some SNAREs interact only with one set of partners, others are more flexible. The extent to which the SNARE combination contributes to specificity is still under debate, as some SNAREs can be exchanged if they belong to the same subfamily. It is also known, that at least some SNAREs can recruit tethering proteins, like VPS (Vesicular protein sorting) proteins, which define intracellular targeting (Koike and Jahn, 2019).

In Figure 2 different membrane fusion events with their corresponding SNARE complexes are illustrated. The SNARE complex of the endoplasmic reticulum (ER) consists of Stx5, GS27, Bet1 and Sec22b and is suggested to act in mediating homotypic fusion of ER-derived

COPII (coat protein complex II) vesicles into ER-Golgi intermediate compartments (ERGIC) (Zhang et al., 1997; Zhang et al., 1999). Another SNARE complex comprising of Stx5, GS28, Bet1 and Ykt6 is likely to be responsible for the fusion of matured ERGICs with the cis-face of the Golgi apparatus (Zhang and Hong, 2001). The recycling trafficking to the ER seems to be mediated by Stx18, Sec20, Slt1 and Sec22b (Burri et al., 2003; Malsam and Söllner, 2011). Stx5 interacts with GS28, GS15 and Ykt6 to function in intra-Golgi traffic (Xu et al., 2002). Stx7, vti1b and Stx8 are enriched in the endocytic pathway. Together with VAMP8 a fusion of early and late endosome is initiated and together with VAMP7 the fusion of the late endosome with the lysosome is catalyzed (Antonin et al., 2000; Pryor et al., 2004). The fusion of autophagosomes with lysosomes is also a subject of SNARE mediation. Stx17, SNAP29 and VAMP8 were described as complex for this process, but also Ykt6, SNAP29 and Stx7 are postulated as parallel complex (Matsui et al., 2018). The retrograde traffic from early endosomes to the Golgi network is supported by Stx16, vti1a, Stx6 and VAMP4 (Mallard et al., 2002). Stx12, with the synonym Stx13, is a SNARE protein involved in the fusion of early endosomes (McBride et al., 1999; Sun et al., 2003). Together with SNAP25 and VAMP2 it also plays a role in recycling endosomes (Prekeris et al., 1998). Moreover, the exocytotic process of hormone secretion is regulated by SNARE proteins. Stx4, SNAP23 and VAMP8 control this process (Wang et al., 2004). Despite high variability in the primary sequences, these different SNARE complexes form structurally conserved four-helix bundles, that show high similarities among themselves in many details (Antonin et al., 2002; Zwilling et al., 2007). The presumably most prominent and paradigmatic representative within the family of SNARE complexes is the neuronal SNARE complex, which is a prerequisite of synaptic vesicle fusion with the plasma membrane and the release of neurotransmitter from synaptic vesicles (Figure 2).

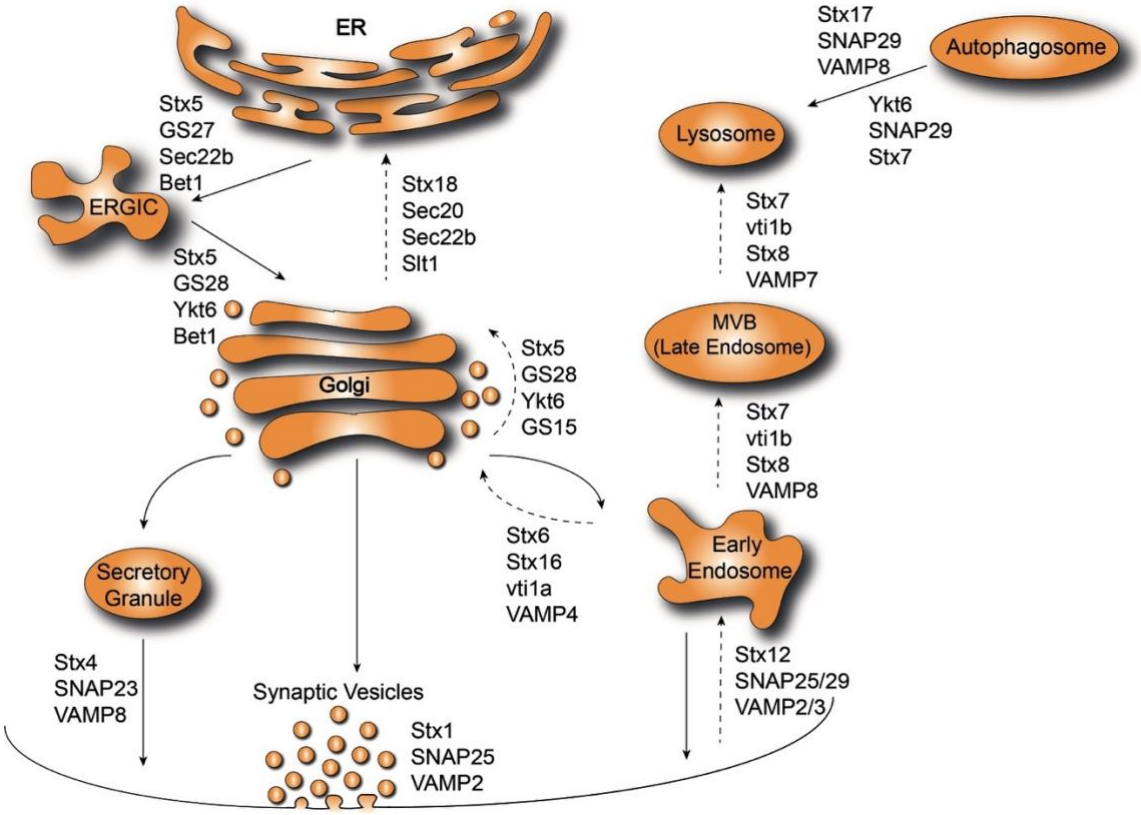

Figure 2: Schematic overview of eucaryotic membrane fusion processes mediated by SNARE complexes in mammals.
SNARE complexes are localized to distinct subcellular compartments and involved in membrane fusion events along exocytic and endocytic pathways. Abbreviations: ER: endoplasmic reticulum; ERGIC: ER-Golgi intermediate compartment; MVB: multivesicular bodies.

1.2.3 SNARE proteins involved in synaptic vesicle exocytosis

Presynaptic nerve terminals release neurotransmitter into the synaptic cleft via synaptic vesicle exocytosis (Figure 3a and b). This process is based on the fusion of vesicles with the plasma membrane which is mediated by the plasma membrane SNARE proteins Syntaxin 1AB (Stx1), synaptosome associated protein of 25 kDa (SNAP25) and the vesicle associated membrane protein 2 (VAMP2), also called Synaptobrevin 2 (Figure 3c) (Hanson et al., 1997; Lin and Scheller, 1997). SNARE proteins play an essential role in this process, which was demonstrated by a series of experiments with genetically modified mice as well as work on various neurotoxins that proteolytically cleave SNAREs. Different strains of the bacteria species *Clostridium botulinum* and *Clostridium tetani* secrete botulinum neurotoxins and tetanus toxins, respectively. They specifically cleave the three different exocytotic SNARE proteins in the C-terminal region of the SNARE motif in the cytoplasm, thereby preventing the formation of SNARE complexes. As a consequence, action potential-induced transmitter release is almost completely inhibited, while the morphology of the synapse remains unchanged (Duchen, 1973; Hunt et al., 1994; Schiavo et al., 2000). It was shown in

permeabilized PC12 cells, an immortalized neuroendocrine cell line, that exocytosis can be restored after treating with the toxin, by incubation with a C-terminal fragment of SNAP25 (Chen et al., 1999). Deletion of Synaptobrevin 2 in mice leads to a nearly complete loss of Ca^{2+}-induced neurotransmitter release in hippocampal neurons, whereas spontaneous neurotransmitter release is only reduced by a factor of 10 (Schoch et al., 2001). In this context, it cannot be excluded that other R-SNAREs may at least partially replace the function of Synaptobrevin. In chromaffin cells, a double-knockout (DKO) of Synaptobrevin and its homolog cellubrevin leads to a complete inhibition of spontaneous fusion of granules (Borisovska et al., 2005).

In the brain, neurotransmitter release occurs in response to an action potential. To ensure a fast and correct propagation of the signal, the membrane fusion mechanism behind exocytosis is different from other membrane fusion processes within the cell. Special characteristics are its tight regulation by Ca^{2+} and the involvement of a variety of specific proteins regulating for instance the precise timing, the high speed and areal precision. (Sudhof, 2004; Hong, 2005; Brose, 2008a; Shih and Shin, 2011; Südhof and Rizo, 2011). Among these important proteins are complexins (Cplx), Munc13, CAPS, Munc18, and Rab-3-interacting molecules (RIM). Munc18 binds both the closed form of Stx1 and a heterodimer of Stx1 and SNAP25. Thus, one possible role of Munc18 may be to serve as a template for the formation of the SNARE complex. Several studies suggest that Munc18 assumes multiple functions during the fusion process and is for example also involved in the priming of the vesicles (Zilly et al., 2006; Gulyás-Kovács et al., 2007; Tareste et al., 2008; Südhof and Rothman, 2009). The action potential initiates the opening of the Ca^{2+} channels, which in turn leads to action of the Ca^{2+} sensor synaptotagmin 1 resulting in the fusion pore opening and the release of neurotransmitter into the synaptic cleft. After this fusion step, the SNARE complex is disassembled by a multiprotein complex consisting of the ATPase NSF (N-ethylmaleimide-sensitive factor) and αSNAP under ATP hydrolysis (Sudhof, 2004; Hong, 2005; Brose, 2008b; Südhof, 2013; Trimbuch and Rosenmund, 2016).

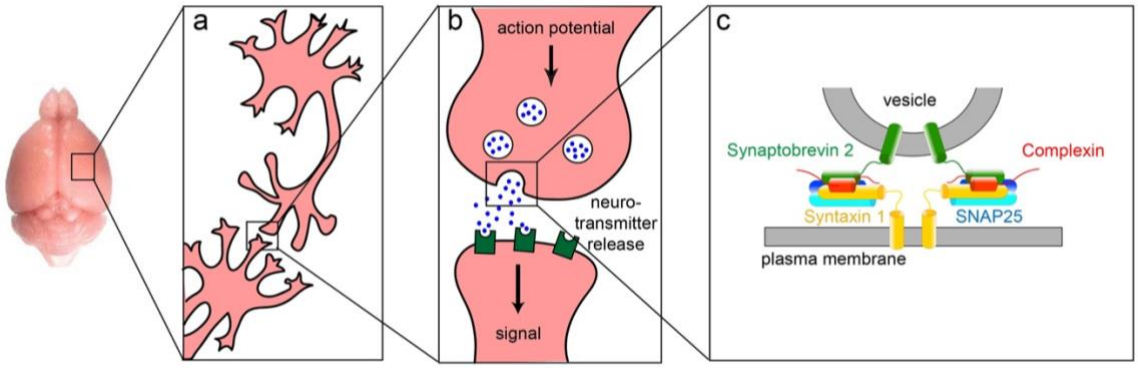

Figure 3: Illustration of synaptic vesicle exocytosis in neurons of the brain.
(a) In the mammalian nervous system, exemplified here by the brain of a mouse, neurons are interconnected via synapses. **(b)** Transmission of the stimulus occurs through an incoming action potential, which leads to an increase in Ca^{2+} concentration. As a result, the vesicles fuse with the plasma membrane and release neurotransmitters into the synaptic cleft. They bind to the receptors of the postsynapse, which propagates the signal to the next cell. **(c)** The fusion of the vesicle with the plasma membrane is mediated by SNARE proteins. Synaptobrevin 2 (green) on the vesicle and Stx1 (yellow) and SNAP25 (blue), which are located on the plasma membrane, form a stable complex via their α helices. As a SNARE regulating protein Cplx binds to this complex via its central α-helical binding domain.

1.3 Complexin

1.3.1 Cplx function in synaptic vesicle exocytosis

To guarantee precise timing, high speed and areal precision in synaptic vesicle exocytosis additional proteins are necessary to regulate SNARE function. Among them is the protein Cplx, also known as Synaphin. Its sequence is conserved in some non-metazoan unicellular organisms and in all metazoans. This suggests a universal role of Cplx in metazoans, which was established and preserved even before metazoan evolution (Yang et al., 2015). Initial biochemical studies showed that Cplx1 binds to assembled SNARE complexes and not to single SNARE proteins (McMahon et al., 1995; Pabst et al., 2000). However, a detailed structure-function analysis on the basis of single-molecule studies revealed that Cplx1 also binds to heterodimers of Stx1A and SNAP25 (Guan et al., 2008; Weninger et al., 2008; Yoon et al., 2008). Isothermal titration calorimetry (ITC) and kinetic studies using stopped-flow fluorescence anisotropy revealed that the binding occurs fast ($k_{on} \approx 5x10^7\ M^{-1}s^{-1}$) and with high-affinity ($K_D \approx 10nM$) (Pabst et al., 2002). Crystal structure analyses demonstrated that one single Cplx1 molecule binds in an anti-parallel fashion to the groove between Stx1 and Synaptobrevin 2 via its central α helix (Figure 4) (Bracher et al., 2002; Chen et al., 2002). Cplx binding cause no major conformational changes in the four-helix bundle of the SNARE complex. Interestingly, Cplx can differentiate between SNARE complex compositions, as

shown in *in vitro* binding assays with full length rat Cplx1 and 2. The exchange of VAMP2 to VAMP8 abolished Cplx binding to the SNARE complex, whereas an exchange of SNAP25 to SNAP29 was tolerated. The replacement of Stx1 by various Stx isoforms also showed different results: Stx3 reconstituted the Cplx binding affinity, Stx2 reduced it, and Stx4 abolished Cplx binding (Pabst et al., 2000).

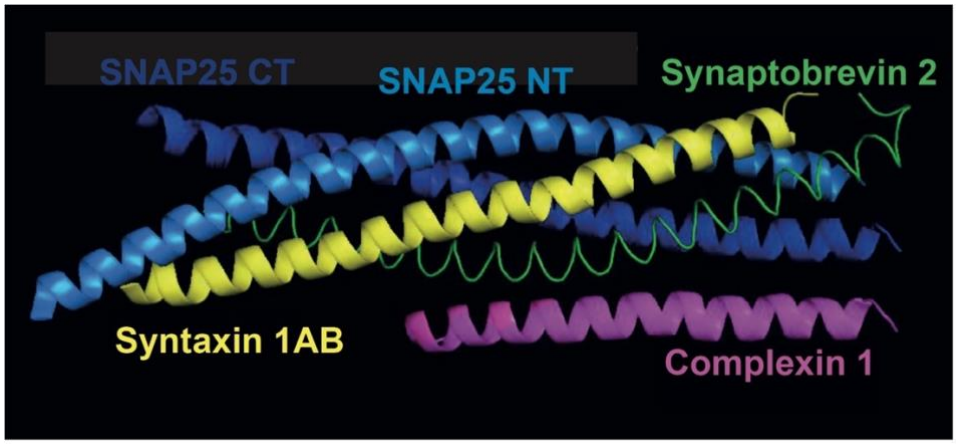

Figure 4: Ribbon diagram of Cplx binding to the neuronal SNARE complex.
The diagram illustrates the twisted parallel four-helical bundle of the SNARE complex which is formed by Syntaxin1AB (yellow), Synaptobrevin 2 (green) and SNAP25 (blue: N-terminal SNARE motif; dark blue: C-terminal SNARE motif). Cplx (magenta) binds in an antiparallel fashion to the groove between Syntaxin and Synaptobrevin. PDB 1KIL (from: Chen et al., 2002).

The exact mode of Cplx action is still under debate. However, that Cplx must play a key role in the central mechanisms of signal transduction from one neuron to the next is underlined by the observation, that a variety of neurological and psychiatric diseases such as e.g. schizophrenia, Huntington's disease, Parkinson's disease and Alzheimer's disease are associated with altered expression levels of Cplxs (Brose, 2008a). Additionally, that Cplxs are essential to maintain normal neuronal activity but that there are probably subtle differences between the Cplx isoforms in the context of the underlying molecular mechanisms is reflected by the phenotypes of different KO mice which were generated to study Cplx function. Likewise, Cplx1 KO mice are suffering from ataxia and Cplx1/2 DKO as well as Cplx1/2/3 TKO mouse mutants die shortly after birth. In contrast, mice deficient of Cplx2, Cplx3 and Cplx4, respectively, as well as Cplx2/3 DKO or Cplx3/4 DKO mutants show no obvious phenotypic alterations (Reim et al., 2001; Xue et al., 2008).

The observation, that hippocampal neurons which were cultured from Cplx1/2/3 triple-knockout (TKO) mice are characterized by a reduced evoked release led to the hypothesis that Cplxs are SNARE regulators that speed up exocytosis. Likewise, this hypothesis was

supported by the observations of a reduced spontaneous release in Cplx1/2 DKO and Cplx1/2/3 TKO mice in mass and autaptic cultures and in Cplx1-KO brain slices (Reim et al., 2001; Xue et al., 2008; Strenzke et al., 2009; Xue et al., 2010; Chang et al., 2015). From the functional data it was concluded that Cplx might stabilize the assembled SNARE complex which enables rapid Ca^{2+}-triggered fusion. Interestingly, a Cplx null mutant of Drosophila melanogaster was also characterized by a reduced evoked release. However, in contrast to the data obtained from Cplx1/2/3 TKO mouse mutants, the Cplx-deficient fly showed a drastic increase in spontaneous release. This was interpreted as clamping effect of Cplx to prevent transmitter release in the absence of an action potential (Huntwork and Littleton, 2007; Cho et al., 2010). These inconsistent findings likely originate in part from different experimental perturbation strategies. Therefore, López et al. generated a conditional Cplx1 KO mouse line and demonstrated that spontaneous, synchronous and asynchronous transmitter release is reduced in hippocampal neurons which are devoid of Cplx 2 and Cplx3 and in which Cplx1 depletion starts after synaptogenesis has finished. These results support the hypothesis of a facilitatory role of Cplx for synaptic vesicle fusion (López-Murcia et al., 2019). The hypothesis of the dual Cplx function was also supported by *in vitro* analyses like lipid-mixing assays, cell-cell fusion assays and structural analyses (Schaub et al., 2006; Yoon et al., 2008; Brunger et al., 2009).

In summary, the fact that in different studies different model organisms, cell types or methods were used for analyses might be one reason why the exact molecular mechanism of Cplx function is not yet completely understood.

1.3.2 Cplx isoforms and their domain structure

So far, four Cplx isoforms have been described in mammals. While Cplx1 and Cplx2 were originally identified as stoichiometric components of the exocytotic SNARE complex (McMahon et al., 1995; Ishizuka et al., 1997), Cplx3 and Cplx4 were discovered 10 years later by using protein profile searches (Reim et al., 2005). All isoforms are similar in their domain structure, which is characterized by an N-terminal domain, an accessory α helix, a central α helix and a C-terminal domain (Figure 5a). Especially the central α helix which mediates the binding to the SNARE complex contains many evolutionary highly conserved amino acids (Yang et al., 2015). Of those, the residues R48, R59, R63, K69 and Y70 are essential for this interaction, since they are involved in salt bridges (R48, R59; R63, K69) or

hydrophobic interactions (R48, R59; R63) interactions or hydrogen bonds (Y70) with residues provided by VAMP2 and Stx1 (Figure 5b, red labeled) (Chen et al., 2002). Binding assays showed that manipulations of these amino acids cause either a reduction (R48L, R59H) of the SNARE binding ability of Cplx1 or they result in a complete elimination (R63A, R48L/R59H, K69A/Y70A) of Cplx1 interaction with the SNARE complex (Xue et al., 2007).

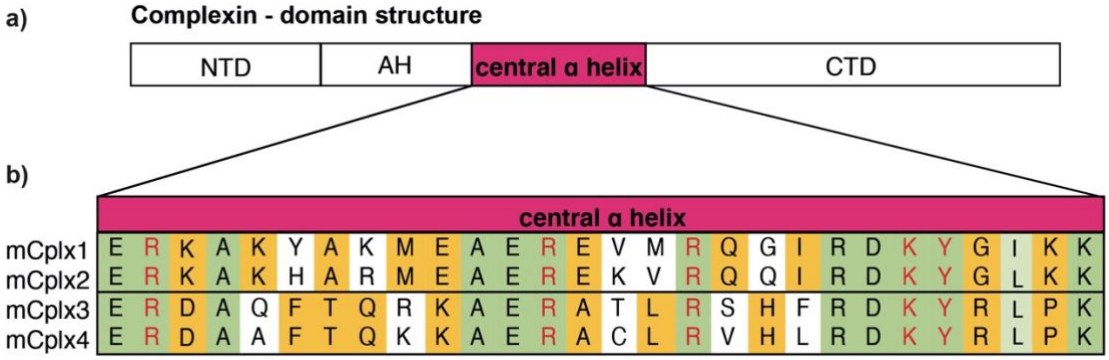

Figure 5: Cplxs are similar in their domain structure.
(a) The four mammalian Cplx isoforms are similar in structure which is characterized by four domains: the N-terminal domain (NTD), the accessory α helix (AH), the central α helix and the carboxy-terminal domain (CTD); **(b)** Sequence alignment of the central helix of the different mouse Cplx isoforms. The amino acids (aa) marked in green label those residues that are conserved in all isoforms. The aa marked in yellow label all residues which are conserved within a certain subgroup and the aa highlighted in red are essential for the interaction with Stx1 and VAMP2.

While the central α helix is essential for binding to the SNARE complex, modulatory roles were assigned also to other domains of Cplx. The N-terminus is thought to have activating properties in vesicle fusion and priming (Xue et al., 2010), while the accessory helix has inhibitory effects on the fusion of synaptic vesicles with the plasma membrane (Trimbuch and Rosenmund, 2016). The C-terminus, the at least conserved portion of the protein, has been shown to exert an inhibitory effect on spontaneous fusion and might play an important role in vesicle priming (Kaeser-Woo et al., 2012).

Apart from the similar domain structure, there are differences between these four isoforms, leading to the classification into two subgroups. Cplx1 und Cplx2 are both soluble, cytosolic and predominantly expressed in the neurons of the brain, which mainly form conventional synapses at their contact sites. The two proteins are 86% homologous to each other and highly conserved between different species. Likewise, Cplx1 homology between human and mouse was found to be 97%, while Cplx2 of these two species are even 100% identical (Brose, 2008b). In hippocampal neurons, the two homologs can substitute for each other

(Fasshauer et al., 1998). Cplx2 is so far the only isoform detected in non-neuronal tissues (Tadokoro et al., 2005; Falkowski et al., 2010).
The other subgroup consists of Cplx3 and Cplx4. Both isoforms contain a CAAX box motif at their C-termini, which is a signal sequence for posttranslational farnesylation. In mice, Cplxs 3 and 4 are 58% homologous but show limited homology (24-28%) to Cplx1 and 2. Cplxs of the second subfamily are also highly conserved between different mammalian species (Brose, 2008b). Furthermore, Cplx3 and Cplx4 are mostly expressed in retina and are the only isoforms in retinal photoreceptors and bipolar cells, which contain a special type of synapses, the ribbon synapses (Reim et al., 2005; Landgraf et al., 2012).

1.4 Sensory ribbon synapses of the retina

1.4.1 Characteristics of ribbon synapses

Sensory ribbon synapses in the visual system release neurotransmitter in a tonical fashion, thereby transmitting information as graded changes in membrane potential. Via this continuous exocytosis thousands of vesicles per second can be released from photoreceptor and bipolar cells of the vertebrate retina, which exceeds the release rate of conventional synapses many times (Heidelberger et al., 1994; Stevens and Tsujimoto, 1995; von Gersdorff et al., 1996; Parsons and Sterling, 2003; Sterling and Matthews, 2005; Moser et al., 2006; Matthews and Fuchs, 2010).

The main morphological feature of ribbon synapses is their unique organization of the active zones (AZ). Typically, it is characterized by a specialized plate-like organelle, the synaptic ribbon (Figure 6a). It is anchored to the plasma membrane in close vicinity to voltage-gated Ca^{2+} channel clusters by the protein Bassoon, protrudes about 200 nm into the presynaptic terminal, curves in a horseshoe shape around the postsynaptic elements and is mainly composed of the protein RIBEYE (Schmitz et al., 2000; tom Dieck and Brandstätter, 2006). Multiple RIBEYE-RIBEYE interactions can form ribbon-like structures (Magupalli et al., 2008). Except RIBEYE, the basic molecular equipment of ribbon synapses is comparable to AZ components in conventional synapses, however in some cases different isoforms are utilized (tom Dieck et al., 2005; Lagnado and Schmitz, 2015). In the context of the release machinery, it was shown for instance, that Stx3b is expressed instead of Stx1. Interestingly, Stx3b is light-dependent phosphorylated by the Ca^{2+}/calmodulin-dependent protein kinase II which generates the potential to form SNARE complexes in an activity-dependent fashion

(Curtis et al., 2008; Liu et al., 2014; Campbell et al., 2020). Another example for synapse type specific expression of different protein isoforms is constituted by the Cplxs.

1.4.2 Role of Cplx in the retina

The retina consists of a mix of ribbon and conventional synapses. The cell bodies of the photoreceptors form the outer nuclear layer (ONL). In the outer plexiform layer (OPL), the synaptic circuitry is applied to the bipolar cells and to the horizontal cells, which are responsible for the lateral circuitry. The inner nuclear layer (INL) includes the cell bodies of the horizontal, bipolar and amacrine cells. In the inner plexiform layer (IPL), the bipolar cells interconnect with the ganglion cells and with the amacrine cells responsible for lateral interconnection. The ganglion cell axons are located in the nerve fiber layer (NFL) and finally form the optic nerve (Figure 6b).

In mouse retina, Cplx1 is mainly expressed in ganglion cells, whereas Cplx2 is the only isoform in conventional synapses of GABAergic, cholinergic and dopaminergic amacrine cells (Lux et al., 2021). Cplx3 has been detected in glycinergic amacrine cells, cone photoreceptor terminals and rod bipolar cells. Cplx4 is localized in rod and cone photoreceptor terminals as well as in cone bipolar cells.

The clear separation between Cplx1 and 2 in conventional synapses and Cplx3 and 4 in ribbon synapses suggests a contribution of Cplx3 and 4 to the unique release machinery of ribbon synapses (Reim et al., 2005; Landgraf et al., 2012). This is supported by various observations. The main structural difference that separates the Cplx3/4 from the Cplx1/2 subgroup is the CAAX-box at the C-terminus of Cplx3 and Cplx4, respectively. In cell culture experiments it was shown that this consensus sequence is used for farnesylation of the two proteins. Moreover, overexpression of Cplx3 and 4 in hippocampal neurons which are deficient of Cplx1 and Cplx2 demonstrated that farnesylation mediates membrane targeting of the CAAX box motif containing proteins. Finally, rescue experiments on the Cplx1/2 DKO background revealed that Cplx3 and 4 were able to functionally replace the missing Cplxs, but the farnesylation was important for that function (Reim et al., 2005).

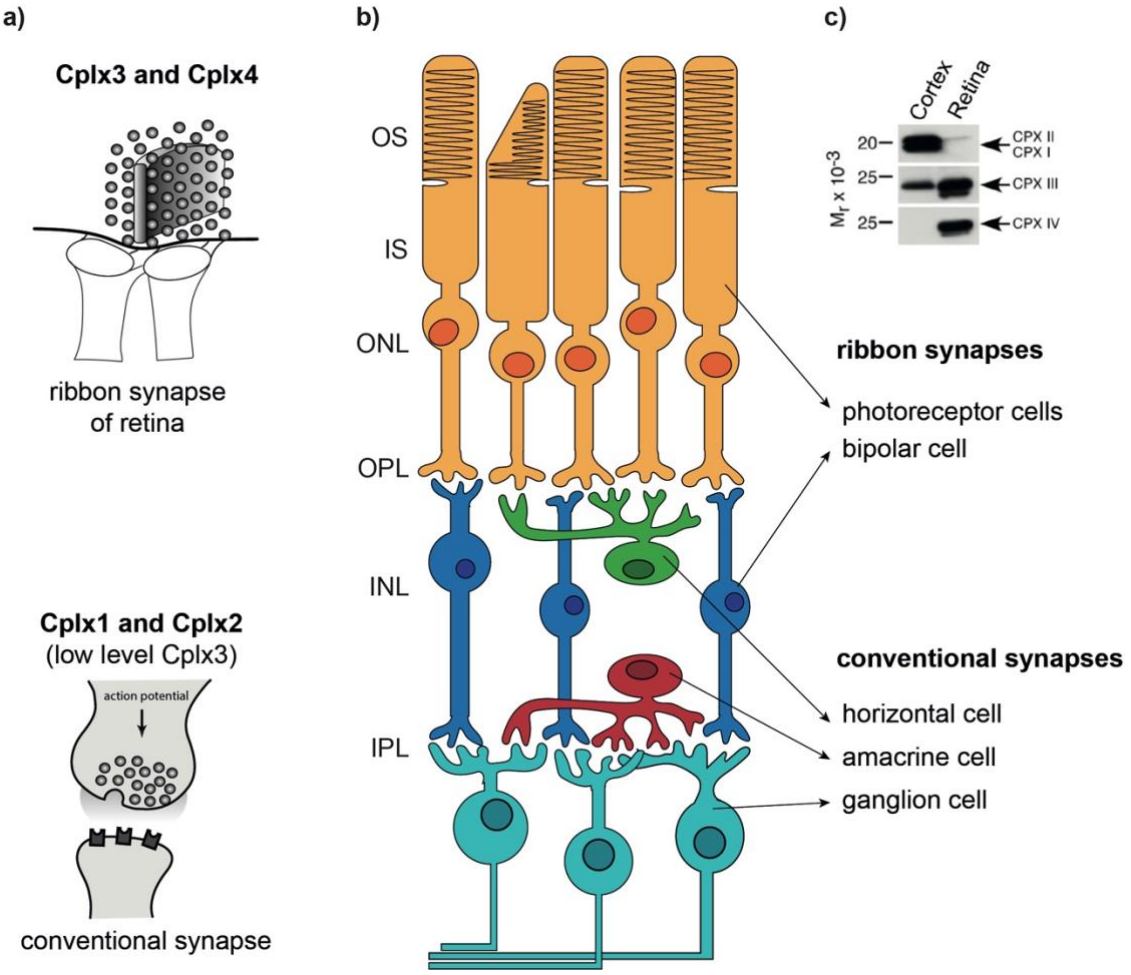

Figure 6: Distribution of Cplx isoforms in different synapse types of the retina.
(a) The Cplx isoforms are distributed distinctly within the different synapse types of the retina. The ribbon synapses contain Cplx3 and Cplx4 and the conventional synapses contain Cplx1 and Cplx2 and small amounts of Cplx3. **(b)** Schematic illustration of retina cell layers and their cell types. The photoreceptor and bipolar cells contain ribbon synapses and the horizontal, amacrine and ganglion cells contain conventional synapses. Abbreviations: OS: outer segment; IS: inner segment; ONL: outer nuclear layer; OPL: outer plexiform layer; INL: inner nuclear layer; IPL: inner plexiform layer. **(c)** Cplx protein expression in cortex and retina tissue was analyzed by Western blot. Cplx1 and Cplx2 isoforms were mainly detected in the cortex, whereas Cplx3 was expressed at low levels. In contrast, Cplx3 and Cplx4 were mainly detected in the retina, whereas the isoforms Cplx1 and Cplx2 were expressed only to a minor extent there (from: (Reim *et al.*, 2005)).

Mice lacking Cplx3 or Cplx4 or both show a normal retinal anatomy as well as no changes in neuronal morphology. However, a more detailed view on the synaptic structure of the photoreceptor ribbons in Cplx3/4 DKO mice revealed a disorganized OPL and, on the ultrastructural level, spherically shaped free-floating ribbons in photoreceptor terminals. Interestingly, in Western blot (WB) experiments a significant decrease of RIBEYE was documented which could explain the disrupted ribbon structure. On the functional level, significant alterations in electroretinographic (ERG) recordings of Cplx3/4 DKO mouse mutants support the idea that the continuous adjustment of vesicle release in photoreceptor ribbon synapses is dependent of Cplx (Reim et al., 2009).

How Cplxs contribute to the unique transmitter release of ribbon synapses is still elusive. Voltage clamp recordings suggested a dual function of Cplx3 and Cplx4, comparable to Cplx1 and Cplx2 in conventional synapses which is expressed as a combination of a facilitatory influence on evoked release and a suppressive function in spontaneous release (Vaithianathan et al., 2015; Babai et al., 2016; Mortensen et al., 2016).

1.5 Peptide-based protein interaction analysis & preliminary data

Although a lot is known about the biochemistry, structure, and function of the interaction between Cplx and the neuronal SNARE proteins, it is still underexplored how the Cplx/SNARE complex is embedded into synaptic protein networks. The systematic analysis of protein interactions is an important requirement for understanding their molecular interplay or pathways. A comprehensive range of methods has been developed for the study of distinct interactions between proteins as well as global interactomes. However, many methods are unable to identify unknown interactors and thus cannot be used in an unbiased approach. For example, the yeast-two-hybrid system has the disadvantage of only investigating binary protein interactions, which eliminates the possibility of studying more complex protein networks, such as interaction partners of assembled SNARE complexes (Fields and Song, 1989). A combination of affinity purification experiments with quantitative mass spectrometry (MS) on the other hand allows the enrichment of multiple and so far, unknown binding partners, their isolation and subsequent identification. For this purpose, enrichment of target proteins together with their interaction partners is often performed by using an immobilized antibody against the bait protein (co-immunoprecipitation) or by using a fusion construct of the bait protein (co-sedimentation, e.g. via GST-glutathione binding). However, as protein-protein interactions are often mediated by a certain domain, it is possible to run the affinity purification not with the full-length protein, but with a peptide covering the binding domain of interest. In particular when such peptides are accessible via solid phase peptide synthesis, they can be easily modified for the generation of negative controls and easily immobilized for the generation of covalent, highly standardized affinity matrices. In this manner, typical antibody- or fusion protein-related problems like unspecific binding or protein aggregation can be reduced (Gururaja et al., 2003; Schulze and Mann, 2004).

Based on these considerations and the high affinity of Cplx to the neuronal SNARE complex (Pabst et al., 2002), it was chosen to use SNARE-binding domain peptides of Cplx for the enrichment of fully assembled SNARE complexes from synaptic protein fractions, rather than co-immunoprecipitation or co-sedimentation of individual SNARE proteins. The basis of our approach was the finding that synthetic peptides representing the central α helix of all four Cplx isoforms retain their affinity to the reconstituted neuronal SNARE complex *in vitro*, with binding affinities spanning the nanomolar (Cplx1) to micromolar (Cplx4) range (K. Reim, O. Jahn, J. Rizo; unpublished observation). The technical proof of concept that the constituents of the neuronal SNARE complex can be enriched from cortical crude synaptosome fractions by immobilized Cplx1 SNARE binding domain peptides was successfully established in my Master thesis entitled "Peptidic tools to study the molecular composition of the SNARE fusion machinery".

1.6 Aim of this study

As described above, all four Cplxs share the conserved central α helix that is necessary for binding of Cplxs to SNARE complexes, as primarily established for Cplx1 and the neuronal SNARE complex consisting of Stx1, SNAP25 and Synaptobrevin 2. The high degree of conservation in this central domain suggests that probably all Cplx isoforms exert their function via an interaction with SNARE complexes. This raises the question whether different Cplxs act upon different SNARE complex types, particularly in view of the observation that Cplx3 and Cplx4 show a considerably decreased affinity to the neuronal SNARE complex (see above). Thus, in ribbon synapses of the retina, where Cplx3 and Cplx4 are specifically expressed, other SNARE complexes may be employed to contribute to the high rate of neurotransmitter release which exceeds that of conventional synapses many times. Moreover, it has not been studied yet whether Cplxs are involved in the regulation of SNARE complex-mediated membrane fusion events apart from neurotransmitter exocytosis. To address these questions in an unbiased and systematic way, the Cplx peptide-based affinity purification approach was expanded to all four Cplx isoforms and applied to different input material, i.e. cortical and retinal protein fractions. With this experimental strategy, it was expected to gain new insights into the molecular composition of SNARE complexes and their interactomes in different synaptic systems.

2 Materials and Methods

2.1 Materials

2.1.1 Animals

Cortical fractions were prepared from mice of C57Bl6N background and retinal fractions from mice of C57Bl6J background. They were kept in compliance with the guidelines for the welfare of experimental animals issued by the Federal Government of Germany (Niedersächsisches Landesamt für Verbraucherschutz und Lebensmittelsicherheit) and the Max Planck Society. The mice were obtained from the animal facility of the MPI of Experimental Medicine Göttingen.

2.1.2 Reagents

Table 1: Reagents with company

Reagent	Company
Acetic acid	Merck
Acetonitrile	J.T. Baker
Acrylamide/Bis Solution 30% (37.5 : 1)	BioRad
Agarose-Beads (SulfoLink® Coupling Resin)	Thermo Scientific
Ammonium bicarbonate (ABC)	Sigma Aldrich
Ammonium persulfate (APS)	Merck
Ammonium sulfate	Merck
Aprotinin	Roth
Aqua-Poly/Mount	Polysciences, Inc.
Bovine serum albumin (BSA)	Thermo Scientific
Bradford reagent	BioRad
Bromphenol blue	Pierce
CHAPS	Serva
Cystein	Pierce
Coomassie Brillant Blue G250	Serva
DAPI (4',6-Diamidino-2-Phenylindole, Dihydrochloride)	Thermo Scientific
Dimethyl sulfoxide (DMSO)	Sigma Aldrich
Dithiothreitol (DTT)	Biomol
Dulbecco's Modified Eagle Medium (DMEM)	Gibco
Dulbecco's phosphate buffer saline (DPBS)	Gibco

Ethanol	Sigma-Aldrich
Ethylendiaminetetraacetic acid (EDTA)	Merck
Ethylenglycoltetraacetic acid (EGTA)	Sigma-Aldrich
Fetal Bovine Serum (FBS)	Gibco
Fibronectin	Sigma Aldrich
Gelantine	Sigma Aldrich
Glycerine	Merck
Goat Serum	Gibco
HEPES (4-(2-hydroxyethyl)-1-piperazineethanesulfonic acid)	Roth
Hydrochloric acid 37%, fuming (HCl)	Merck
L-Cysteine	Pierce
Leupeptin	Peptide Institute
Lipofectamin 2000	Invitrogen
Magnesium chloride ($MgCl_2$)	Merck
Methanol	J.T. Baker
NP-40	Fluka BioChemika
Odyssey®-Blocking buffer	LI-COR
Opti-MEM	Gibco
Ortho-phosphoric acid	Sigma-Aldrich
PageRuler prestained protein ladder	Thermo Scientific
Paraformaldehyde (PFA)	Serva
Penicillin (1000U/mL)/Streptomycin (1000 µg/mL)	Gibco
Phenylmethylsulfonylfluoride (PMSF)	Sigma-Aldrich
Ponceau S	Sigma-Aldrich
Potassium chloride (KCl)	Merck
Potassium hydrogen phosphate (KH_2PO_4)	Merck
Sodium acetat	Fluka BioChemika
Sodium acide	Merck
Sodium Chloride (NaCl)	Merck
Sodium-Cholate	Wako
Sodiumdodecylsulfate (SDS)	Roche
Sodium hydroxide (NaOH)	Merck
Sodium phosphate dibasic dihydrate (Na_2HPO_4 x $2H_2O$)	Merck
Sodium phosphate monobasic monohydrate (NaH_2PO_4 x H_2O)	Merck
Sucrose	Merck

Tetramethylethylenediamine (TEMED)	Serva
Thio-Urea	Sigma-Aldrich
Transferrin-AlexaFluor568	Thermo Scientific
Trizma®-base (Tris)	Sigma-Aldrich
Triton X-100	Roche
Trypsin-EDTA (0.05%)	Gibco
Tween 20	Sigma-Aldrich
Urea	Merck

2.1.3 Solutions and Buffer

If not mentioned otherwise solutions and buffer were dissolved in ddH_2O. The pH was adjusted with HCl or NaOH.

Table 2: Solution and Buffer

Biochemistry	
3x SDS sample buffer:	10 % SDS, 140 mM Tris-HCl pH 6.8, 3 mM EDTA, 30 % sucrose 0.1 % bromphenol blue before use 150 mM DTT were added
Coomassie dye stock solution	0.1 % Coomassie Billant Blue G250 2.0 % ortho-phophoric acid 10 % ammonium sulfate
Coomassie fixation solution	40 % ethanol 10 % acetic acid
Coupling Buffer: (Peptide Coupling)	50 mM Tris 5 mM EDTA The pH was adjusted to 8.5. Buffer was sterile filtrated.
FASP Buffer:	7 M Urea 2 M Thio-Urea 2 % CHAPS 0.1 M Tris (pH 8.5) 10 mM DTT (add immediately before use)

Homogenization Buffer:	0.32 M Sucrose, 1 µg/mL Aprotinin, 0.5 µg/mL Leupeptin 17.4 µg/mL PMSF.
Phosphate Buffered Saline (PBS) Solution:	137 mM NaCl, 2.68 mM KCl, 8.09 mM Na_2HPO_4 x H_2O 1.76 mM KH_2PO_4 pH was adjusted to 7.4.
Ponceau S staining buffer:	0.1 % Ponceau S 5 % acetic acid
SDS-PAGE Running Buffer:	25 mM Tris, 250 mM glycine 0.1 % SDS
Separating Polyacrylamid (PAA) gel:	10-18% acrylamide, 375 mM Tris-HCl pH 8.8, 0.1 % SDS, 0.1% APS 0.1 % TEMED.
Solubilisation Buffer:	150 mM NaCl 10 mM Hepes-NaOH (pH 7.4) 1 mM EGTA 2 mM $MgCl_2$ 1% NP40 (or 1 % CHAPS or 1 % sodium cholate) 0.1 % of each proteinase inhibitor (Aprotinin, Leupeptin, PMSF) 1 mM DTT
Stacking PAA gel:	5 % acrylamide, 125 mM Tris-HCl pH 6.8, 0.1 % SDS, 0.1 % APS 0.1% TEMED.
Storage Buffer (Peptide Coupling):	0.05 % NaN_3 in PBS The pH was adjusted to 7.2.

	Buffer was sterile filtrated.
Transfer Buffer:	25 mM Tris, 190 mM glycine 20 % methanol
Immunoblotting	
Blocking buffer	50 % PBS 50 % Odyssey Buffer
Primary Antibody solution	49.95 % PBS 49.95 % Odyssey Buffer 0.1 % Tween20 corresponding dilution of antibody
Secondary Antibody solution	49.95 % PBS 49.95 % Odyssey Buffer 0.1 % Tween20 0.01 % SDS corresponding dilution of antibody
Washing Buffer	0.1 % Tween in PBS
Cell Biology	
Acid wash buffer:	0.1 M Sodium acetat pH 5.3 0.5 M NaCl
Cell culture medium:	DMEM 100 U/ml Penicillin / Streptavidin 10 % FBS
Freezing medium:	10 % FBS 10 % DMSO in cell culture medium
Immunocytochemistry	
Permeabilization buffer	0.3 % Triton-X-100 in Sorensen phosphate buffer
Blocking buffer	20 % Goat serum 0.1 % Triton X-100 0.2 % gelantine in Sorensen phosphate buffer
Antibody Solution	1 % Goat serum

	0.1 % Triton X-100 0.2 % gelantine in Sorensen phosphate buffer
Sorensen Phosphate buffer	M NaH_2PO_4 x H_2O M Na_2HPO_4 x $2H_2O$
Fixation buffer	4 % PFA in Sorensen phosphate buffer pH 7.4 Buffer was sterile filtrated.

2.1.4 Antibodies

Table 3: Primary and Secondary Antibodies
Abbreviations: WB: Western Blot; ICC: Immunocytochemistry

Antigen	Host	Company	Dilution	Use
Primary Antibodies				
Bassoon	Guinea pig	SYSY	1:1000	WB
Cplx1/2	Rabbit	SYSY	1:2000	WB
			1:500	ICC
Cplx3	Rabbit	SYSY	1:500	WB
Cplx4	Rabbit	SYSY	1:500	WB
CtBP2/RIBEYE	Mouse	BD Biosciences	1:5000	WB
Munc18	Mouse	SYSY	1:1000	WB
Sec22b	Rabbit	SYSY	1:1000	WB
SNAP23	Rabbit	SYSY	1:500	WB
SNAP25	Mouse	SYSY	1:5000	WB
SNAP29	Rabbit	SYSY	1:1000	WB
Synaptobrevin 2	Mouse	SYSY	1:7500	WB
Syntaxin 1 AB	Mouse	SYSY	1:10 000	WB
Syntaxin 3	Rabbit	SYSY	1:1000	WB
Syntaxin 5	Rabbit	SYSY	1:1000	WB
Syntaxin 6	Rabbit	SYSY	1:2000	WB
Syntaxin 7	Rabbit	SYSY	1:1000	WB
Syntaxin 8	Rabitt	SYSY	1:250	WB
Syntaxin 12/13	Rabbit	SYSY	1:500	WB
Syntaxin 16	Rabbit	SYSY	1:500	WB
Syntaxin 17	Rabbit	Novus Biological	1:500	WB

VAMP4	Rabbit	SYSY	1:500	WB
VAMP7	Mouse	SYSY	1:1000	WB
VAMP8	Rabbit	SYSY	1:1000	WB
vti1a	Rabbit	SYSY	1:1000	WB
vti1b	Rabbit	SYSY	1:1000	WB
Ykt6	Rabbit	Abiocode	1:500	WB
Secondary Antibodies				
Anti-Mouse - AlexaFluor680	Goat	Life	1:5000	WB
Anti-Mouse - IRDye800	Goat	LI-COR	1:5000	WB
Anti-Rabbit- AlexaFluor555	Goat	Thermo Fisher	1:500	ICC
Anti-Rabbit - AlexaFluor680	Goat	Life	1:5000	WB
Anti-Rabbit - IRDye800	Goat	LI-COR	1:5000	WB

2.1.5 Peptides

Table 4: Peptides with amino acid sequence

Peptides	Amino Acid Sequence
Cplx1_WT	CERKA KYAKM EAERE VMRQG IRDKY GIKK-($CONH_2$)
Cplx1_K69A/Y70A	CERKA KYAKM EAERE VMRQG IRDAA GIKK-($CONH_2$)
Cplx2_WT	CERKA KHARM EAERE KVRQQ IRDKY GLKK-($CONH_2$)
Cplx2_K69A/Y70A	CERKA KHARM EAERE KVRQQ IRDAA GLKK-($CONH_2$)
Cplx3_WT	CERDA QFTQR KAERA TLRSH FRDKY RLPK-($CONH_2$)
Cplx3_K79A/Y80A	CERDA QFTQR KAERA TLRSH FRDAA RLPK-($CONH_2$)
Cplx4_WT_abu	CERDA AFTQK KAERA (Abu)LRVH LRDKY RLPK-($CONH_2$)
Cplx4_ K79A/Y80A _abu	CERDA AFTQK KAERA (Abu)LRVH LRDAA RLPK-($CONH_2$)
RBP_WT_monomer	CEQTV PVDLS VARPR-($CONH_2$)
RPP_control_monomer	CEVRQ DAPSV LTPRV-($CONH_2$)
RBP_WT_dimer	CEQTV PVDLS ARPR (PEG12) EQTV PVDLS ARPK-(COOH)
RBP_control_dimer	CEVRQ DAPSV LTPRV (PEG12) EVRQ DAPSV LTPVK-(COOH)

The peptides were synthesized according to the standard solid phase fluorenylmethoxycarbonyl (Fmoc) chemistry and kindly provided by Lars van Werven (Proteomics group). In Cplx4 peptides α-aminobutyric acid (abu) was used as replacement for internal cysteine residues to ensure that peptide coupling only happens via the N-terminal cysteine residue.

2.1.6 Vector plasmids

Table 5: Vector plasmids with background vector

Construct	Mutation	Vector
Cplx2_WT-IRES-EGFP	-	pcDNA3
Cplx2_M-IRES-EGFP	K69A/Y70A	pcDNA3

The plasmid constructs were kindly prepared by Manuela Schwark.

2.1.7 Software

Table 6: Software

Software	Company
Adobe Illustrator 2020	Adobe
FIJI-ImageJ 2.1.0	Open Source
Imaris 9.8.0	Oxford Instruments
Image Studio Lite	LI-COR
Leica LAS AF	Leica
Microsoft Exel & Word 16.54	Microsoft 365

2.2 Biochemical methods

2.2.1 Protein preparation from cortex and retina

Cortex or retina of mice were dissected and taken up in homogenization buffer. Tissue disruption was performed within a glass teflon homogenizer by using a Potter (Braun) at 900 rpm for 10 strokes (referred to as "homogenate"). If fractionation was necessary, the homogenate was centrifuged at 1.000 g for 10 min to remove nuclei. The supernatant ("S1") was optionally further fractionated by centrifugation at 20.000 g for 30 (retina) or 60 min (cortex) to yield a crude membrane enriched fraction ("P2"). The resulting pellets were resuspended in homogenization buffer and all fractions were stored at -80°C. All steps were performed at 4°C. To determine protein concentration, Bradford protein assays were executed. BSA samples served as standard curve and the absorbance of the samples was measured at 595 nm with a spectrophotometer (Amersham Bioscience).

2.2.2 Peptide coupling

SulfoLink® resins are porous agarose beads activated with iodoacetyl groups for covalent immobilization of cysteine peptides and other sulfhydryl molecules. The beads were equilibrated by washing four times with coupling buffer before coupling with the peptide. 375 µg peptide were dissolved in coupling buffer and added to 100 µL agarose beads for 60 min while end-to-end rotation. In this way a covalent thioether bound was formed between the free iodoacetyl group on the agarose bead and the N-terminal cysteine of the peptide. The beads were washed four times with coupling buffer before adding 50 mM L-Cysteine for 60 min for quenching. The beads were washed five times with 1 M NaCl and three times with storage buffer. All steps were performed at room temperature und beads were treated with gently shaking and centrifugation (1000 g). The success of coupling was verified by high performance liquid chromatography (HPLC) analysis of the supernatant before and after the coupling.

2.2.3 Affinity purification experiment

As input material for the affinity purification assays different tissue (cortex or retina), fractionations (homogenate, nucleus-free fraction or crude synaptosomal fraction) from different origins (mouse tissues or HEK cells) were used. To generate detergent extracts, input material at a protein concentration of 2 mg/mL was added to the solubilization buffer for 15 min while rotation. The non-solubilized proteins were removed by ultracentrifugation at 356200 g for 15 min. The supernatant, further also called Load, was added to the peptide-coupled agarose beads with the ratio 40:1 (v/v) for 3 hours during rotation. Afterwards beads were washed 5 times with solubilization buffer. So far, all steps were performed at 4°C. After the last washing step residual buffer was removed. In preparation of MS analyses, the beads were suspended in FASP buffer (1:6 ratio), incubated 20 min while rotation und centrifuged at 16.000 g. The supernatant was transferred to a fresh tube and subjected to proteomic analysis. In preparation of WB analyses, the beads were resuspended in SDS sample buffer (1:2 ratio) und boiled at 95 °C for 5 min.

2.2.4 Sodium dodecyl sulfate polyacrylamide gel electrophoresis (SDS-PAGE)

Two-layer polyacrylamide gels (stacking and separation gel) were made according to the needed grade of protein separation based on the molecular weight. The porous gel was

loaded with a protein molecular weight standard (PageRuler, Thermo Scientific) and the denatured samples, which were diluted in SDS sample buffer. The anionic detergent SDS adds a negative charge to the proteins, which therefore will migrate in an electric field toward the anode. In a gel electrophoresis system, filled with running buffer, the proteins were separated according to their size by applying 180 V and 25 mA (Laemmli, 1970).

2.2.5 Colloidal Coomassie Staining

To visualize the protein bands on the gel and quantify the protein amount, the gel was stained with a colloidal Coomassie solution. Following electrophoresis, the gel was fixed with a standard fix solution for 1h, washed twice with ddH_2O for 10 min and stained over night with 80 % Coomassie dye stock solution and 20 % methanol. On the following day the gel was washed with ddH_2O, scanned, and protein amounts of the individual lanes were quantified by near-infrared fluorescence with the Odyssey system of LICOR.

2.2.6 Immunoblotting

After separating the proteins by SDS-PAGE, they were transferred onto a nitrocellulose membrane in transfer buffer by using a tank-blot-system. The transfer was carried out at 4°C for 740-860 mAh, depending on the expected protein weight. Subsequently, the membrane was stained with Ponceau S to visualize the transferred proteins. To remove the dye, the membrane was then washed with PBS. For the immunoblotting analysis the fluorescence systems by LI-COR was used. Therefore, blocking buffer was added to the membrane for 1 h. After incubation with the primary antibody in the corresponding dilution for 1h, the membrane was washed five times with washing buffer. The secondary antibody solution was added for 1h in the dark and the membrane was washed again for five times. All steps were performed at RT and during the incubation steps the membrane was shaking.

2.2.7 Visualization and Quantification

For detection and quantification of the fluorescent signal, the Odyssey Imaging System uses two-color near-infrared detection (700 nm and 800 nm) and multiplexing options. The signals were quantified with the software Image Studio Lite from LI-COR, based on the densiometric method. The software calculates the background at a border width of 3 for the top and bottom segment for immunoblotting analysis. Also Coomassie dye staining could be

visualized at 700 nm. The only difference is that the background for quantification is measured here in the right and left segments.

2.2.8 Tissue extraction

To study protein expression in different mouse organs, the tissues must be prepared. Therefore, tissue of the different organs (heart, lung, pancreas, liver, spleen, ilium; colon, kidney, testis, thyroid gland, brain) were dissected and resuspended in PBS with proteinase inhibitors. The tissue was dispersed by an ULTRA-TURRAX® and with a centrifugation step with 1000 g for 10 min the coarse particles were removed. The protein concentration of the supernatant was determined and the samples were resuspended in SDS-sample buffer.

2.3 Quantitative mass spectrometry

For proteome analysis, the eluted fractions from affinity purification experiments were submitted to the Proteomics Group of the Max Planck Institute of Experimental Medicine. Briefly, samples from the screening approach were eluted in lysis buffer (7 M urea, 2 M thiourea, 10 mM DTT, 2% CHAPS, 0.1 M Tris pH 8.5) and directly subjected to automated in-solution digestion with trypsin according to the filter-aided sample preparation (FASP) protocol as established for synaptic protein fractions (Ambrozkiewicz et al., 2018). Alternatively, samples from the validation approach were eluted in SDS sample buffer, separated on precast Tris/glycine gradient 4-12% gels (TG PRiME, Serva), and subjected to automated in-gel digestion with trypsin. All digests were spiked with 10 fmol/µl Hi3 EColi standard (i.e. quantified synthetic peptides derived from E. coli. Chaperone protein ClpB; Waters Corporation) for quantification purposes and analyzed by liquid chromatography coupled to electrospray mass spectrometry (LC-MS). Tryptic peptides were separated by nanoscale reversed-phase ultra-performance liquid chromatography. Mass spectrometric analysis of tryptic peptides was performed using a Synapt G2-S (Waters Corporation) quadrupole (Q-TOF) time-of-flight mass spectrometer equipped with ion mobility option. For label-free quantification, a data-independent acquisition (DIA) workflow with alternating low and elevated energy (MS^E) and an ion mobility-enhanced version thereof (referred to as $UDMS^E$) was utilized (Distler et al., 2016), as described for samples derived from in-solution and in-gel digestion, respectively (Ambrozkiewicz et al., 2018; Sondermann et al., 2019). Continuum LC-MS data processing and protein identification by database search was performed with the software Waters ProteinLynx Global Server (PLGS) version 3.0.2, using

the UniProtKB/Swiss-Prot mouse proteome to which the sequence information for E. coli. Chaperone protein ClpB and porcine trypsin was added. Appending the reversed entry sequence enabled determination of false discovery rate (FDR). Precursor and fragment ion mass tolerances were automatically determined by PLGS 3.0.2. Carbamidomethylation of cysteine was set to fixed whereas oxidation of methionine was assumed as variable modification. One missed trypsin cleavage was allowed and minimal ion matching requirements was: two fragments/peptide, five fragments/protein, one peptide/protein. Threshold of FDR protein identification was set to 1%. For post-identification analysis, the freely available software ISOQuant (http://www.isoquant.net) was used to calculate the absolute in-sample amounts for each detected protein according to the TOP3 quantification approach (Silva et al., 2006; Kuharev et al., 2015). False discovery rate (FDR) for both peptides and proteins was set to 1 % threshold and only proteins reported by two and more peptides were quantified.

2.4 Cell biological methods

2.4.1 Mammalian Cell Culture

As mammalian cell lines HEK293FT and HeLa cells were used. They are fast growing and easy to transfect. In contrast to the HEK293FT cells, the HeLa cells have a smaller nucleus and are therefore better suited for experiments with subsequent microscopy. The handling is identical for both cell lines. The cells were maintained in 10 cm culture dishes at 37 °C, 5 % CO_2 level and 95 % humidity. At a confluence of about 80 %, the cells were split to ensure continued viability. Therefore, the cells were washed with PBS, detached from the dish with 0.05% Trypsin for 2 min at 37 °C and resuspended in fresh cell culture medium. The cell suspension was diluted according to the desired number of cells into a new culture dish.

2.4.2 Freezing and thawing of mammalian cells

For storage of mammalian cells, they were frozen at -80 °C. Therefore, the washed and trypsin-detached cells were resuspended in freezing medium and slowly frozen. Cells frozen as descripted above, were thawed at 37°C for maximal 2 min and diluted with cell culture medium. After centrifugation at 200 g for 3 min, the pellet was again resuspended in cell culture medium.

2.4.3 Harvesting

Cells in the cell culture dish were washed three times with PBS to get rid of excess supplements of the cell culture medium. 0.32 M Sucrose with proteinase inhibitors were added and cells were detached from the plate using a cell scraper. The cell suspension was homogenized with 27G canula (0.4 mm diameter) to burst the cells. After centrifugation for 10 min at 1000 g at 4 °C the nuclei are removed in the pellet and by centrifuging again the supernatant for 1 h at 20.000 g at 4°C the membrane containing fraction was enriched in the pellet. The pellet was resuspended in 0.32 M sucrose and proteinase inhibitors. This protocol was adapted from the P2 fractionation of the cortex.

2.4.4 Coating of coverslips

If the cells should be used for a following microscopy experiment, they need to be seeded on top of glass coverslips. To degrease and decontaminate the coverslips they were washed in 1 M HCl for 48 h, followed by several washing steps with ddH_2O and two washing steps in 70% ethanol. The coverslips were stored in 100% ethanol. For better adhesion of the cells to the glass coverslip, they are coated with fibronectin. Therefore, the coverslips were set up for one hour under UV radiation for ethanol evaporation and decontamination. The coverslip is placed on a drop of fibronectin and incubated at 37°C for 30 min. Excess fibronectin is removed by washing twice with PBS. Cell suspension can be added in desired density, whereby 60.000 cells/mL was an optimal range for a following transfection after 24 h.

2.4.5 Lipofectamin transfection

After reaching a confluence of about 60-70%, the cells could be transfected. For each coverslip 0,5 µg cDNA and 1 µl Lipofectamin2000 were mixed with OptiMEM medium and let stand still at RT for 30 min. In parallel, the cell culture medium on top of the cells was removed and replaced by pure DMEM medium without any supplements. The complexes of lipofectamine with cDNA were added to the cells, incubated at 37 °C and after 1 h cell culture medium was added.

2.4.6 Transferrin uptake assay

When cell confluence reaches approximately 70 %, cells were washed twice with PBS and starved for 1 h by adding serum free DMEM medium with 20 mM HEPES pH 7,4. The Transferrin, coupled with the fluorophore AlexaFluor-568, was prepared as uptake solution with a final concentration of 20 µg/ml. Droplets of this fluorescent ligand were added onto parafilm and the coverslips with the cells were transferred upside-down onto one droplet of ligand and incubated at 37°C. After 1 to 8 minutes the cells were placed on ice to stop the uptake immediately. The coverslips were transferred into ice-cold PBS with 10 mM $MgCl_2$, incubated in an acid wash buffer for 1 min on ice, washed again two times with ice-cold PBS with 10 mM $MgCl_2$ and fixed with 4% PFA for 10 min. To stain the nuclei, the cells were incubated with DAPI for 15 min. Afterwards they were washed with PBS and mounted with Aqua-Poly/Mount.

2.4.7 Immunocytochemistry

To check the Cplx expression after transfection, immunostaining was performed. Therefore, transfected cells were washed three times with Sorensen phosphate buffer and fixed with 4 % PFA for 10 min. After another three washing steps with PB, samples were treated with permeabilization buffer for 30 min at gently shaking. Next, blocking buffer was added for 1.5 h. The corresponding primary antibody against Cplx1/2 was diluted (see 2.1.3), added to the sample and incubated at 4 °C over night. After three washing steps with PBS, an incubation with the secondary antibody AlexaFluor-633 (see 2.1.3) for 1.5 h at room temperature followed. The cells were washed three times with PB and stained with the nuclei marker DAPI for 15 min and again washed three times with PB. Finally, the cells were mounted with Aqua-Poly/Mount on a glass slide.

2.5 Confocal fluorescence microscopy

2.5.1 Image acquisition

All microscopic images of the cells were taken on the confocal laser scanning microscope Leica SP5. With this, high-resolution images of several channels could be acquired in all three dimensions (x,y,z). The 40x oil-immersion objective with a numerical aperture of 1.25 was used to acquire images with the resolution of 1024 x 1024 pixels. For the excitation

wavelength of 405 nm UV light was used, for 488 nm an argon laser with 20 % power and for 561 nm a helium-neon laser. For the emission a photomultiplier tube (PMT) detector was chosen for the 405 nm excitation and more sensitive hybrid detectors (HyD) for the 488 nm and 561 nm excitation. All excitation wavelengths were defined in channels with emission detection spectrum, individually optimized laser power and gain (Tab. 7 and 8) to avoid oversaturation of the signal. Images were taken with a z-step size of 0.21 µm to cover the whole cell.

Table 7: Settings for Transferrin uptake experiment

channel	excitation wavelength	emission detection spectrum	laser power	gain
3	405	415-478	4 %	
2	488	498-558	22 %	-
1	561	578-700	11 %	-

Table 8: Settings for ICC experiment

channel	excitation wavelength	emission detection spectrum	laser power	gain
3	405	415-478	3 %	
2	488	498-545	24 %	-
1	561	565-650	2 %	-

2.5.2 Image analysis

The three-dimensional confocal images were analyzed by using IMARIS (bitplane). First the files in LEICA format need to be converted in IMARIS 3D files. The surface tool was used at channel 2 to identify the EGFP-transfected cells and define them as region of interest. The parameters to create such a surface were defined in table 9. The settings were applied to all quantification. In this way the mean intensity and the summed intensity of the transferrin signal was determined for each transfected cell and could be statistically analyzed.

Table 9: Parameter for the IMARIS software to identify the cell surface of EGFP positive cells

Parameter	Value
Surface Grain Size (µm)	0.758 µm
Diameter of Largest Sphere (µm)	30,0 µm
Manual Threshold Value	44.29
Region Growing Estimated Diameter (µm)	10 µm
Filter Volume above (μm^3)	10 μm^3
Filter Quality above	0.73

Some representative immunostained 2D-images were processed in FIJI for figure 21b. A maximum projection of the z-stacks was created, and brightness and contrast were adjusted for each channel. To compare the conditions, all images were processed the same way.

2.6 Statistical Analysis

All statistical analyses were performed using Prism 8 (GraphPad). All data are represented as mean with standard error of the mean (SEM). N refers to the total number of transfected cells, whereby three biological replicates were generated to reach this number. Whether a normal distribution occurs was checked by means of D'Agostino-Pearson normality test. When all data sets were normally distributed, the samples were analyzed for significance using an unpaired two-tailed Welch's t-test to compare WT and mutant. For non-parametric data, the Mann-Whitney test was used for comparing. The significance level for p was set at < 0.05.

3 Results

3.1 Development of the experimental design

3.1.1 Principle of the peptide-based affinity purification assay

To study whether Cplxs act upon different SNARE complex types and if these SNARE complexes are Cplx isoform-dependent, peptides representing the central α helix of all four Cplx isoforms were synthesized and covalently immobilized on agarose beads (Figure 7a). These affinity matrices were used to enrich fully assembled SNARE complexes and their interactomes from detergent-solubilized protein fractions, either derived from cortical crude synaptosome preparations or from retinal lysate. Such affinity purification approaches need to be tightly controlled to be able to distinguish between specific and non-specific binding. Here it was realized by using SNARE-binding deficient Cplx mutant peptides, differing by only two amino acids from the wildtype (WT) peptide sequence (Figure 7b). For screening purposes, eluted proteins were subjected to in-solution digestion with trypsin, following identification and quantification by mass spectrometry (Figure 7c).

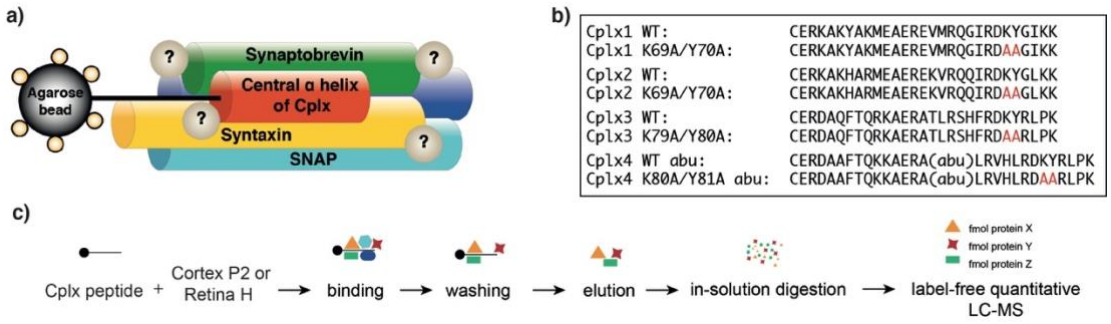

Figure 7: Affinity purification experiment with Cplx peptides.
(a) Schematic illustration of the Cplx-tool. The peptide, covering the central α helix of Cplx is coupled to agarose beads. Because this central α helix mediates SNARE complex interaction, the binding of SNARE proteins / assembled SNARE complexes is expected. Moreover, the identification of additional interacting molecules, that bind to the Cplx peptides or to already bound proteins is possibly. **(b)** Sequence of wildtype (WT) Cplx peptides and their respective negative controls. Mutations were generated on the basis of Xue et al., 2007. **(c)** Flowchart of affinity purification experiment. Cplx peptides, immobilized to agarose beads, were incubated with protein extracts from different sources (cortex pellet 2 – P2, retina homogenate – H). Proteins of the input material bind to the peptides and unspecific binding partners were washed away. After elution of the remaining proteins, they were digested with trypsin according to the filter-aided sample preparation (FASP) protocol and identified and quantified by label-free mass spectrometry (MS).

3.1.2 Influence of detergents on SNARE binding

Affinity assays like the used one, are prone to reveal false results, because the protein-protein interactions are sensitive regarding the detergent used and the ratio between protein and detergent. On the one hand the proteins in the input material need to be solubilized successfully and on the other hand the detergent should not interfere with the protein-protein interactions. Detergents are composed of both a hydrophobic and a hydrophilic part and when a critical limit is exceeded, micelles are formed. Because these micelles mimic the lipid-bilayer environment, they are useful tools to solubilize membrane proteins. Based on the nature of their hydrophilic head groups, detergents can be divided into three groups: non-ionic (e.g. NP-40), zwitterionic (e.g. CHAPS) and ionic (e.g. sodium cholate). Detergents from these different classes were tested, with the aim of finding optimal conditions for the affinity purification approach. For this set of experiments, we used the Cplx1, Cplx2 and Cplx3 peptides as well as their corresponding mutants as negative controls (Fig. 7b) and crude synaptosomes from cortex as protein source. For verification, WBs were performed with antibodies against the neuronal SNARE proteins. To examine the possibility of detecting even interaction partners of the SNARE complex with our approach, WBs were also conducted with the known SNARE complex interaction partner Munc18. Total protein amounts in the eluted fraction were visualized by gel electrophoresis followed by colloidal Coomassie staining.

When the affinity purification was performed with 1% NP-40, a mild non-ionic detergent, the protein pattern seen on the Coomassie stained PAA gel was as expected: separated proteins distributed over the whole lanes with a slightly higher concentration in the WT samples (Fig 8a). The corresponding WBs showed that the neuronal SNARE proteins Stx1AB, SNAP25, VAMP2 and Munc18 were detected in the WT samples whereas in the negative controls specific signals for the indicated proteins could not be observed or only to a minor extent (Figure 8 d, g). With 1% of the zwitterionic detergent CHAPS, lower total protein amounts were observed in the Coomassie stained gel in comparison to the NP-40 experiment. Consequently, in the WBs the specific signals for the indicated proteins were weaker but the signal pattern was comparable to the WBs of the NP-40 experiment (Figure 8b, e, h). It was concluded that the CHAPS mediated solubilization occurs suboptimal under our experimental conditions.

The use of 1% of the ionic sodium cholate resulted in the enrichment of higher protein amounts, however the neuronal SNARE proteins as well as Munc18 were also detected with

the SNARE binding deficient mutants (Figure 8c, f, i). As the proteins bind unspecifically to the peptides in the presence of sodium cholate, it was concluded that the detergent interferes with the Cplx peptide – SNARE interaction.

Only with the detergent NP-40 the SNARE proteins seem to be solubilized successfully, the protein interaction with Cplx is not interfered and the negative controls behave as expected. Consequently, the following experiments were performed with 1% NP-40.

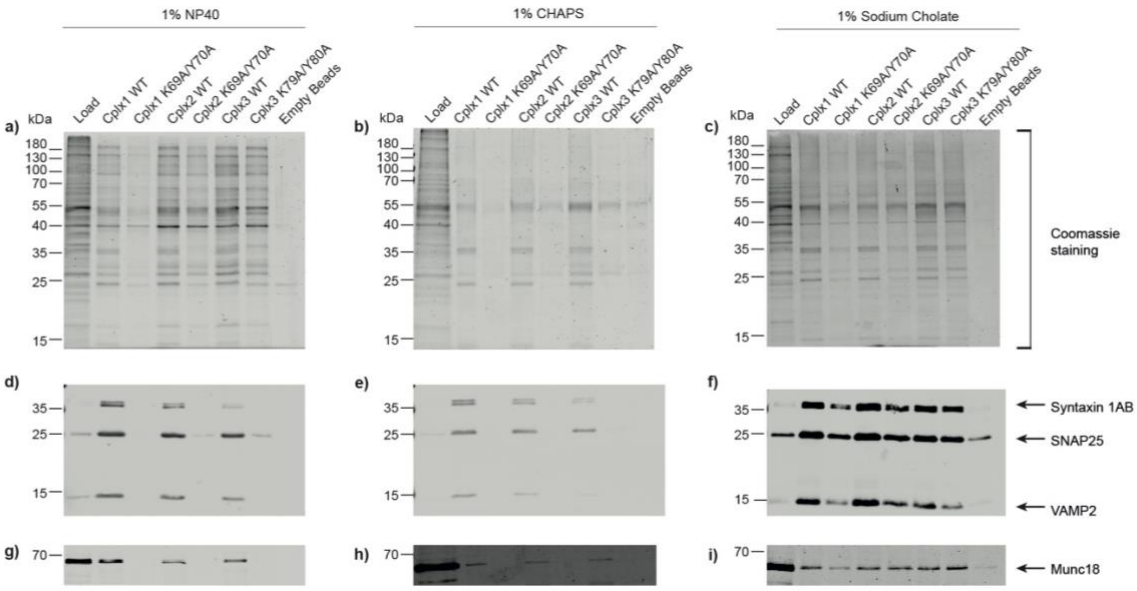

Figure 8: Influence of detergents regarding SNARE protein solubilization and their binding affinity. **(a-c)** After affinity purification experiments with Cplx1, Cplx2 and Cplx3, the quality of the samples was monitored by Coomassie stained SDS gels. The protein bands were quantified to adapt the amount of sample for the following Western blots. This adaptation process was done individually for each experiment. **(d-f)** Western Blots of neuronal SNARE proteins Stx1AB, SNAP25 and VAMP2, as known Cplx interactors, proofed that the experimental setting is working and the SNARE binding deficient mutant is sufficient. **(g-i)** Western Blot of Munc18, which was also detected as known interactor of the SNARE complex. The experiments were conducted with different detergents in the solubilization buffer. The experiment with 1 % NP-40 **(a,d,g)** was considered best, regarding SNARE und Munc18 enrichment in wildtype (WT) samples and no SNARE enrichment in mutants. With CHAPS as detergent **(b, e, h)** the mutants were also free of SNARE and Munc18 proteins, but the enrichment in WT samples was lower. The detergent sodium cholate **(c, f, i)** on the other hand enriched the SNARE proteins and Munc18 successfully, but also in large amounts with the mutant peptide.

3.1.3 General workflow

To ensure a high level of data quality, in each experiment peptides of two Cplx isoforms were used in parallel, whereas in the several independent repeats different Cplx isoforms were combined. By this procedure, multiple protein lists for each Cplx isoform were generated by quantitative MS (Table 10 and 11). Based on the experimental design it was possible to compare the results of the independent approaches.

Moreover, parallel runs of MS-based and gel-based approaches allowed the monitoring of each affinity purification experiment. For that purpose, the same amounts of samples were seperated on PAA gels which were stained with Coomassie. Because Coomassie Brillant Blue G250 can be excited by 700 nm laser light it was possible to use the corresponding scans not only for inspection of sample quality but also for estimation of protein amounts detected in each lane. Subsequently, the loading volumes for the different isoforms could be adjusted for the MS injection and WBs, whereas the negative control is not adjusted and is applied with the same volume as the corresponding WT variant. Due to the parallelism, WBs can be used as validation of the MS results in the following. For one screen (cortex screen II), such an adjustment is shown exemplarily in the appendix (Figure 31).

To analyze the multiple protein lists, following specific filter criteria were determined to condense the list to the most robust interactors. Just if a protein is enriched with the WT peptide compared to the mutant peptide and the enrichment factor is stable across all experiments, the protein is classified as a possible Cplx interaction partner. The individual enrichment thresholds were in the range of 2-fold and were experimentally determined depending on the total amount of proteins in the WT and mutant samples. The reproducibility of the results was checked, the affinity purification was repeated with gel-based MS, as complementary proteomic method, and bioinformatics analysis was used to sort all interacting proteins with respect to GO terms and synaptic function. After this approach was evaluated as a robust screen, the protein lists were examined for nonneuronal SNARE proteins or other interacting partners of interest. This general workflow was applied for affinity purification experiments using both cortex and retina as input material (Figure 9).

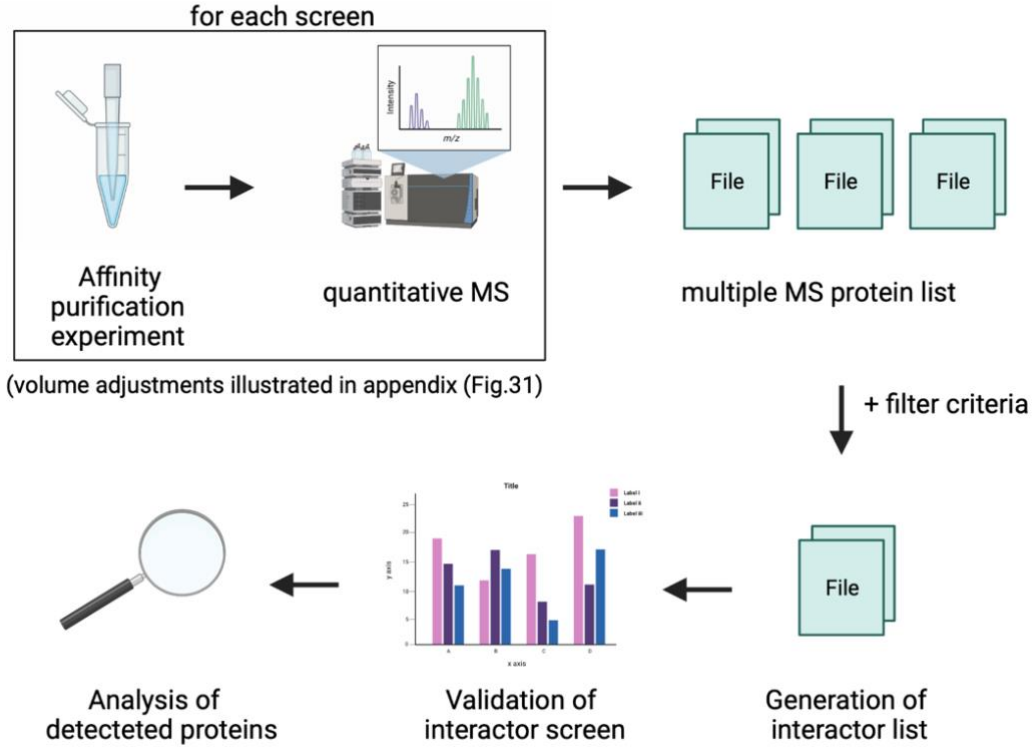

Figure 9: Schematic representation of the general workflow.
After affinity purification experiments, the samples were analyzed by FASP-based quantitative mass spectrometry (MS). Multiple passages with different Cplx peptides end in a big dataset of several MS protein lists. The application of strict filter criteria resulted in a final comprehensive protein list with enrichment ratios. To validate the interactor screens, reproducibility was checked by analysis of single screens and validated by Western Blot. In addition, the whole protein list was analyzed via the bioinformatic GO-term analysis tool. Afterwards the searching for new direct or indirect interaction partner of Cplx started. This workflow was applied for both cortex and retina samples. The figure was created with BioRender.com.

3.2 Affinity purification experiments with cortical fractions

3.2.1 Generation of interactor lists

To focus on potential interactors of the presynaptic Cplxs, crude synaptosomal fractions of isolated mouse cortices were prepared for the subsequent peptide-affinity approaches. Such fractions are enriched in synaptic proteins whereas nuclear proteins are reduced. Corresponding to the cortex material, Cplx1, Cplx2 and Cplx3 peptides were used for the screens, because these Cplx isoforms are expressed in this brain region (Reim et al., 2005). Three experiments were performed in which each isoform was compared with each other. After applying all filter criteria, the number of proteins which were enriched in WT vs SNARE binding-deficient mutant was calculated. In all screens 797 proteins were exclusively enriched with the WT peptides, however the number of identified proteins varied in the different approaches (Table 10). A closer inspection of the data revealed that 106 of these

proteins were found independently of the respective Cplx isoform, whereby others were exclusively found in only one isoform (Figure 10).

Table 10: FASP-based screens with Cortex input material
Screen I was run with Cplx1 and Cplx2 and 248 proteins were enriched with the wildtype (WT) peptide in comparison to the mutant (M) peptide. Screen II was run with Cplx1 and Cplx3 and 554 proteins were enriched. Finally, Screen III was run with Cplx2 and Cplx3 and 606 enriched proteins. The enrichment factor threshold was calculated individually for each screen, based on the total protein amounts and was in the range of 2-fold.

Screen	I	II	III
Cplx1	x	x	
Cplx2	x		x
Cplx3		x	x
proteins WT>M	248	554	606

797 proteins (WT>M)

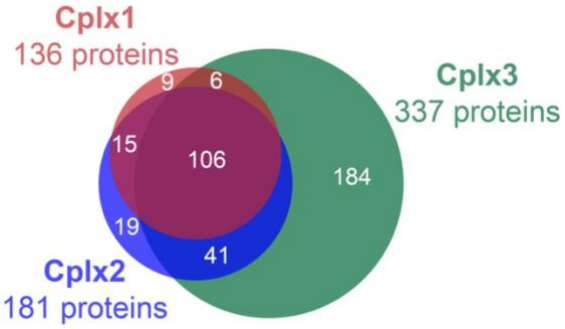

Figure 10: Venn diagram of Cplx1, Cplx2 and Cplx3 peptide interactome.
797 proteins were identified as proteins of the Cplx peptide interactome of one or several Cplx isoforms. Of these proteins were 106 found with all Cplx isoforms. 136 just with Cplx1, 181 just with Cplx2 and 337 just with Cplx3.

3.2.2 Validation of interactor screens

Before the 797 identified proteins were examined in more detail, the screens were tested on functionality and reproducibility. Because Cplx is known to bind to the assembled neuronal SNARE complex, all values obtained in the three quantitative MS screens for the individual SNARE components Stx1AB, SNAP25 and Synaptobrevin 2 were visualized as relative bar graphs (Figure 11a). The evaluation allows the following conclusions: (1) as expected, the SNARE proteins don't bind to the SNARE binding-deficient mutants, (2) with respect to the tested Cplx peptides, Cplx1 showed the best binding ability to the neuronal SNARE complex. In addition, Munc18 was tested because it is described to interact with the SNARE complex (Dulubova et al., 2007; Shen et al., 2007; Rodkey et al., 2008; Tareste et al., 2008; Ma et al., 2015). Interestingly, Munc18 was found in all screens and its appearance was

comparable to the pattern of the neuronal SNAREs. This result suggests that our experimental design is suitable to detect not only SNARE complexes that are recognized by the Cplx SNARE binding domain peptides but also additional proteins that probably interact with these SNARE complexes.

Another approach to validate the screening results is to reproduce the results with another proteomic approach. Therefore, the in-solution digestion was replaced by gel-based sample preparation, i.e. with prefractionation at protein level (Figure 11b). Although not as straightforward by means of label-free quantification, the MS-based readout from gels can be more directly compared with Western blot data (Figure 8d and g). As shown in figure 11c this method further confirmed the findings from the MS-based screen and from Western-blot analysis. It was thus concluded that the affinity purification approach is suitable to address SNARE complexes and their interactomes.

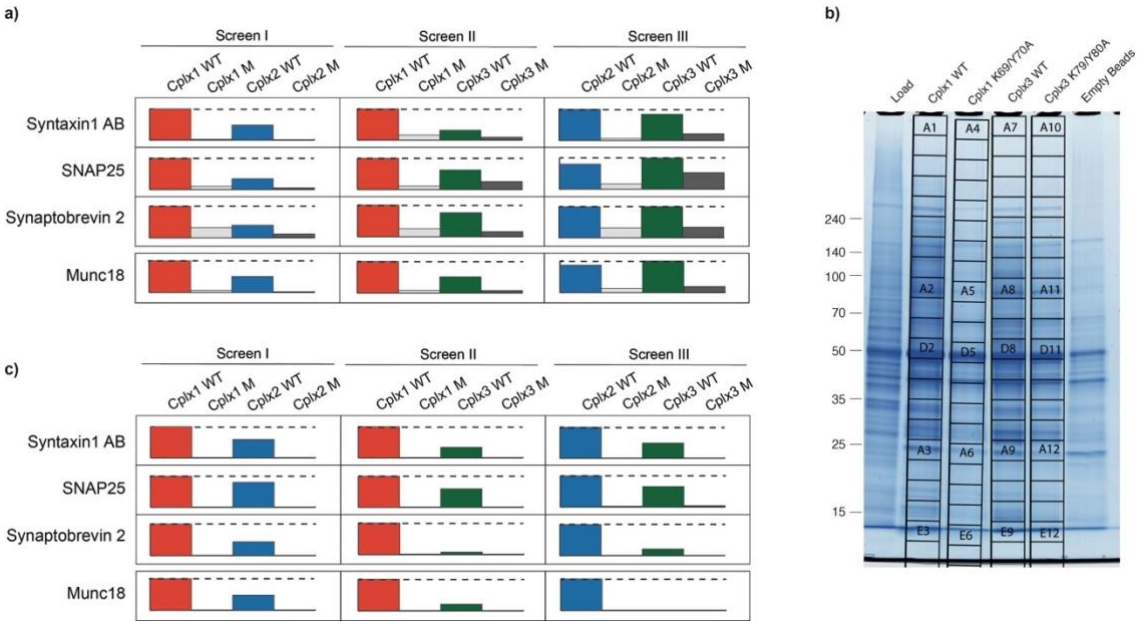

Figure 11: Mass spectrometry-based quantification of neuronal SNARE proteins and Munc18.
(a) Visualization of the three FASP based screen data for Syntaxin1, SNAP25, Synaptobrevin 2 and Munc18. Data are shown as relative amounts, whereas Cplx1 wildtype (WT) data were always set as 100 %. The stitched line indicates 100%. **(b)** Visualization of the three gel-based screen data, as described for (a). **(c)** Exemplary SDS-PAGE gel, before a gel-based MS. The grid shows where the gel is cut to get 24 pieces per lane, for separately digested MS samples.

3.2.3 Analysis of detected proteins by bioinformatic tools

In the three screens, a total of 797 proteins were identified as potential interactors of Cplx1, 2, and 3. To analyze these proteins, bioinformatics tools such as DAVID (Database for Annotation, Visualization and Integrated Discovery) and SYNGO were used. These

databases have deposited word-like information about proteins, such as Gene Ontology (GO) terms. A comparison of the own protein lists with the database shows whether some terms are associated with an above-average frequency with the own protein list.

With the free database DAVID the proteins were analyzed regarding the Gene Ontology (GO) terms *biological processes* and *cellular components* as well as the *KEGG pathway* terms (Figure 12a). For *biological processes* the top three terms listed by p-value were intracellular protein transport, transport, and vesicle-mediated transport. For the *cellular compartment* terms, the cytoplasm, cytosol, and SNARE complex were ranked with the highest values and for the *KEGG pathway* the enriched terms were SNARE interactions in vesicular transport, oxidative phosphorylation, and synaptic vesicle cycle. All in all, SNARE related terms we enriched, which showed that the approach is working and that false-positive candidates were not enriched excessively.

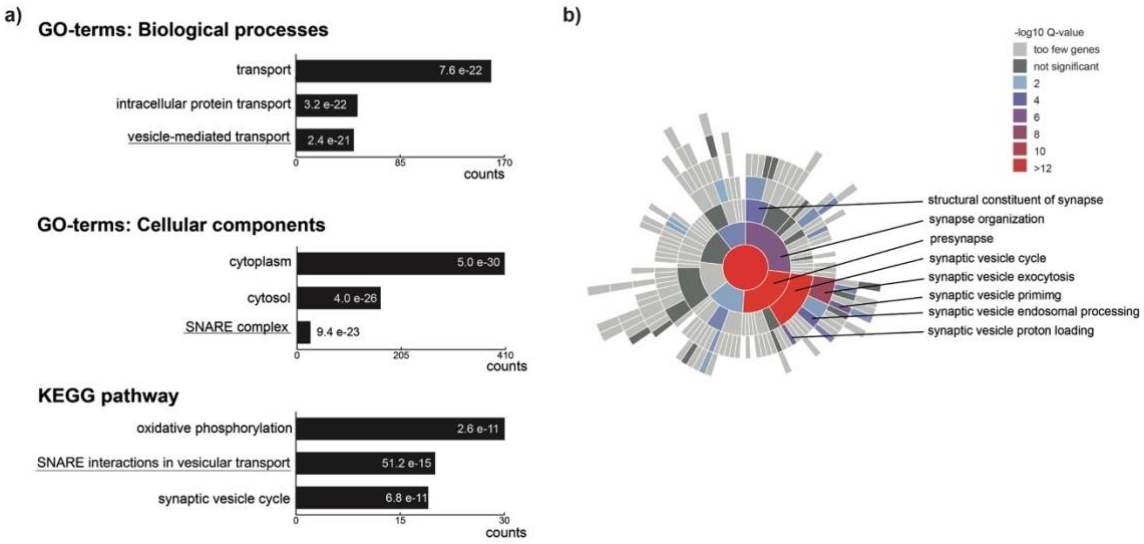

Figure 12: GO-term and SYNGO analysis of total Cplx-peptide interactome.
(a) 797 proteins, identified by MS were analyzed with the freely available bioinformatic database DAVID corresponding to the GO terms *Biological processes*, *Cellular components* and *KEGG pathway*. The top three listed terms regarding to p-values (numbers are given within the bars) are displayed for each category. The x-axis shows the number of protein counts for the terms. **(b)** Sunburst plot of 146 proteins, which were found in the SYNGO database. The color scale is indicating the -log Q-value.

The 797 proteins were also analyzed via SYNGO (Figure 12b). It is a database with synaptic proteins, curated by experts regarding evidence, as resource for studies concerning synaptic function and gene enrichment. 146 proteins were found in the database. The sunburst plot in figure 12b displaying the results of analysis in a hierarchical fashion illustrates that a lot of the found proteins were related to the group "presynapse" and within this category to the subgroup "synaptic vesicle cycle". Interestingly, among those proteins probably involved in

this process, molecules were identified not only mediating exocytosis but also endosomal processing.

3.2.4 Cplxs enrich non-neuronal SNARE proteins

After validation of the screening approach with the neuronal SNAREs, the lists of specific Cplx binders were checked for other SNARE proteins (Figure 13). We found, that beside the neuronal SNAREs additional 15 non-neuronal SNAREs were detected in relation to Cplx. Next, these SNARE proteins were quantified on the basis of the MS results. For each protein the highest value of a screen was determined as to be 100 % and the comparable dataset was related to this value (Figure 13). The quantitative profiles revealed a slight preference for Cplx1 for all SNARE proteins. However, a preference of any of these proteins for Cplx2 or Cplx3 was not detected. Some SNAREs, e.g. Stx16, VAMP4, VAMP7, vti1b or Sec22b, were not consistently detected with Cplx3, but a continuously loss of affinity to Cplx3 was also not observed.

In order to compare the relative amounts of the SNARE proteins among each other within a sample, further diagrams were created from the FASP-based screening data. Figure 14a shows the relative amount of SNARE proteins with Cplx1 (Screen II), figure 14c shows the SNARE proteins with Cplx2 (Screen III) and figure 14d the SNARE proteins with Cplx3 (Screen I). The three parallel datasets were shown in the appendix (Figure 32). The neuronal SNARE proteins SNAP25, Synaptobrevin 2 and Stx1AB were quantified with the highest values. However, also some non-neuronal SNAREs were considerably enriched. The most abundant SNAREs were validated via WB (Figure 14b). The non-neuronal SNAREs Stx6, SNAP47, Stx7, Ykt6 and Stx12 showed an enrichment with the Cplx1 WT peptide but not with the mutant Cplx1_K69A/Y70A, as seen with the neuronal SNAREs. Additional SNARE protein WBs are shown in the appendix (Figure 33).

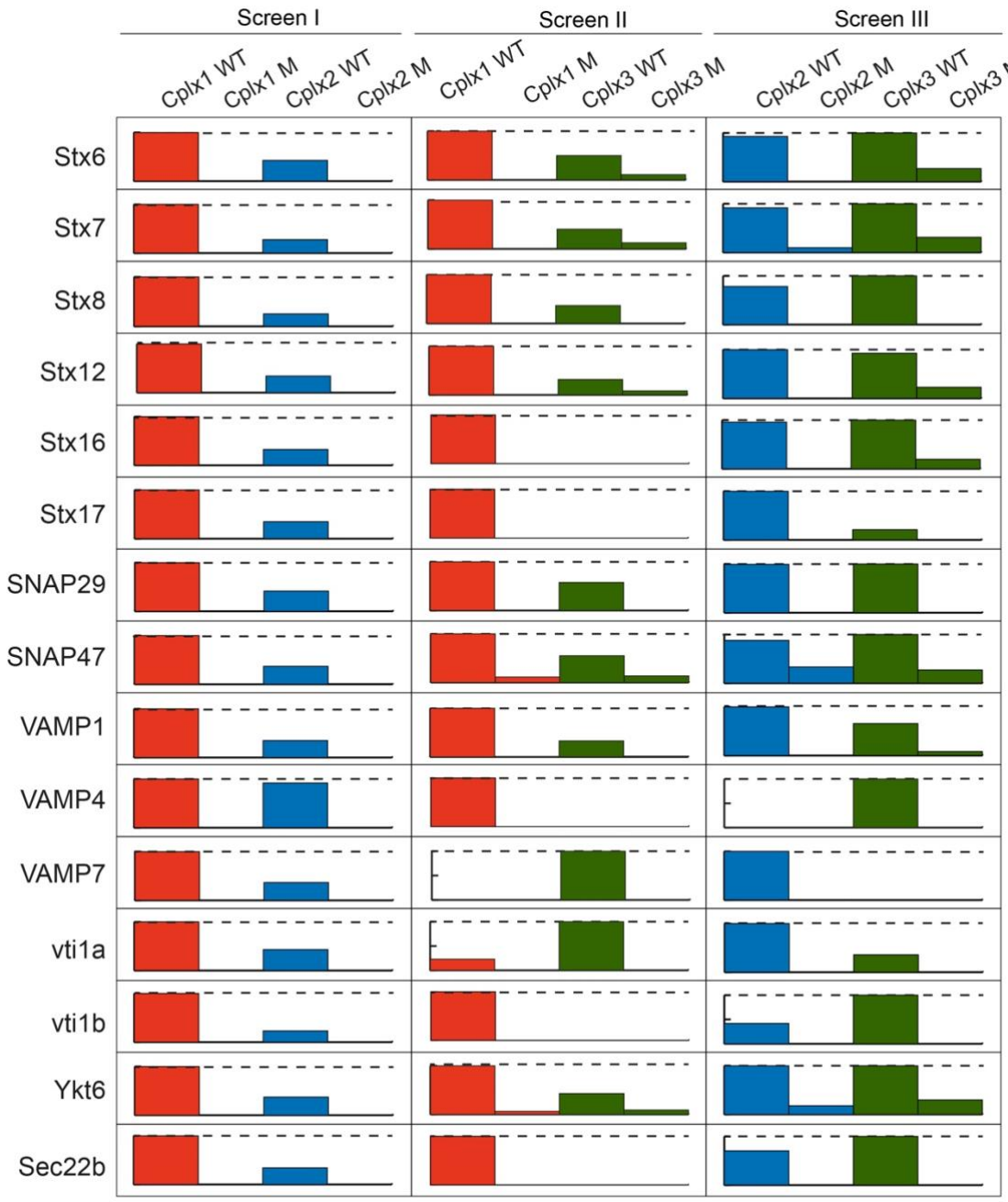

Figure 13: MS-based quantification of non-neuronal SNARE proteins.
Visualization of the three FASP based screen data for 15 non-neuronal SNARE proteins. Data are shown as relative amounts, whereas Cplx1 wildtype (WT) data were always set as 100 %. The stitched line indicates 100%.

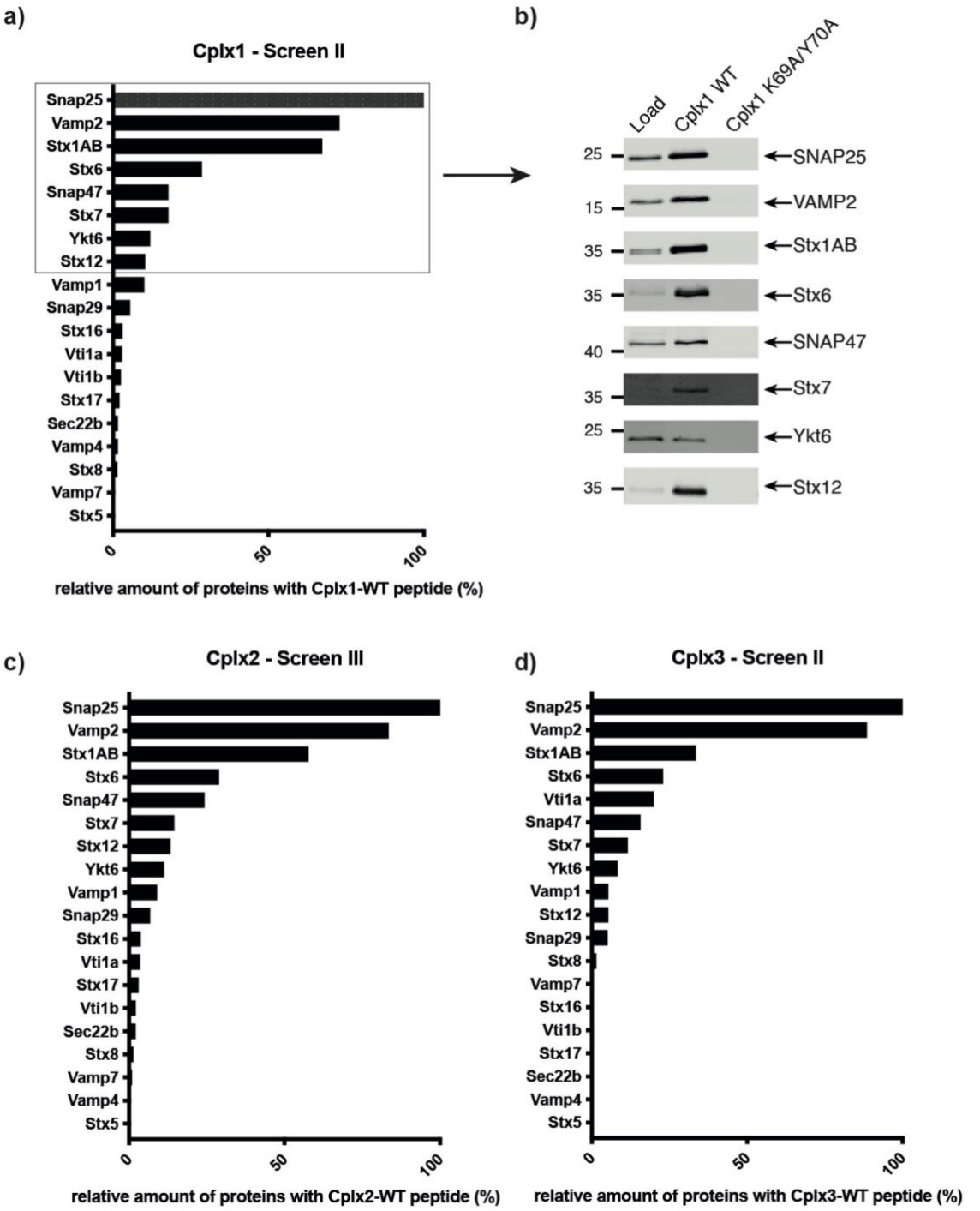

Figure 14: Relative amount of SNARE proteins analyzed via quantitative MS and verified by WB. **(a,c,d)** SNARE proteins binding to Cplx peptides were listed regarding their amounts and set in relation to the SNARE protein with the highest amount. For each isoform are two datasets available, one is shown here (Cplx1, screen II; Cplx2, screen III; Cplx3, screen II) and the other in the appendix (Cplx1, screen I; Cplx2, screen I; Cplx3, screen III). **(b)** The eight SNARE proteins with the highest amount with the Cplx1 peptide in screen II were selected for verification by WB.

As the interaction of Cplx with non-neuronal SNARE proteins seems to be independent of neuronal SNARE proteins, the literature on the localization of these proteins was studied. In Figure 15 all SNAREs associated with Cplx1 in the affinity purification experiment were marked. The blue marked proteins were identified by MS and the green marked proteins were verified by WB. It is noticeable that the SNARE complexes, that drive the membrane fusion processes of the endosomal and/or lysosomal pathway were completely detected in the Cplx peptide screen.

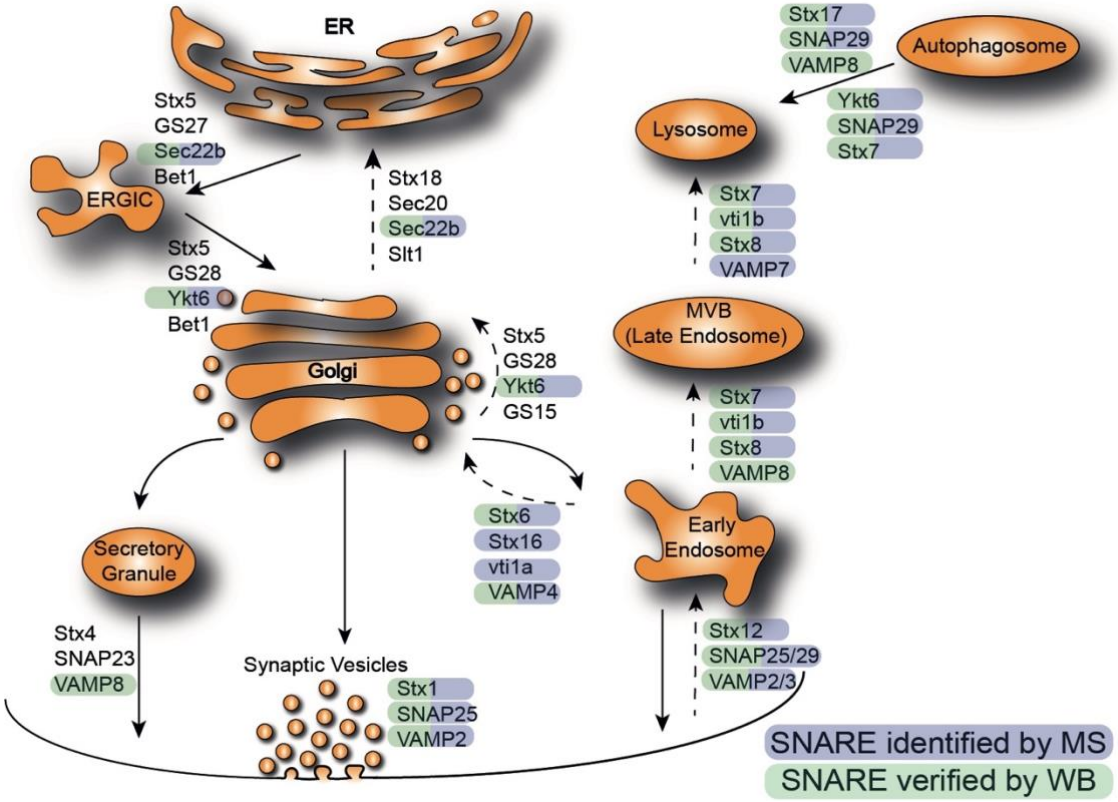

Figure 15: Schematic overview of membrane fusion processes mediated by SNARE complexes. Proteins identified by mass spectrometry were marked in blue and proteins verified by WB were marked in green. Abbreviations: ER: endoplasmic reticulum; ERGIC: ER-Golgi intermediate compartment; MVB: multivesicular bodies.

3.2.5 Validation of Cplx interaction with non-neuronal SNAREs

3.2.5.1 Validation with HEK cells as input material

To exclude the possibility that non-neuronal SNARE proteins were only detected because of co-enrichment with the neuronal SNARE proteins present in excess in cortical protein preparations, we performed an affinity purification experiment using Cplx1 peptides and membrane-enriched fractions from HEK cells (Fig. 16a), and thus in the absence of

endogenous Cplx and the synaptic exocytotic machinery. The absence of Cplxs and neuronal SNARE proteins from different cell lines as HeLa, COS and HEK cells was shown in WBs using cortex and retina material as positive controls (Appendix Figure 34).

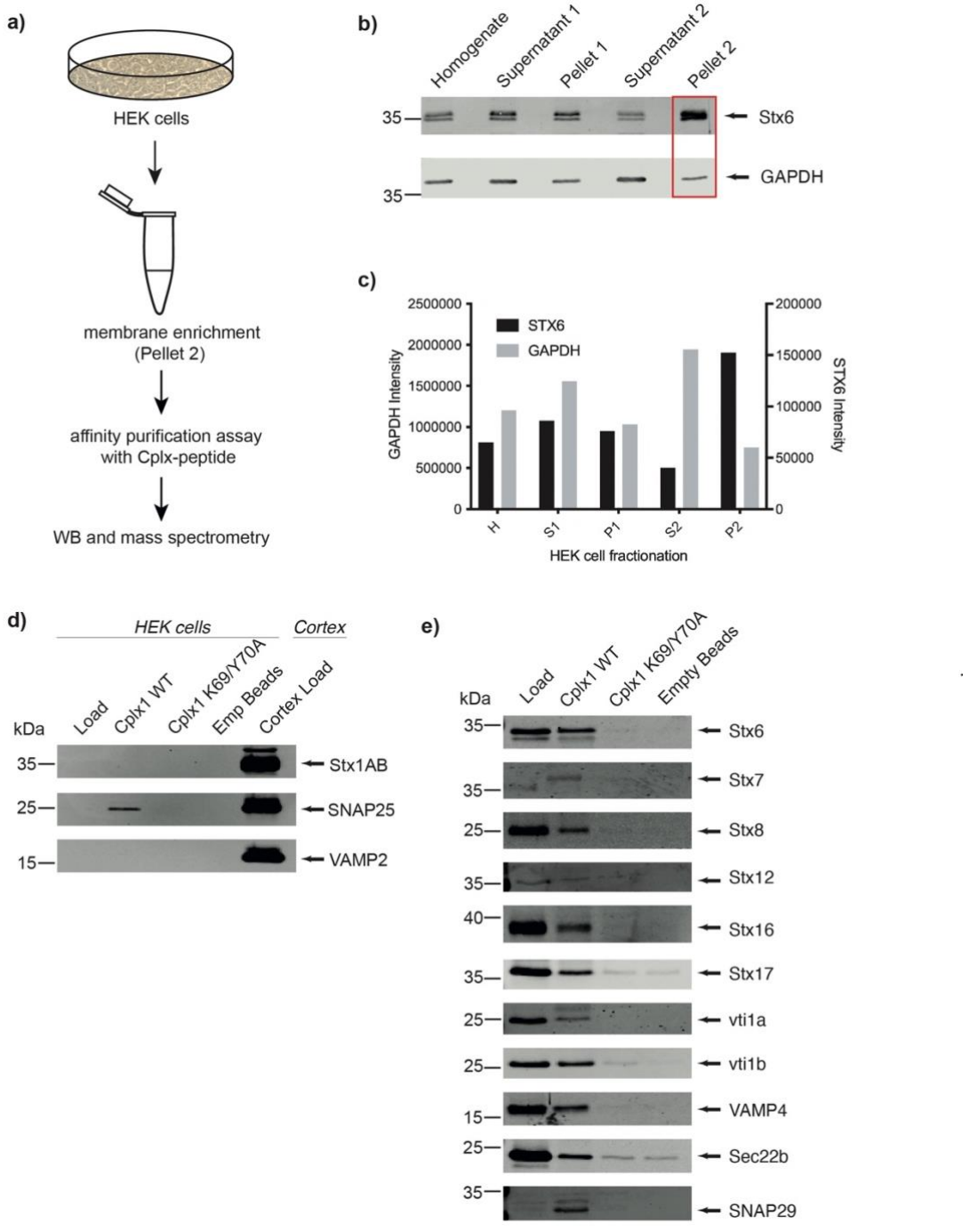

Figure 16: Validation of results in absence of neuronal SNAREs in HEK cells.
(a) Schematic workflow of affinity purification experiment with HEK cells. **(b)** WB of protein fractions regarding Syntaxin 6 as membrane protein and GAPDH as cytosolic protein. **(c)** Quantification of WB shown in (b). **(d)** WB of neuronal SNAREs in HEK cells and cortex load as positive control. **(e)** WB of selected SNARE proteins after affinity purification experiment with HEK cells as input material and Cplx1 WT and mutant as peptides.

To work with input material comparable to the cortex samples, HEK cell proteins were fractionated following a protocol similar to the preparation of crude synaptosomal fractions from cortex (see chapter 2.4.3). To verify the adapted protocol, the obtained fractions were tested by WB using Stx6 for monitoring the distribution of membrane proteins as well as GAPDH as a marker for soluble proteins (Figure 16b and c). The WB analysis and the subsequent quantification of the data showed an enrichment of Stx6 and a decrease of GAPDH in the Pellet2 fraction which is comparable to the enrichment of synaptosomes if cortex is used as input material. Following the affinity purification experiment using the Cplx1 peptides, the lack of neuronal SNAREs was verified by WB (Figure 16d). A cortex Load was added to the WB as positive control. Stx1 and Synaptobrevin 2 were not detected and SNAP25 just in small amounts. In contrast to the neuronal SNAREs, a variety of non-neuronal SNAREs (Stx6, Stx7, Stx8, Stx12, Stx16, Stx17, vti1a, vti1b, VAMP4 and Sec22b, SNAP29) which were previously identified to be part of the Cplx1 interaction network in cortex could be detected in the Cplx1 WT sample (Figure 16e).

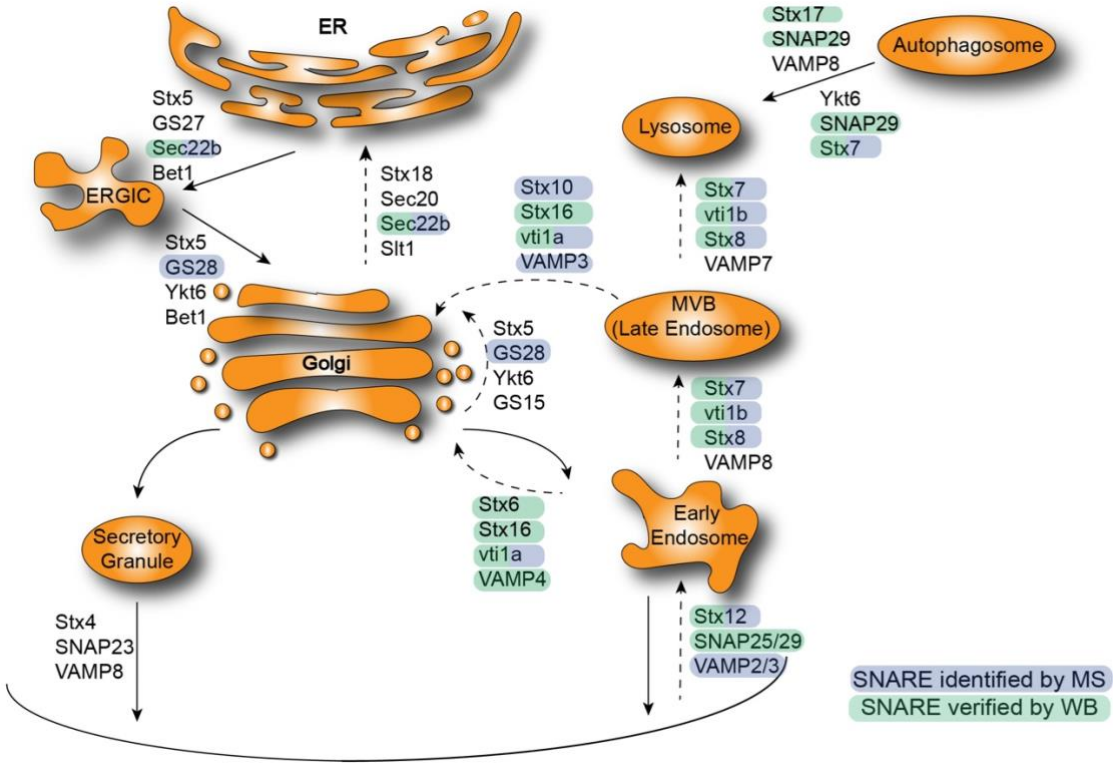

Figure 17: Schematic overview of membrane fusion processes mediated by SNARE complexes in HEK cells.
Proteins identified by mass spectrometry were marked in blue and proteins verified by WB were marked in green. Abbreviations: ER: endoplasmic reticulum; ERGIC: ER-Golgi intermediate compartment; MVB: multivesicular bodies.

Complete SNARE complexes could be mapped here as well, especially complexes of the endosomal pathway (Figure 17). In contrast to the previous findings the lysosomal complexes were less well covered. This favors the hypothesis that Cplx is involved in endosomal processes. Therefore, in the next step a functional effect of Cplx in endosomal processes was studied.

3.2.5.2 Functional validation by transferrin uptake assays

So far, the results of the peptide-based affinity enrichment approaches indicate, that Cplxs are involved in SNARE related processes beside synaptic vesicle exocytosis, probably the endosomal pathway. In order to cover this on a more physiological level, a transferrin uptake assay was conducted. In brief, at the cell surface iron binds to transferrin, followed by the binding of iron-loaded transferrin to the transferrin receptor. Transferrin internalization occurs through clathrin-mediated endocytosis. Then transferrin is trafficked via the endosomal pathway to early endosomes, where it delivers the iron. Finally, transferrin is trafficked back to its initial position at the cell surface via the recycling pathway (Figure 18). The use of fluorescently labeled transferrin allows to follow the internalized ligand on its trafficking pathway and to monitor its sorting into different populations of endosomes under the microscope.

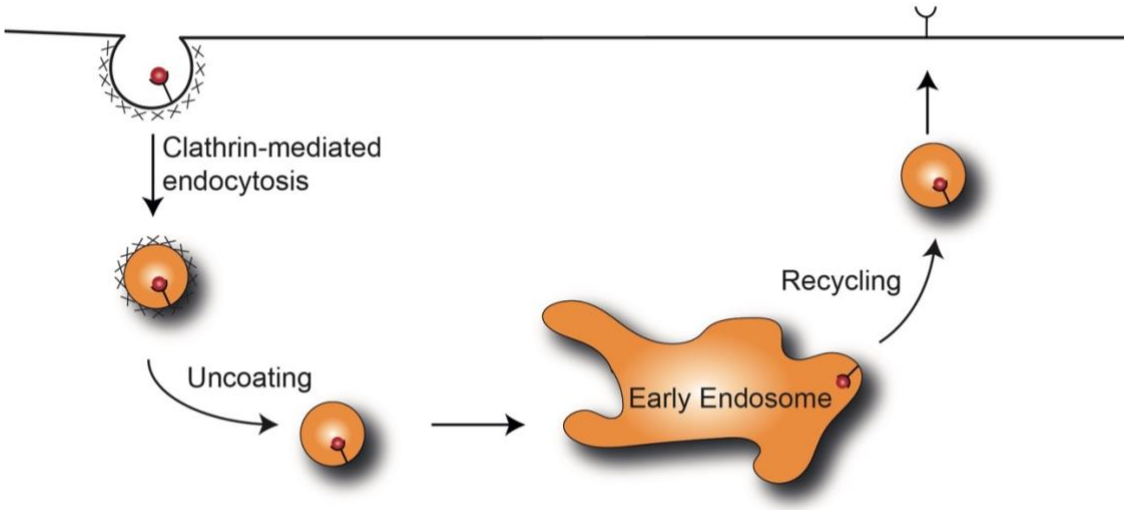

Figure 18: Transferrin uptake assay
At the cell surface iron-loaded transferrin binds to the transferrin receptor and is internalized through clathrin-mediated endocytosis. Then transferrin is trafficked via the endosomal pathway to early endosomes, where it delivers the iron. Finally, transferrin is trafficked back to the cell surface via the recycling pathway.

HeLa cells were chosen as the cell culture system because the smaller nucleus makes subsequent microscopic analysis easier compared to HEK cells. Since HeLa cells lack endogenous Cplx (Appendix Figure 34), it was necessary to choose a Cplx isoform for

transfection. Listed proteins from screens for Cplx1, Cplx2, and Cplx3 show just little differences in relative amounts (Figure 13). Because the validation experiment with HEK cells was performed with the Cplx1 peptide and in view of the high homology between murine Cplx1 and Cplx2 (see chapter 1.3.2), the further selection process was restricted to Cplx1 and 2. The decision to express Cplx2 rather than Cplx1 was made after protein expression analysis in different mouse organs (Appendix, Figure 35). Cplx1 is the main isoform in the brain, but the more widely expressed isoform is Cplx2. It was detected in kidney, spleen, colon and brain, whereas the isoform Cplx 1 was just detected in the brain and in smaller amount in the colon. As negative control samples of a Cplx2-KO mouse were run in addition and Tubulin was used as loading control (Figure 19).

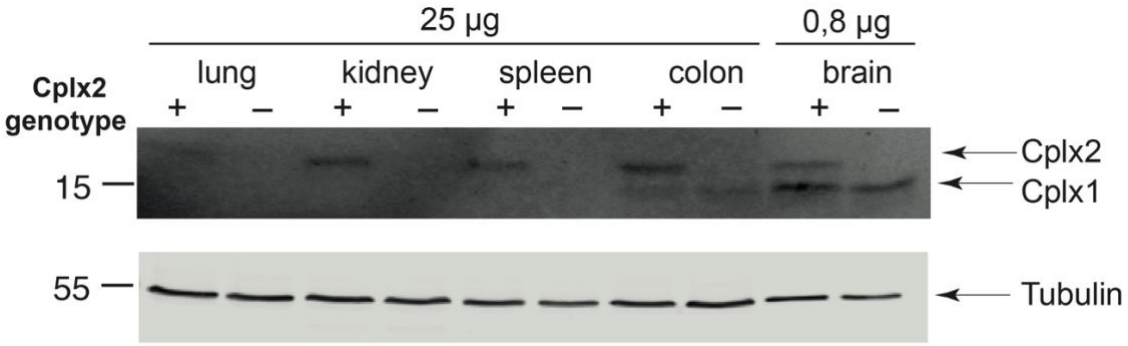

Figure 19: WB of Cplx1, Cplx2 and Tubulin with organ samples of a Cplx2 WT and KO mouse. Lung, kidney, spleen, colon and brain of a Cplx2 WT and KO mouse pair were homogenized, protein concentrations were measured and 25 µg of the sample or 0.8 µg of the brain sample were loaded for SDS-PAGE. The protein expression of Cplx1 and Cplx2 was checked by immunoblotting. Kidney, spleen, colon and brain of the WT mouse show Cplx2, whereas no signal could be detected in the negative control samples of the Cplx2 KO mouse. The Tubulin amount was checked as loading control.

For transfection a plasmid was used expressing Cplx2_WT-IRES-EGFP under the control of the CMV promoter. The configuration of this construct allows the consecutive synthesis of Cplx2 and EGFP providing the possibility to identify Cplx2 overexpressing cells by green fluorescence of EGFP. To control the expression of Cplx2 in EGFP positive cells, the latter were fixed and stained with Cplx1/2 antibody and DAPI (Figure 20). A successful co-staining of EGPF and Cplx1/2 could be confirmed as well as a lack of Cplx2 in non-transfected cells. As in the previous experiments, the SNARE binding-deficient Cplx2 K69A/Y70A mutant (Cplx2_M-IRES_EGFP) was used as a control. To exclude a general influence of the transfection process, cells were also transfected only with an empty EGFP vector, serving as a negative control.

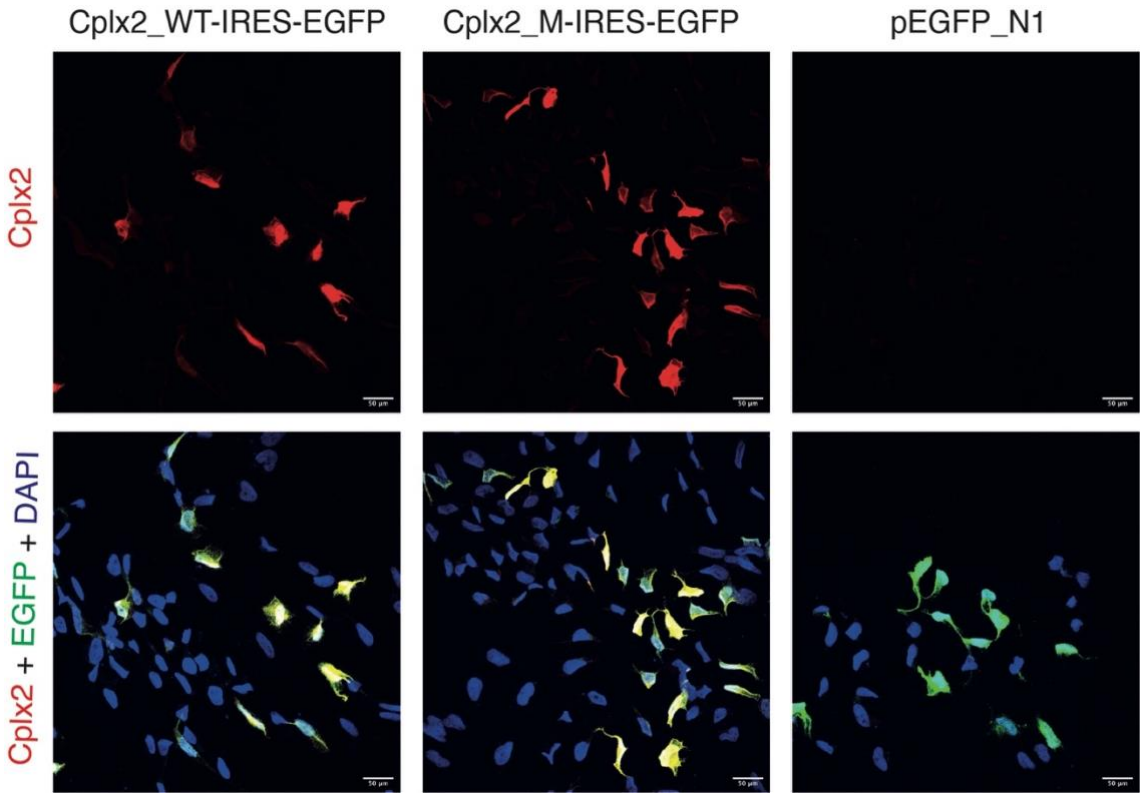

Figure 20: Cplx staining of transfected HeLa cells
Representative images of HeLa cells after 16 h transfection with Cplx2_WT-IRES-EGFP, Cplx2_M-IRES-EGFP or pEGFP-N1 cDNA, fluorescently labeled with antibody against Cplx2. The nuclei are stained with DAPI. Scale bar = 50 µm.

The transferrin uptake assay was conducted in triplicate from three independent transfections. After reaching a cell confluence of 60% on coated coverslips, the parallel sets of cells were transfected with the plasmids described before (Figure 21a). 16 h later, the cells were starved for 1 h to synchronize the cells and the transferrin, which is coupled to AlexaFluor 568, was added at 37 °C to the cells for 0 to 8 min. The coverslips were cooled directly on ice after the respective incubation to stop the uptake and transferrin which was bound to the membrane surface was removed by an acidic wash. After fixation and staining the nuclei with DAPI, the cells were imaged under a fluorescent microscope (Figure 21b). With the IMARIS software a 3D surface was created for each EGFP-positive cell and within these the mean signal intensity and summed signal intensity of Tranferrin-Alexa568 was calculated. After pooling the data obtained from all three experiments (at least 92 cells for each condition), the results were statistically analyzed by calculating the mean, SEM and significance between Cplx2-WT and mutant.

Up to 6 min transferrin uptake, the summed intensity of fluorescent transferrin in a cell is comparable between cells expressing Cplx2 WT (WT; blue), Cplx2 mutant (M; red) and the negative control (C; green). Strikingly, after 7min and 8min of uptake, cells expressing Cplx2

WT differ significantly in comparison to cells expressing the Cplx2 mutant or the negative control (Figure 21 d). With Cplx2 WT the summed transferrin intensity is higher, whereas the size of the cells remained constant (Figure 21c).

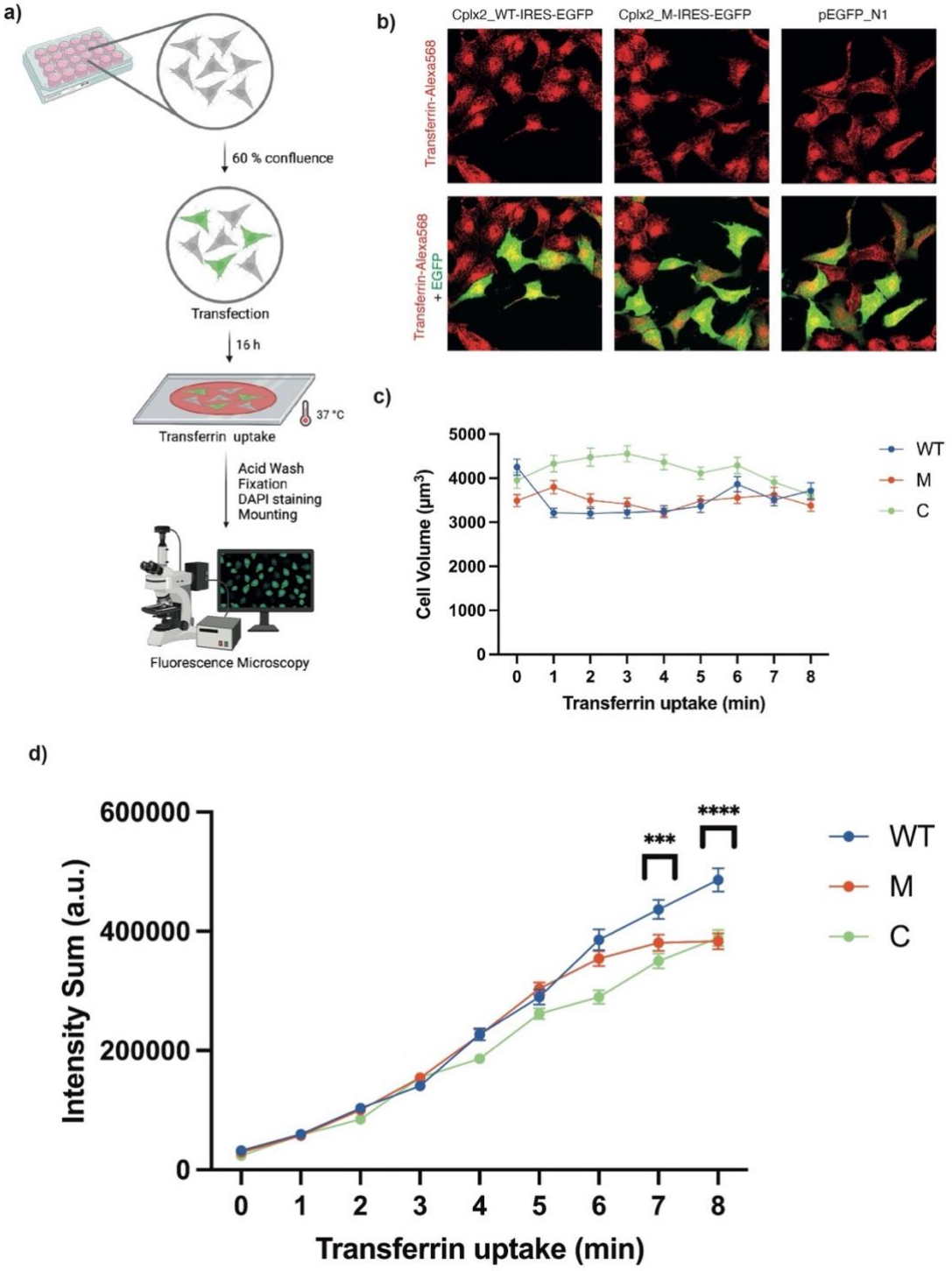

Figure 21: Transferrin uptake of HeLa cells expressing Cplx2_WT, Cplx2_M and EGFP, respectively. **(a)** Schematic workflow of transfection and transferrin uptake, created with BioRender.com. **(b)** Representative images of HeLa cells after 16 h transfection with Cplx2_WT-IRES-EGFP, Cplx2_M-IRES-EGFP or pEGFP-N1 cDNA and after 8 min of transferrin uptake. **(c)** Cell volume (µm³) after creation of 3D-surface of EGFP positive cells **(d)** Time course of summed fluorescence intensity (mean +/- SEM) upon uptake of Transferrin-AlexaFluor568. Legend: WT=Wildtype; M= mutant; C=control; a.u.= arbitrary unit; ***: $p<0.001$; ****: $p<0.0001$.

3.2.6 Extended Cplx interaction networks

So far, a number of SNARE proteins were identified possibly belonging to the Cplx interaction network of Cplx1, Cplx2 and Cplx3. However, regarding these SNAREs no enrichment pattern was observed which tends to be specific for one of the tested Cplx isoforms. Therefore, in a second round of MS data analysis it was tried to identify proteins which represent probably specific interaction partners of only one Cplx isoform. For this purpose, the log2 ratio of one Cplx vs the other isoform was calculated for each protein of the screens. If a protein showed a log2 ratio over 1 in both screens it was defined as an isoform specific protein. With this stringent selection process 597 of the 797 proteins were found to be not isoform specific. Out of the remaining 200 proteins, 33 proteins appeared to be specific for the Cplx1 interactome, 21 proteins for the Cplx2 interactome and 79 proteins for the Cplx3 interactome. Although no proteins were synapse related the Cplx3 specific proteins were pursued by bioinformatic analysis because their number was comparatively high. This analysis revealed an accumulation of proteins partially assigned to the groups "cytoskeleton organization", "regulation of actin cytoskeleton" and "microtubule-based movement" (Figure 22a).

As SNARE binding domain peptides are used for affinity enrichment and as the filter criteria of a specific binding to the WT peptide in comparison to the SNARE binding-deficient mutant were still applied, the found SNARE proteins can be imagined as first shell Fig 22b, green), whereas the extended interaction network can be seen as second shell (Figure 22b, yellow). Therefore, the presumably Cplx3-specific cytoskeleton proteins may be related to the SNARE binding of Cplx3.

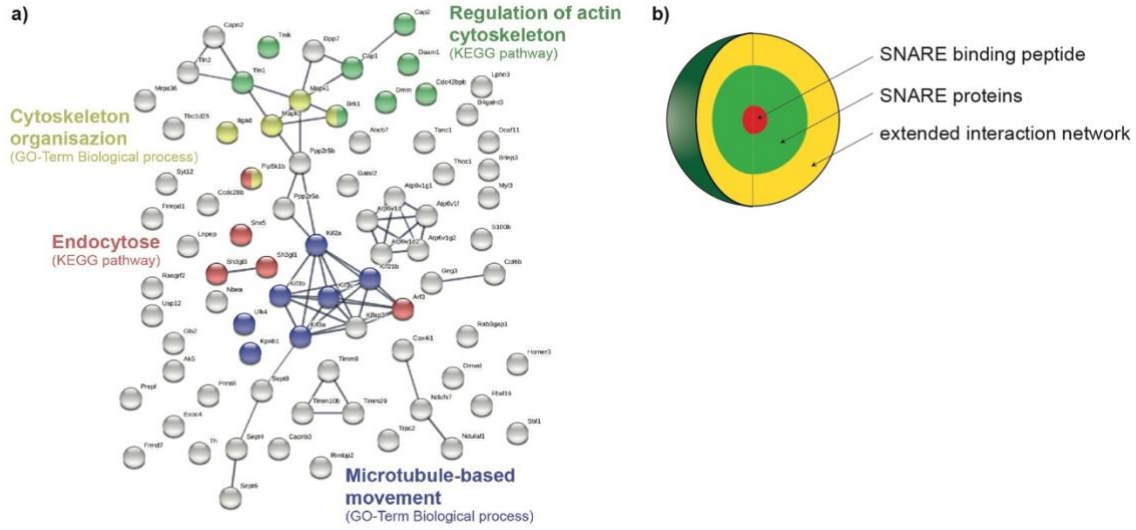

Figure 22: Systematic analysis of the extended Cplx3 interaction network.
(a) STRING analysis of proteins with log2 ratio over 1 for the Cplx3 peptide in both screens. **(b)** Shell model with the SNARE binding peptide as central unit. The SNARE proteins form the first layer and the extended interaction network the second layer.

3.3 Affinity purification experiments with retina homogenate

3.3.1 Generation of interactor lists

So far, experimental results were reported obtained from peptide affinity purification approaches using Cplx1, Cplx2 or Cplx3 peptides and crude synaptosomal fractions as protein source. However, the mammalian Cplx protein family consists of four members which are differentially distributed throughout the nervous system. Whereas Cplx1 and Cplx2 are restricted to conventional synapses and Cplx3 is found in both conventional and ribbon synapses, Cplx4 is expressed exclusively in ribbon synapses (Figure 6). The morphology of the release sites in such synapses is characterized by a specialized plate-like organelle, the synaptic ribbon. This particular structure was discussed to be one of the main factors contributing to the high rate of neurotransmitter release which exceeds that of conventional synapses many times (Sterling and Matthews, 2005). Another factor could be a unique protein equipment which enables this special kind of synapses to respond to light stimuli in an adaptation-dependent manner.

In order to address the question whether Cplx3 and Cplx4 are contributing to the functional characteristics of ribbon synapses by themselves and/or by their corresponding interaction networks, a second set of affinity purification experiments was conducted.

The design of the peptides representing the SNARE binding domains of Cplx1, Cplx3 and Cplx4 (Figure 7) was comparable to the experiments described before. In Cplx4 peptides α-aminobutyric acid (abu) was used as replacement for internal cysteine residues to ensure that peptide coupling only happens via the N-terminal cysteine residue. In contrast to the previous approaches, detergent extracts of whole retina homogenate served as protein source.

Based on our experience, information about interacting proteins were obtained by quantitative MS. Two screens with Cplx3 and two independent screens with Cplx4 were performed. In each of these screens, Cplx1 was used in parallel, which offered the possibility to compare the results of all screens (Table 11). After applying the established filter criteria, the number of proteins which were enriched in WT vs negative control were calculated. Accordingly, 461 proteins were identified for the Cplx3 and 281 for the Cplx4 interactome, respectively (Figure 23).

Table 11: MS based screens with retina as input material.
Screens I and II were performed using the Cplx1 and Cplx3 peptides, whereas for screens III and IV Cplx1 and Cplx4 peptides were used.

Screen	I	II	III	IV
Cplx1	x	x	x	x
Cplx3	x	x		
Cplx4			x	x

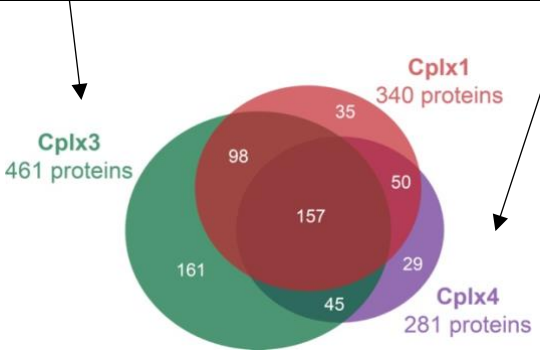

Figure 23: Venn diagram of Cplx1, Cplx3 and Cplx4 peptide interactome.
461 proteins were identified as proteins forming the Cplx3 interactome. They were enriched with the wildtype (WT) peptide in comparison the mutant (M) peptide. 281 proteins were identified as proteins of the Cplx4 interactome. The significance threshold was calculated individually for each screen, based on the total protein count.

3.3.2 Analysis of detected proteins by bioinformatic tools

In order to analyze the enriched proteins in more detail, the GO term algorithm was used again. For both Cplx3 and Cplx4, the same subgroups were identified under *Biological processes*.

The top three categories regarding p-values were protein transport, vesicle-mediated transport and intracellular protein transport (Figure 24). Among the vesicle-mediated transport proteins are for example also the SNARE proteins.

Interestingly, although whole retina homogenate was used as input material in the respective experiments, the ranked categories were similar to the subgroups classified in context with the affinity purification experiments using crude synaptosomal preparations from cortex. This was not expected, because the used cortical fractions are enriched in synaptosomes, whereas retina homogenates contain the whole spectrum of proteins including nuclear components for instance.

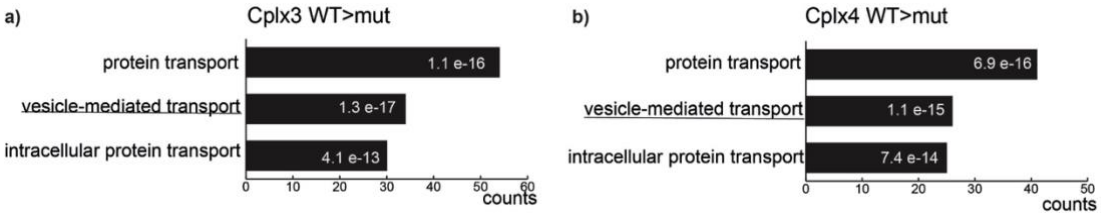

Figure 24: GO-term analysis of Cplx3 and Cplx4-peptide interactome.
(a) The 461 proteins, identified with the Cplx3 peptide after affinity purification experiments and **(b)** the 281 proteins, identified with the Cplx4 peptide, were analyzed with the freely available bioinformatic database DAVID regarding the GO term *Biological processes*. Visualized are the top three listed terms regarding p-values, which are written in the bars. The x-axis shows the number of protein counts for the terms.

3.3.3 Analysis of SNARE proteins

In line with experiments with cortex input material, we first focused on the quantitative analysis of SNAREs (Figure 25). The neuronal SNAREs Stx1AB, SNAP25 and VAMP2 were detected with all three Cplx peptides. Comparable to the previous cortex screens, a slight preference for Cplx1 was observed.

Moreover, the analysis revealed, that a number of SNAREs which were related to the cortex interactomes of Cplx1, Cplx2 and Cplx3 were also identified as members of the retina interactomes of Cplx1, Cplx3 and Cplx4 (e.g. Stx12 or VAMP4). Others, as for instance Sec22b or vti1a/b, were not identified. Interestingly, one protein was exclusively detected within the affinity purification experiments with retina homogenate: Stx3b, which was described to be a ribbon synapse-specific t-SNARE (Curtis et al., 2008). Exocytosis in the ribbon synapse is also thought to be SNARE-mediated, with a SNARE complex of Stx3b, SNAP25, and Synaptobrevin 2.

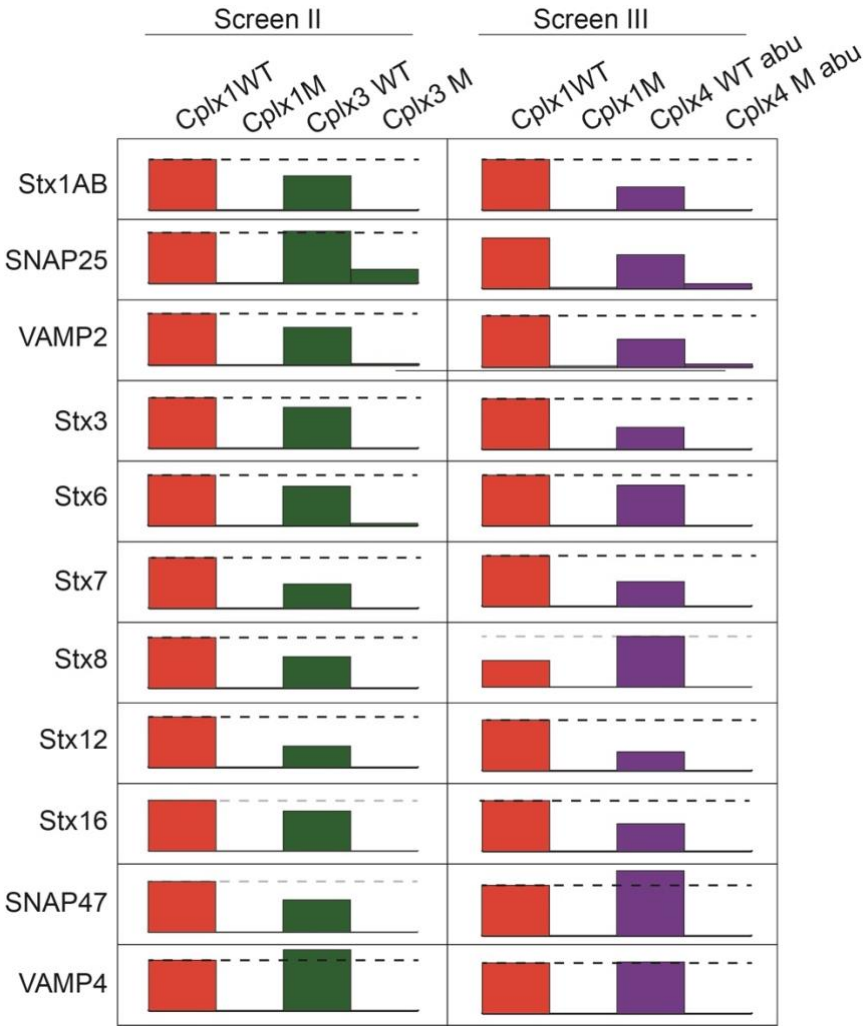

Figure 25: MS-based quantification of SNARE proteins.
Visualization of two out of the four FASP based screen datasets for neuronal and non-neuronal SNARE proteins. Data are shown as relative amounts, whereas Cplx1 wildtype (WT) data were always set as 100 %. The stitched line indicates 100%.

3.3.4 Extended interaction networks

In view of the question whether Cplx3 and Cplx4 are contributing to the functional characteristics of ribbon synapses, the SNARE proteins gave no hints, as their enrichment with Cplx3 and 4 did not differ considerably from that with Cplx1. Therefore, the extended interaction network was studied with the same stringent selection process as applied for the cortex. For each protein the ratio between Cplx1 and Cplx3 for both screens was calculated. If a protein had an enrichment factor of log2 over 1 in both screens for Cplx3, it was indicated as specific for Cplx3 (Figure 26a, green box). So, 245 Cplx3 specific proteins were identified and used for another GO term enriched analysis for biological processes. Because of their high p-values the categories protein transport, protein localization to cilium as well as cilium morphogenesis were ranked to the first three positions (Figure 26b). Because the outer segments of photoreceptors are modified sensory cilia (Khanna, 2015), our dataset of

Cplx3-specific retina network was aligned with a published cilium interactome (Boldt et al., 2016). Interestingly, this alignment revealed an overlap of 74 proteins.

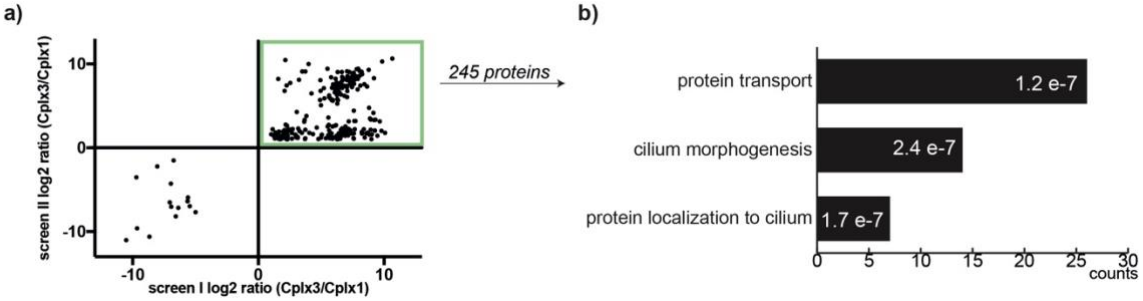

Figure 26: Systematic analysis of the extended Cplx3 interaction network.
(a) Calculation of the log2 ratio Cplx3 vs Cplx1 for each protein for screen I (x-axis) and screen II (y-axis). Green bordered are the 245 Cplx3 specific proteins. **(b)** These 245 proteins were analyzed with the freely available bioinformatic database DAVID regarding the GO term *Biological processes*. Visualized are the top three listed terms regarding p-values, which are given in the bars. The x-axis shows the amount of protein counts for the terms.

3.3.4.1 RIBEYE as part of the Cplx3 and Cplx4 interactome

Beside the interesting link to the dataset of cilium proteins the list of Cplx3 and Cplx4 interacting network contained another surprising candidate: the ribbon synapse-specific protein RIBEYE (Figure 27a and b). It was described as the main component forming the ribbon structure (Schmitz et al., 2000). RIBEYE is composed of two domains, the A domain without homology to other proteins, and the B domain, whose amino acid sequence is identical to that of the transcription factor CtBP2 (Figure 27c). By a subsequent WB it could be demonstrated that RIBEYE is exclusively contained in the Cplx3 and Cplx4 WT samples (Figure 27d and e) which confirmed the MS results. Note that only specific RIBEYE signals were observed which are represented on the WB by the 120 kDa band, but no specific signals for CtBP2 could be detected.

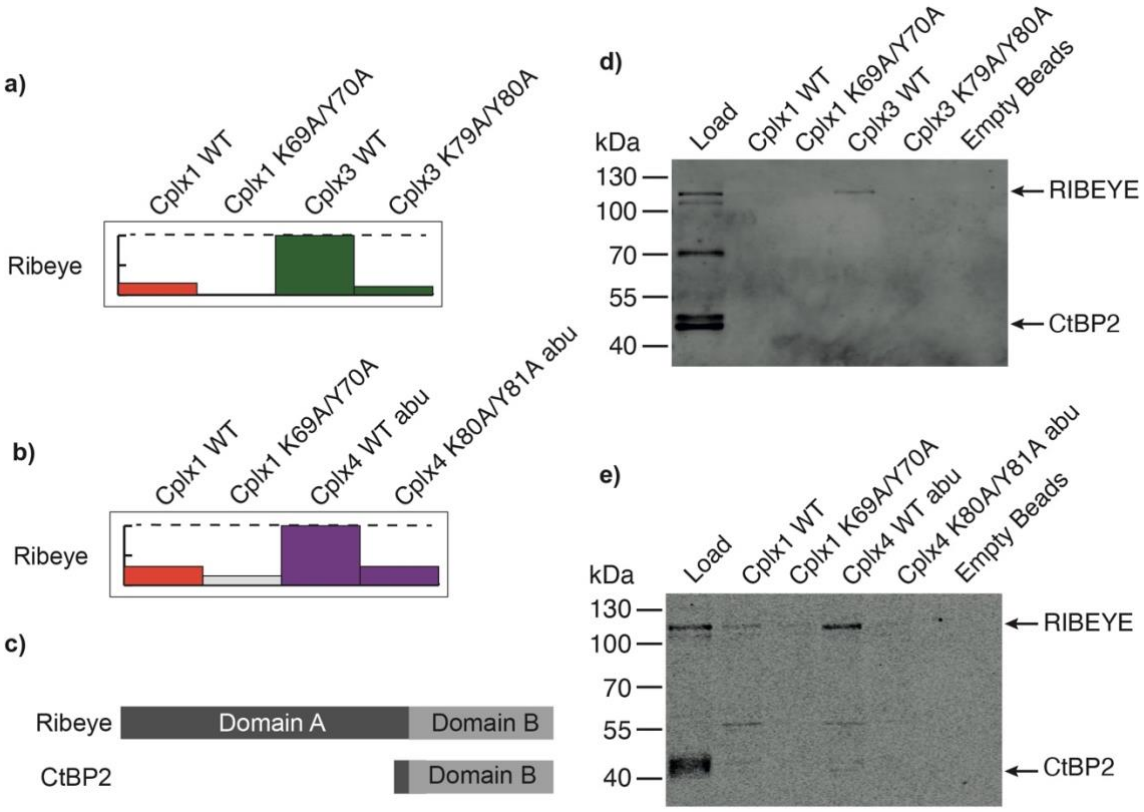

Figure 27: RIBEYE as interacting protein in the affinity purification experiment with Cplx3 peptide. **(a)** MS-based relative quantification of the protein RIBEYE in screen II with Cplx1 and Cplx3 and **(b)** in screen III with Cplx1 and Cplx4. The stitched line indicates 100%. **(c)** Schematic domain structure of RIBEYE and CtBP2. **(d**) Immunoblot with CtBP2/RIBEYE antibody after affinity purification experiment with Cplx1 and Cplx3 peptides and **(e)** with Cplx1 and Cplx4.

To validate the interaction between Cplx3 or Cplx4 and RIBEYE, a reverse affinity purification experiment was conducted using the monomeric ribbon-binding peptide (RBP), which was described to have a high binding affinity (K_D of 27 μM) to RIBEYE (Figure 28a). As control a peptide with randomly scrambled amino acid sequence was used (Zenisek et al., 2004). For the subsequent experiments retina homogenate was used as input material comparable to the experiments done with the Cplx peptides. While RIBEYE was successfully enriched with the RBP, neither Cplx3 nor Cplx4 could be identified via MS or WB (Figure 28b). Bassoon as known RIBEYE interactor (tom Dieck et al., 2005) was also not detected.

An insufficient affinity of the monomeric RBP could be a conceivable cause for the failed detection of RIBEYE interactors. Therefore, a tandem RBP dimer was used in the following experiment. This dimer was described to have a higher binding affinity (K_D = 1.5 μM) because two peptides were coupled with a PEG spacer along to each other (Figure 28a) (Francis et al., 2011). Another conceivable cause would be the high complexity of the input

material. As shown in figure 36 in the appendix the second most enriched protein groups regarding *cellular component* terms were nuclear proteins (47 out of 71 proteins). Therefore, the mouse retina homogenate was fractionated and the content of Cplx3, Cplx4, RIBEYE, CtBP2 and the nuclear protein Histone H3 were examined by WB (Figure 28c). In the S1 fraction was the nuclear protein Histone H3 removed and the amount of the Cplx isoforms and RIBEYE was still high. Hence, this fraction was used for another affinity purification experiment, along with the tandem RBP dimer.

RIBEYE could be enriched again with the dimer peptide and not with the corresponding control (Figure 28d). Nevertheless, Cplx3 and Cplx4 could not be detected by WB.

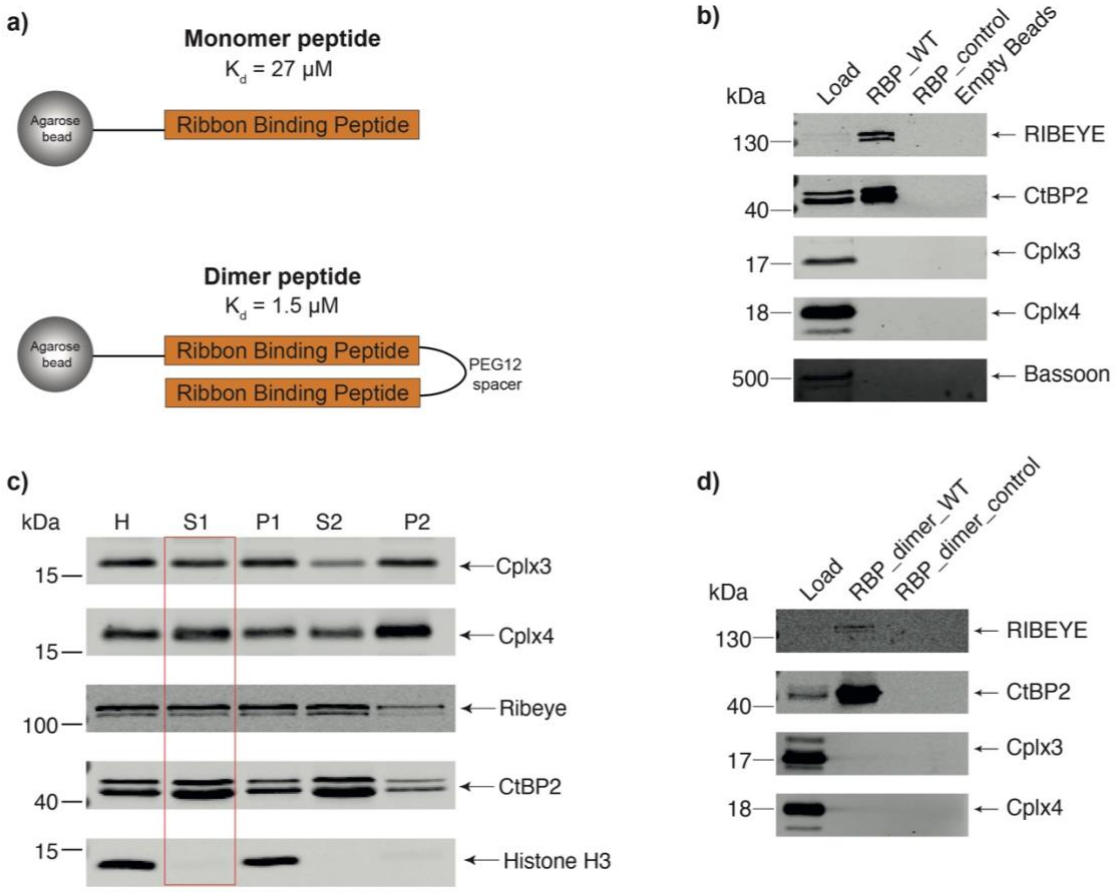

Figure 28: Reverse affinity purification experiment with ribbon binding peptide.
(a) Schematic illustration of the monomer ribbon binding peptide (RBP) with a K_d of 27 µM and the tandem RBP dimer, in which the monomers are connected by a PEG spacer. The dimer peptide has a K_d of 1,5 µM. **(b)** Immunoblot after affinity purification with the monomer RBP and retina homogenate. RIBEYE and CtBP2 were detected with the WT peptide, but not with the control peptide or empty beads. Cplx3, Cplx4 or Bassoon were just detected in the load but not in any peptide sample. **(c)** Immunoblot of different fractions of the retina regarding Cplx3, Cplx4, RIBEYE, CtBP2 and Histone H3. Abbreviations: H: homogenate, S1: supernatant 1, P1: pellet 1, S2: supernatant 2 and P2: pellet 2. **(d)** Immunoblot after affinity purification with the dimer RBP and retina supernatant 1 fraction. RIBEYE and CtBP2 were detected with the WT peptide and not with the mutant peptide or empty beads. Cplx3 and Cplx4 were just detected in the load but not with any peptide.

3.3.4.2 Transducin as part of the Cplx3 and Cplx4 interactome

The advantage of an unbiased MS screen is that it can also be used as a data basis for new questions. Thus, the screens were investigated with respect to the G-protein transducin, as collaboration partners had identified a link between Cplx3 and Cplx4 and different subunits of transducin (Lux et al., Abstract, NWG Conference Göttingen 2019). Therefore, the MS data regarding the transducin subunits were visualized (Figure 29a) and for the rod specific protein Gnat1 a WB was conducted with affinity-purified samples for validation (Figure 29b). The transducin γ-subunits Gngt1 (rods) and Gngt2 (cones) are not displayed as they were identified by MS only sporadically, likely because of their small size of <9 kDa.

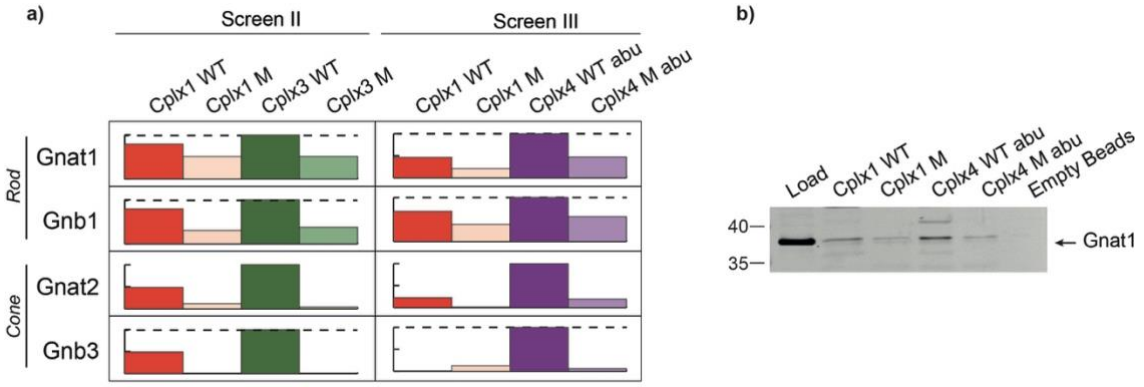

Figure 29: Transducin as interacting protein in the affinity purification experiment with Cplx3 and Cplx4 peptides
(a) MS-based relative quantification of the transducin subunits Gnat1 and Gnb1 of Rod photoreceptor cells and Gnat2 and Gnb3 of cone photoreceptor cells in screen II and III. The stitched line indicates 100%. **(b)** Immunoblot with Gnat1 antibody after affinity purification experiment with Cplx1 and Cplx4 peptides.

4 Discussion

4.1 Cplx peptide-based affinity purification as a robust screening method for the identification of SNARE complexes and their interaction partners

To study in an unbiased and systematic way whether Cplxs act upon different SNARE complex types and if these SNARE complexes are Cplx isoform-dependent, an Cplx peptide-based affinity purification approach was expanded to all four Cplx isoforms and applied to different input material, i.e. cortical and retinal protein fractions. As basic for such an unbiased screening method it is important to ensure that specificity and robustness of the data are given. Therefore, the data were analyzed and validated from different angles. First, for each Cplx isoform a double dataset exists (cortex: Screen I and II for Cplx1, Screen I and III for Cplx2 and Screen II and III for Cplx3; retina: Screen I and II for Cplx3, Screen III and IV for Cplx4 and Screen I-IV for Cplx1) (Table 10 and 11). Second, the findings from the initial cortex screens were validated by gel electrophoresis, either read out by MS as a complementary unbiased approach, or – in the case of expected targets like the neuronal SNARE proteins – by WB (Figure 11 and 8d). Third, the fact that the neuronal SNAREs were found in higher amount with the Cplx1 peptide as with the other isoforms, with quantitative MS (Figure 11) and WB (Figure 8d), reflects the binding data (K. Reim, O. Jahn, JS. Rhee unpublished observation) showing that the Cplx1 peptide has the highest affinity to the neuronal SNARE complex.

After generating the datasets, they were analyzed with bioinformatic tools. With both, the cortex P2 fraction and the retinal homogenate, proteins involved in the vesicle-mediated transport were enriched (Figure 12a and 24). As the SNARE complexes are part of these vesicle-mediated transport processes and they are in focus with the used SNARE binding peptide the results of the GO-term analysis were considered as confirmation of the principle of the approach. The 1:1:1 stoichiometry of the neuronal SNARE complex is reflected in the quantification of the results just partly (Figure 14) but could be explained with the involvement of the single proteins in other SNARE complexes in the mammalian cell. For example, SNAP25 and VAMP2 play an additional role in the fusion of early and recycling endosomes. All in all, the assay worked successfully and robustly delivered valid datasets.

4.2 Cplx binds to non-neuronal SNARE proteins

So far, the best studied mammalian Cplx isoform is Cplx1. It binds with high affinity to the assembled neuronal SNARE complex and thereby regulates synaptic vesicle exocytosis in conventional synapses. Interestingly, the four known mammalian Cplx isoforms are characterized by a high homology in the central α helix which mediates SNARE complex binding. On the other hand, neuronal SNARE complexes consisting of Stx1AB, SNAP25 and Synaptobrevin 2 are formed via SNARE motifs, that are conserved among the SNARE proteins. This leads to the question whether Cplx1 can act upon different SNARE proteins.

To address this question, the known interaction of Cplx1 to the assembled complex of Stx1AB, SNAP25 and VAMP2 was used as internal control. As negative control the SNARE-binding deficient mutant Cplx1 K69A/Y70A, was run always in parallel with the respective WT peptides. Since the other Cplx isoforms Cplx2, Cplx3 and Cplx4 were also studied, their mutant peptides Cplx2 K69A/Y70A, Cplx3 K79A/Y80A and Cplx4 K80A/Y81A abu were also running simultaneously with the corresponding WT peptides.

Indeed, among the proteins identified by MS analysis were some non-neuronal SNARE proteins binding to the SNARE-binding domain of Cplx1, supporting the assumption about an interaction of Cplx1 and non-neuronal SNARE complexes (Figure 13). The amount of bound non-neuronal SNARE proteins was less in comparison to the neuronal SNARE proteins (Figure 14), which was expectable, because of the high endogenous levels of neuronal SNAREs in neuronal tissue and the already described high affinity of Cplx1 to this complex. Nevertheless, Stx6, SNAP47, Stx7, Ykt6 and Stx12 were quantified with 10% - 30 % in comparison to the most abundant SNARE protein SNAP25 (Figure 14). These proteins were absent in the negative control with the SNARE binding deficient mutant so unspecific binding could be excluded and the most abundant SNARE proteins of the Cplx1 screen were confirmed exemplarily by WB. The question whether other SNARE proteins also bind to Cplx1 could be answered positively. Consequently, the question arises whether specific SNARE complexes can be assigned to a Cplx isoform. This issue was not resolvable with the present assay. All SNARE proteins seem to prefer Cplx1 (Figure 13). The reason for this could be that the SNARE proteins in the lysate are present in a mixed form and not locally separated like *in vivo*.

To exclude the possibility that non-neuronal SNAREs were identified because they were interacting with the neuronal SNAREs and therefore specific for the WT peptides and Cplx1, an affinity purification experiment with HEK cells was conducted. HEK cells, derived from embryonic kidney, do not contain the neuronal SNARE complex (Appendix Figure 34). Just SNAP25 could be detected (Figure 16d), as only protein of the complex, because it is also involved in other SNARE mediated processes, like in the endosome recycling pathway (Aikawa et al., 2006). As input material the P2 fraction was used, to treat the material in the same way as the cortex material. As side effect the nucleus fraction could be removed, which is in HEK cells disproportionally large because of a big nucleus. Same as with the cortex and retina input material, the HEK cell experiment showed a specific binding of non-neuronal SNARE proteins to the Cplx peptide (Figure 16e). It must be noted that HEK cells lack endogenous Cplx (Appendix Figure 33). On the one hand this experiment is not reflecting a biological system but on the other hand the peptides do not need to compete with the endogenous Cplx protein isoforms. All in all, a co-sedimentation effect with the neuronal SNARE proteins and therefore false-positive results of the non-neuronal SNARE proteins can be excluded.

Another theoretical explanation for the finding of non-neuronal SNAREs could be the exchange of single proteins of the neuronal SNARE complex because the SNARE proteins are so similar in their SNARE motif and the use of a crude lysate could bring proteins in proximity, which usually cannot interact because of their local distribution. For example, it was shown for Cplx1 and Cplx2 that the exchange of SNAP25 to SNAP29 would be tolerated. In contrast, the exchange from VAMP2 to VAMP8 is not tolerated by Cplx1 and Cplx2 (Pabst et al., 2000), but VAMP8 was nonetheless detected with Cplx1 by WB (Appendix Figure 33). Therefore, an exchange of single SNARE proteins could be excluded at least as general explanation for the binding of Cplx to non-neuronal SNAREs.

An additional argument for binding of Cplx to non-neuronal SNARE proteins was shown by assignment of the found SNARE proteins to their involved membrane fusion process. Therefore, it is striking that for same processes all proteins necessary for this complex could be identified and not just randomly single SNARE proteins. As Cplx binds to fully assembled SNARE complexes and not to single proteins it is an additional hint that this interaction of Cplx and non-neuronal SNARE proteins is relevant and not a false-positive result of a crude affinity experiment.

Moreover, the analysis revealed, that a number of SNAREs which were related to the cortex interactomes of Cplx1, Cplx2 and Cplx3 were also identified as members of the retina interactomes of Cplx1, Cplx3 and Cplx4 (e.g. Stx12 or VAMP4). Others, as for instance Sec22b or vti1a/b, were not identified. A possible explanation for the differences would be the different fractions of the input material. While in the cortex P2 material crude synaptosomes were enriched with membrane proteins, in the retina homogenate not such a high enrichment of SNARE proteins was achieved. These differences in the input material may be reflected in the depth of the interaction list. Another explanation is a different functioning of Cplx3 and Cplx4 in the different synaptic systems of conventional synapses in the cortex and the ribbon synapses in the retina. In summary, it could be said that Cplx can bind to SNARE proteins beside the synaptic exocytosis.

4.3 Is Cplx involved in endosomal pathways?

As already mentioned, the assignment of the found SNARE proteins to their involved membrane fusion process revealed that full complexes were found (Figure 15). Striking was the identification of mainly complexes of the endosomal pathway. The endocytic pathway is essential for the cell to communicate with its environment, control cell growth and regulate nutritional uptake. About 70-80% of the endocytosed material is recycled back to the plasma membrane, while the remainder will either be transported to the TGN or fuses with the lysosome resulting in the degradation. Defects in the recycling pathway led to serious diseases like cancer, Bardet-Biedel-syndrome or Alzheimer's disease (Solinger et al., 2020).

To examine a functional effect of Cplx in endosomal pathways, HeLa cells expressing EGFP and Cplx2 (WT and mutant) were studied regarding transferrin uptake. The transfected (EGFP-stained) cells were incubated for 0 to 8 min with Alexa 568–labeled transferrin and assessed for concentration of fluorescent transferrin. After 7 and 8 minutes of transferrin uptake a significantly different summed intensity of transferrin was observed between cells expressing Cplx2 WT or the SNARE binding deficient mutant (Figure 21). As the summed intensity is dependent on the volume of the cell, this parameter was also analyzed and no significant differences were observed between WT and mutant cells (Figure 21e). Therefore, the increased transferrin amount is most possibly a consequence of the expressed Cplx2 in the cell, which may be involved in membrane fusion events. The pathways which could be followed by transferrin are the uptake and recycling pathways of the cell. As the effect is

visible quite late, after 7 and 8 min of uptake, an involvement in the endocytosis is unlikely, whereas an effect on the recycling is possible.

This recycling can occur via two ways, i.e. fast and the slow recycling. The fast recycling route guides transferrin-loaded vesicles directly back to the cell surface where they fuse with the plasma membrane, whereas in the slow recycling route vesicles fuse first with the recycling endosome which afterwards fuse with the plasma membrane. All these fusion steps are regulated by SNARE proteins, the localization of which is in part not yet completely assignable. Several proteins have been suggested to play a role in endocytic recycling fusion events. These include Stx12 (Prekeris et al., 1998; McBride et al., 1999; Trischler et al., 1999; Lee et al., 2001; Hoogenraad et al., 2010), Stx6 (Brandhorst et al., 2006; Watson et al., 2008; Tiwari et al., 2011; Riggs et al., 2012), Stx16 (Proctor et al., 2006; Gee et al., 2010), vti1a (Kreykenbohm et al., 2002; Bose et al., 2005), VAMP3 (McMahon et al., 1993; Galli et al., 1994; Daro et al., 1996; Riggs et al., 2012) and VAMP4 (Mallard et al., 2002; Brandhorst et al., 2006). The exact composition of the SNARE complex remains to be determined. All of these SNARE proteins were identified with the Cplx affinity purification approach with cortex (Figure 13 and 15), HEK cells (Figure17) and partly with retina (Figure 25) as input material. Thus, an effect of Cplx on membrane fusion processes during endosomal recycling is possible.

Even if the exact SNARE composition of this recycling pathway is unknown, some tethering proteins were already identified. Rab4 was described in association with fast recycling endocytic vesicles and Rab11 with slow recycling endocytic vesicles (Wandinger-Ness and Zerial, 2014). Additionally involved in slow recycling is the so called FERARI complex that consists of VPS45, Rabenosyn5 and Rab11FIP5. Another multisubunit complex was detected with the Rab4-dependent fast recycling pathway. The so called EARP complex is composed of VPS51, VPS52, VPS53 and VPS50 and interacts with Stx6. Depletion of VPS50 showed an increased transferrin concentration in late phases, but not earlier phases of transferrin uptake. Pulse chase experiments confirm delayed recycling of internalized transferrin for VPS50 and also Stx6 KD cells (Schindler et al., 2015). As the results of Schindler et al. and the present results with the Cplx2 expressing cells regarding transferrin internalization were comparable, it is possible that Cplx plays a role in the balance between fast and slow recycling process. As a possible model it is conceivable, that Cplx change with an inhibitory effect on the fast recycling the balance between fast and slow recycling (Figure 30). This could lead to an accumulation of transferrin after 7 min. A pulse chase experiment would be a future experiment to further test this hypothesis.

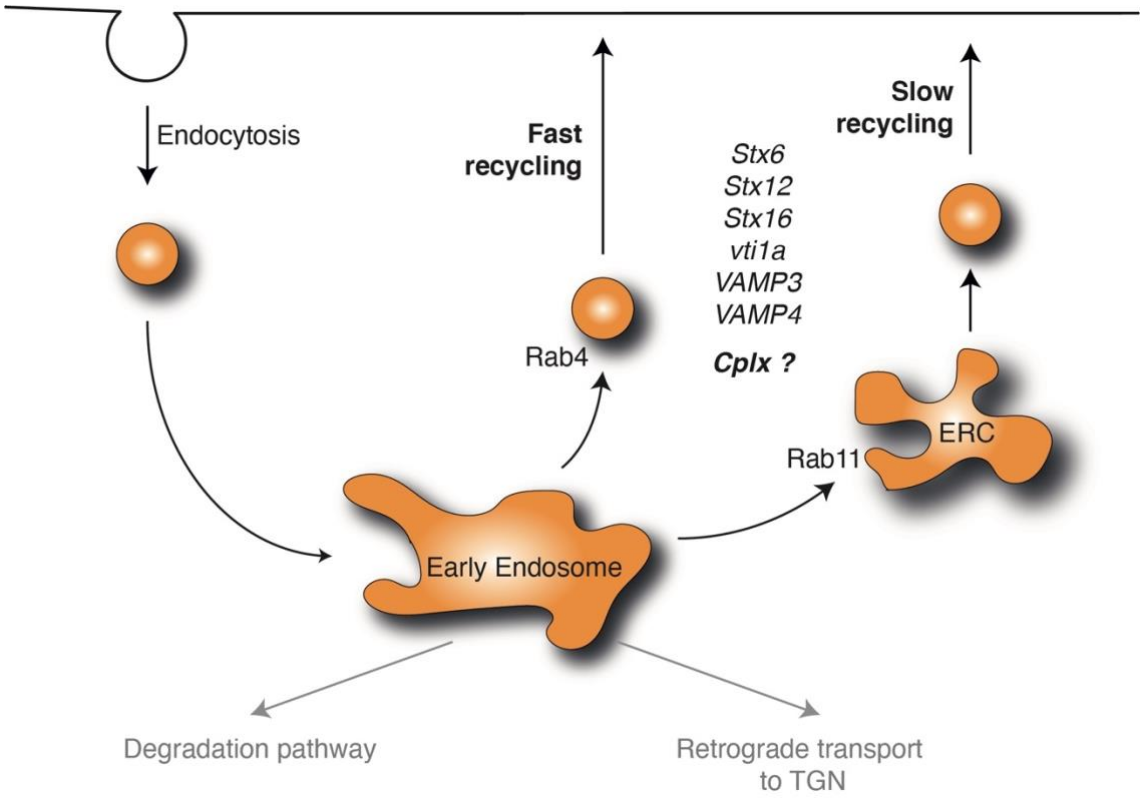

Figure 30: Overview of endocytic pathways with transferrin uptake and recycling pathway
After internalization of the transferrin with its receptor via clathrin-mediated endocytosis, the vesicle will be uncoated and fuse with the early endosome. Here the proteins will be sorted into different pathways. As transferrin will not be degraded via the late endosome and lysosome or transported retrograde to the TGN, the receptor with the transferrin ligand will be recycled to the cell surface. Two pathways are possible, the fast recycling via Rab4 marked vesicles or the slow recycling via Rab11 marked vesicles and the endosomal recycling compartments (ERC). Some SNAREs involved in this recycling pathway are known but so far not fully assigned.

As the advantage of the present approach is the unbiased comprehensive dataset of interacting proteins, interesting candidates of the extended interaction network could be searched. Whereas the Rab4 and Rab11 proteins were not detected, same as most of the Rab proteins, Rabenosyn5 and Rab11FIP5, different VPS proteins were found (Appendix Figure 37). The VPS of the EARP complex, VPS50, VPS51, VPS52 and VPS53 have a similar binding pattern. They were found mainly with the WT peptides and not with the mutants and they were found in larger amounts with Cplx3 than Cplx1 or Cplx2. For VPS45, part of the FERARI complex, the binding pattern was comparable with the binding pattern of the SNARE proteins, no binding to the SNARE binding deficient mutants and preference to Cplx1. The identification of these proteins with the Cplx affinity purification approach is a hint to an involvement of Cplx in these recycling processes. As none of the SNARE proteins showed a Cplx3 preference like VPS50, VPS51, VPS52 and VPS53, a direct connection to specific SNARE proteins cannot be drawn.

The possible involvement of Cplx in the endosomal recycling pathway did not exclude the possibility that Cplx could also be involved in the endo-lysosomal degradation pathway or in the retrograde transport to the TGN. The SNARE complexes involved in these fusion steps were also identified as interaction partner of the Cplx peptide (Fig. 15). To study the endo-lysosomal pathway for degradation, other dedicated uptake assays (LDL, EGF) would be interesting to perform.

As HeLa cells lack endogenous Cplx, these functional experiments were conducted in an artificial *in cellulo* system. Therefore, after identifying a possible Cplx influence on recycling endosomal processes, the next step would be a change in the studied system to neurons. They contain endogenous Cplx and Cplx KO mice are available as negative control. Here, the named processes can then be specifically studied for functional changes and colocalizations.

In the context of neurons, another indication of the involvement of Cplx in key membrane fusion events came from López-Murcia et al. (López-Murcia et al., 2019). They had observed that Cplx can influence neuronal health. Cplx1flox/flox Cplx2/3 DKO hippocampal mass cultures were infected at DIV 7 with Cre-RFP virus, fixated at DAI 12 and immunolabeled against Cplx1/Cplx2 and the presynaptic marker protein vGlut1 (Appendix Figure 38). Striking was the smaller cell size and the accompanied decrease of the number of boutons per neuron at this stage of the Cplx free aged neurons. This could be a hint for deregulated membrane fusion events apart from synaptic vesicle exocytosis, especially as other synaptic exocytosis regulating proteins like Munc13, do not disturb the growth of neurons (Sigler et al., 2017).

The assumption that Cplx also plays a role beside the synaptic exocytosis, is encouraged by the fact that the importance of Cplx has also been demonstrated for a completely different fusion process, namely the regulated acrosomal exocytosis that sperm undergo in preparation of fertilization of the egg. Compared to neuronal exocytosis, this process is also Ca^{2+} regulated and SNARE mediated, but much slower. Moreover, there is simultaneous fusion of membrane segments and no vesicle recycling. Although Cplx1 and 2 are expressed in spermatozoids, only loss of Cplx1 limits fertility (Zhao et al., 2007; Zhao et al., 2008).

All in all, there are multiple effects of Cplx, beside the synaptic vesicle exocytosis described and the functional data of the transferrin uptake indicate an effect of Cplx on the recycling endocytosis.

4.4 Extended interaction network of Cplx3

The extended interaction networks identified with cortex material were not discussed further since these were seen as interactors of the SNARE complexes and these do not differ between the isoforms in these experiments. However, it was striking that comparatively many proteins were specifically found in the Cplx3 interactome (Figure 10). Network analysis showed an enrichment of cytoskeletal proteins (Figure 22). A possible explanation would be that due to the lower affinity of Cplx3 for the SNARE complex (Figure 11), Cplx3 peptides cannot displace endogenous Cplx1 proteins from the SNARE complex and thus the free peptides interact with cytoskeletal proteins in contrast to Cplx1 and Cplx2 peptides.

Since Cplx3 is mainly expressed in the retina, their extended interaction networks, were also studied in the retina. Striking was there the enrichment of cilia proteins with Cplx3 (Figure 26). The cilia of photoreceptor cells are localized at the OS, in close location to the disks (Appendix Figure 39), where the light signal is processed. Since vesicle mediated membrane fusion is more expected in the IS, ON and OPL, where the cell organelles are located, an Cplx-mediated process in the cilium is so far unlikely. A possible explanation for this finding is based on the observation of the accumulation of cytoskeletal proteins with Cplx3 in the cortex assays. The cilium is a microtubule-based protrusion, which cannot synthesize its own proteins and thus a lot of trafficking between the cytosol and primary cilia is driven by the concerted action of kinesin and dynein motor proteins (Luo et al., 2017). Therefore, it is possible that the enrichment of cilia proteins in the Cplx3 network of the retina based on the higher affinity of Cplx3 to cytoskeletal proteins. In contrast to this explanation an influence of Cplx4 on the OS structure was observed after Cplx4a KD in larval zebrafish (Vaithianathan et al., 2013).

4.5 Connection between ribbon synapse specific Cplx and RIBEYE

Cpx3 and Cplx4 are preferentially expressed in ribbon synapses of the retina. In contrast, Cplx1 und Cplx2 are mainly expressed in conventional synapses. To answer the question whether Cplx3 and Cplx4 contribute to the unique high rates of neurotransmitter release, in the retina assay proteins were searched exclusively interacting with Cplx3 and Cplx4. One of these proteins was the ribbon scaffolding protein RIBEYE. RIBEYE is an isoform of the transcription factor CtBP2, which was not enriched in the Cpx3 and Cplx4 interactome. The differentiation between RIBEYE and CtBP2 was performed in the MS analysis by identification of specific peptide sequences of the A-Domain of RIBEYE and confirmed by WB (Figure 27).

If a direct or indirect interaction between Cplx3/4 and RIBEYE exists, cannot be answered with this kind of assay. As the Cplx peptide represents just the SNARE binding domain, an interaction via SNARE proteins is conceivable. The fact that no SNARE protein could be detected with preference to Cplx3/4 (Figure 25), like the RIBEYE protein, could be explained with the mixed type of synapses in the retina lysate.

As validation approach of the interaction between Cplx3 and Cplx4 and RIBEYE, a reversed affinity purification experiment was conducted with an established ribbon-binding peptide. While the enrichment of the RIBEYE protein worked successfully Cplx3 and Cplx4 could not be identified as interaction partner in this assay. Similarly, the known interaction partner Bassoon (tom Dieck et al., 2005) was also not detectable. To improve the assay the affinity of the peptide was increased by using a dimer peptide (Francis et al., 2011). Furthermore, the occupation of the binding sites by the nuclei protein CtBP2 was tried to be reduced by using the nuclear free fraction S1 as input material for the assay. It should be noted that after separation of the nuclear proteins, Histone H3, as a nuclear-specific marker, could no longer be detected in the S1 fraction, but CtBP2 is still present. However, also with the improvements Cplx3 and Cplx4 could not be identified as interaction partner. A possible explanation would be the occupation of the Cplx binding side on RIBEYE by the ribbon binding peptide, as this peptide was developed based on a recurrent amino acid sequence of ribbon interaction proteins.

A link between Cplx3/4 and RIBEYE was described already in Cplx3/4 DKO mice (Reim et al., 2009). The RIBEYE expression levels, determined by quantitative immunoblotting, are reduced to 62%, whereas the other synaptic proteins are not altered. Furthermore, light and electron microscopy analysis discovered a disorganized OPL in the retina with club-shaped and 24% free floating ribbons in synaptic terminals. A hypothetical explanation of the interaction between Cplx3/4 and RIBEYE would be a tethering link between the synaptic vesicles and the RIBEYE composed ribbon. In this way Cplx3/4 would be part of the ribbon specific mechanism of high rates of neurotransmitter release, beside of the general synaptic vesicle exocytosis. This explanation approach is supported by the finding of an interaction between Cplx and Bruchpilot in Drosophila melanogaster. Bruchpilot as component of the cytomatrix at the active zone in Drosophila participates in tethering of synaptic vesicles via its C-terminus. Cplx was identified as a linker for the tethering (Scholz et al., 2019).

In summary, a link between the ribbon synapse specific Cplx3 and Cplx4 and the ribbon specific protein RIBEYE was promising regarding the MS and WB data and the effects in Cplx3/4 DKO mice. It would be interesting regarding the unique vesicular release machinery of ribbon synapses but could not be validated yet, at least not with the reserve affinity purification approach.

4.6 Connection between Cplx and Transducin

Another interacting protein complex was analyzed in more detail, not because of the obvious enrichment values, but because of findings from collaboration partners of the Department of Biology of the Universität Erlangen. Babai et al. described already 2016 a role of Cplx3/4 in adaption dependent availability of synaptic vesicles at photoreceptor ribbon synapses. While wildtype (WT) photoreceptor ribbons showed in the light-adapted state a significantly reduced number of vesicles in comparison to the dark-adapted state, the Cplx3/4 DKO mice lack such an adaption-dependent change of vesicles. This observation indicated that the synaptic ribbon resembles a capacitor that charges with vesicles in the light, which can then be released in response to a dark stimulus in a phasic burst followed by the tonic release of neurotransmitter (Jackman et al., 2009). It was concluded that Cplx3 and 4 could have, beside of their role in synaptic vesicle exocytosis, also a role in adaption dependent availability of

synaptic vesicles at photoreceptor ribbon synapses. Additionally, the cone circadian clock seems to control Cplx3 expression at transcriptional level (Bhoi et al., 2021).

Our collaboration partners found several transducin subunits as interactors of full-length Cplx3 and 4 in a tandem affinity purification tag screen from HEK cells. Transducin subunits translocate in the rods after light stimulus within minutes from the disks in the OS to the OPL, where the synapses of the photoreceptor cells are located. In the OPL a co-localization with Cplx4 was observed via a proximity ligation assay (Lux et al., Abstract, NWG Conference Göttingen 2019). Therefore, the present large database of the Cplx/SNARE interactome was used and studied regarding the transducin subunits of the photoreceptor cells. The α/β subunits of the rod cells (Gnat1 and Gnb1) and cone cells (Gnat2 and Gnb3) were found in the present assay partly with higher affinities to Cplx3 or Cplx4 in comparison to Cplx1 (Figure 29). However, also the SNARE binding deficient negative control enriched some subunits of transducin in smaller amount, so that a specific interaction is only indicated for Gnat1 so far. One reason could be the high affinity of transducin subunits to agarose beads, which is a common problem working with these proteins (Dr. Andreas Gießel, personal communication). Nevertheless, an interaction depending on the SNARE complex is possible, as the beta and gamma subunit of G-proteins can interact with the SNARE complex at low Ca^{2+} levels. After Ca^{2+} influx, the affinity of synaptotagmin 1 for the SNARE complex increases, thereby displacing the transducin subunits (Yoon et al., 2007). The results of our screen are surprising insofar as there seems to be an interaction between Cplx4 (rod specific) and the transducin α subunit. The question is whether the interaction is mediated directly or indirectly via the SNARE complex. The last would be possible since the SNAREs for the exocytosis complex were also detected in the screen. Therefore, it would be possible, that Cplx3 and 4 are involved in the vesicular fusion of transducin containing vesicles, which were transported depended on the light adaption.

4.7 Outlook

The transferrin uptake experiments indicated a role of Cplx in the endosomal recycling pathway. To confirm this, pulse chase experiments with transferrin are planned to investigate the recycling pathway in more detail and exclude the influence of endocytosis. Since also SNARE complexes of the lysosomal pathway were almost completely detected with the Cplx peptide affinity purification approach, an additional investigation of the degradation pathway

would be interesting. For this purpose, uptake experiments with EGF or LDL in HeLa cells are suitable, probably revealing more precise information about which fusion processes may be influenced by Cplx. Based on this knowledge, uptake assays can be performed in cultured primary neurons endogenously expressing Cplx and neurons deficient for Cplx can be used as negative controls. As different Cplx mouse mutants ($Cplx1^{flox/flox}$Cplx2/3 DKO; Cplx1 KO, Cplx2 KO, Cplx3 KO and Cplx4 KO) are available to us, conclusions can be drawn, which Cplx isoforms specifically act beyond synaptic exocytosis. Additional colocalization experiments with specific markers for the endosomal or lysosomal pathway would allow differentiation between the membrane fusion processes regulated by Cplx.

For a further study of Cplx interactors the switch to *in vivo* systems would be possible. One common problem of working with crude lysate, is the number of proteins which can interact with each other, although they are localized in the cell separately and therefore cannot interact *in vivo*. One possible solution could be an extension of the peptide with additional tags to conduct an *in vivo* affinity approach. First, a cell penetrating peptide (CPP) tag could bring the Cplx peptide *in vivo* in the cell in a cell culture system. Second, an additional photophor and UV light could covalently crosslink the interacting proteins. Third, a biotin tag could be used to purify the peptide with the interacting proteins. With this multifunctional Cplx peptide the question regarding non-neuronal SNARE complexes could be addressed directly under cellular conditions because SNARE complexes cannot assemble spontaneously anymore.

The peptide assay could also be extended regarding the employed protein domain. The central α domain, which mediates the binding to the SNARE complex is the most essential domain of Cplx, where protein interaction was described. Therefore, this domain was used in the peptide-based affinity purification approach. So far, no interaction partners of the other domains like NTD, AH or CTD were described, but especially the CTD would be interesting to study further. Differences in the expression pattern of the two Cplx subfamilies (Cplx1/2 vs. Cplx3/4) are accompanied by differences in the configuration of their C termini. In contrast to Cplxs1/2, Cplxs3/4 carry a C-terminal extension terminated by the posttranslational farnesylation motif CAAX. A farnesylated protein could be available in two states. It could be bound to the membrane because of its farnesyl residue or it could stay in the cytosol because of protein-protein interactions of chaperones. This flexibility between soluble and insoluble Cplx state would help the synapse to react quickly on light stimuli.

Therefore, further affinity purification approaches would be interesting with other Cplx domains, like the CTD with its farnesylation.

5 Summary

To study in an unbiased and systematic way whether Cplxs act upon different SNARE complex types and if these SNARE complexes are Cplx isoform-dependent, an Cplx peptide-based affinity purification approach was expanded to all four Cplx isoforms and applied to different input material, i.e. cortical and retinal protein fractions.

The detailed analysis shows that basically there are differences in the Cplx interactomes. In the cortex samples, a variety of possible regulators and effectors were identified, among them different members of the of SNARE protein family including Stx1, SNAP25 and VAMP2. Moreover, the samples also contained the complete set of SNAREs which are known to form complexes of the endosomal and lysosomal pathway, respectively. Surprisingly, these SNARE proteins were found to be Cplx isoform independent. A co-enrichment with neuronal SNARE proteins was excluded by repeating the affinity purification approach with HEK cells, which do not contain neuronal SNARE proteins. A functional effect of Cplx on non-exocytotic pathways was shown with a transferrin uptake assay, indicating an effect on the recycling endocytosis.

In addition, a link between the ribbon synapse specific Cplx3 and Cplx4 and the ribbon specific protein RIBEYE was promising regarding the MS and WB data. It would be interesting regarding the unique vesicular release machinery of ribbon synapses but could not be validated yet, at least not with the reserve affinity purification approach.

Furthermore, transducin was detected as part of the Cplx3 and Cplx4 interactome, which allows a speculation about a light dependent mechanism of Cplx action.

6. Bibliography

Aikawa, Y., Lynch, K.L., Boswell, K.L., and Martin, T.F. (2006). A second SNARE role for exocytic SNAP25 in endosome fusion. Mol Biol Cell *17*, 2113-2124. 10.1091/mbc.e06-01-0074.

Ambrozkiewicz, M.C., Schwark, M., Kishimoto-Suga, M., Borisova, E., Hori, K., Salazar-Lázaro, A., Rusanova, A., Altas, B., Piepkorn, L., Bessa, P., et al. (2018). Polarity Acquisition in Cortical Neurons Is Driven by Synergistic Action of Sox9-Regulated Wwp1 and Wwp2 E3 Ubiquitin Ligases and Intronic miR-140. Neuron *100*, 1097-1115.e1015. 10.1016/j.neuron.2018.10.008.

Antonin, W., Fasshauer, D., Becker, S., Jahn, R., and Schneider, T.R. (2002). Crystal structure of the endosomal SNARE complex reveals common structural principles of all SNAREs. Nat Struct Biol *9*, 107-111. 10.1038/nsb746.

Antonin, W., Holroyd, C., Fasshauer, D., Pabst, S., Von Mollard, G.F., and Jahn, R. (2000). A SNARE complex mediating fusion of late endosomes defines conserved properties of SNARE structure and function. Embo j *19*, 6453-6464. 10.1093/emboj/19.23.6453.

Babai, N., Sendelbeck, A., Regus-Leidig, H., Fuchs, M., Mertins, J., Reim, K., Brose, N., Feigenspan, A., and Brandstätter, J.H. (2016). Functional Roles of Complexin 3 and Complexin 4 at Mouse Photoreceptor Ribbon Synapses. J Neurosci *36*, 6651-6667. 10.1523/jneurosci.4335-15.2016.

Bhoi, J.D., Zhang, Z., Janz, R., You, Y., Wei, H., Wu, J., and Ribelayga, C.P. (2021). The SNARE regulator Complexin3 is a target of the cone circadian clock. J Comp Neurol *529*, 1066-1080. 10.1002/cne.25004.

Boldt, K., van Reeuwijk, J., Lu, Q., Koutroumpas, K., Nguyen, T.M., Texier, Y., van Beersum, S.E., Horn, N., Willer, J.R., Mans, D.A., et al. (2016). An organelle-specific protein landscape identifies novel diseases and molecular mechanisms. Nat Commun *7*, 11491. 10.1038/ncomms11491.

Bonifacino, J.S., and Glick, B.S. (2004). The mechanisms of vesicle budding and fusion. Cell *116*, 153-166. 10.1016/s0092-8674(03)01079-1.

Borisovska, M., Zhao, Y., Tsytsyura, Y., Glyvuk, N., Takamori, S., Matti, U., Rettig, J., Südhof, T., and Bruns, D. (2005). v-SNAREs control exocytosis of vesicles from priming to fusion. Embo j *24*, 2114-2126. 10.1038/sj.emboj.7600696.

Bose, A., Guilherme, A., Huang, S., Hubbard, A.C., Lane, C.R., Soriano, N.A., and Czech, M.P. (2005). The v-SNARE Vti1a regulates insulin-stimulated glucose transport and Acrp30 secretion in 3T3-L1 adipocytes. J Biol Chem *280*, 36946-36951. 10.1074/jbc.M508317200.

Bracher, A., Kadlec, J., Betz, H., and Weissenhorn, W. (2002). X-ray structure of a neuronal complexin-SNARE complex from squid. J Biol Chem *277*, 26517-26523. 10.1074/jbc.M203460200.

Brandhorst, D., Zwilling, D., Rizzoli, S.O., Lippert, U., Lang, T., and Jahn, R. (2006). Homotypic fusion of early endosomes: SNAREs do not determine fusion specificity. Proc Natl Acad Sci U S A *103*, 2701-2706. 10.1073/pnas.0511138103.

Brose, N. (2008a). Altered complexin expression in psychiatric and neurological disorders: cause or consequence? Mol Cells *25*, 7-19.

Brose, N. (2008b). For better or for worse: complexins regulate SNARE function and vesicle fusion. Traffic *9*, 1403-1413. 10.1111/j.1600-0854.2008.00758.x.

Brunger, A.T. (2005). Structure and function of SNARE and SNARE-interacting proteins. Q Rev Biophys *38*, 1-47. 10.1017/s0033583505004051.

Brunger, A.T., Weninger, K., Bowen, M., and Chu, S. (2009). Single-molecule studies of the neuronal SNARE fusion machinery. Annu Rev Biochem *78*, 903-928. 10.1146/annurev.biochem.77.070306.103621.

Burri, L., and Lithgow, T. (2004). A complete set of SNAREs in yeast. Traffic *5*, 45-52. 10.1046/j.1600-0854.2003.00151.x.

Burri, L., Varlamov, O., Doege, C.A., Hofmann, K., Beilharz, T., Rothman, J.E., Söllner, T.H., and Lithgow, T. (2003). A SNARE required for retrograde transport to the endoplasmic reticulum. Proc Natl Acad Sci U S A *100*, 9873-9877. 10.1073/pnas.1734000100.

Campbell, J.R., Li, H., Wang, Y., Kozhemyakin, M., Hunt, A.J., Jr., Liu, X., Janz, R., and Heidelberger, R. (2020). Phosphorylation of the Retinal Ribbon Synapse Specific t-SNARE Protein Syntaxin3B Is Regulated by Light via a Ca(2 +)-Dependent Pathway. Front Cell Neurosci *14*, 587072. 10.3389/fncel.2020.587072.

Chang, S., Reim, K., Pedersen, M., Neher, E., Brose, N., and Taschenberger, H. (2015). Complexin stabilizes newly primed synaptic vesicles and prevents their premature fusion at the mouse calyx of held synapse. J Neurosci *35*, 8272-8290. 10.1523/jneurosci.4841-14.2015.

Chen, X., Tomchick, D.R., Kovrigin, E., Araç, D., Machius, M., Südhof, T.C., and Rizo, J. (2002). Three-dimensional structure of the complexin/SNARE complex. Neuron *33*, 397-409. 10.1016/s0896-6273(02)00583-4.

Chen, Y.A., Scales, S.J., Patel, S.M., Doung, Y.C., and Scheller, R.H. (1999). SNARE complex formation is triggered by Ca2+ and drives membrane fusion. Cell *97*, 165-174. 10.1016/s0092-8674(00)80727-8.

Cho, R.W., Song, Y., and Littleton, J.T. (2010). Comparative analysis of Drosophila and mammalian complexins as fusion clamps and facilitators of neurotransmitter release. Mol Cell Neurosci *45*, 389-397. 10.1016/j.mcn.2010.07.012.

Curtis, L.B., Doneske, B., Liu, X., Thaller, C., McNew, J.A., and Janz, R. (2008). Syntaxin 3b is a t-SNARE specific for ribbon synapses of the retina. J Comp Neurol *510*, 550-559. 10.1002/cne.21806.

Daro, E., van der Sluijs, P., Galli, T., and Mellman, I. (1996). Rab4 and cellubrevin define different early endosome populations on the pathway of transferrin receptor recycling. Proc Natl Acad Sci U S A *93*, 9559-9564. 10.1073/pnas.93.18.9559.

Di Paolo, G., and De Camilli, P. (2006). Phosphoinositides in cell regulation and membrane dynamics. Nature *443*, 651-657. 10.1038/nature05185.

Distler, U., Kuharev, J., Navarro, P., and Tenzer, S. (2016). Label-free quantification in ion mobility-enhanced data-independent acquisition proteomics. Nat Protoc *11*, 795-812. 10.1038/nprot.2016.042.

Donaldson, J.G., and Jackson, C.L. (2011). ARF family G proteins and their regulators: roles in membrane transport, development and disease. Nat Rev Mol Cell Biol *12*, 362-375. 10.1038/nrm3117.

Duchen, L.W. (1973). The effects of tetanus toxin on the motor end-plates of the mouse. An electron microscopic study. J Neurol Sci *19*, 153-167. 10.1016/0022-510x(73)90159-7.

Dulubova, I., Khvotchev, M., Liu, S., Huryeva, I., Südhof, T.C., and Rizo, J. (2007). Munc18-1 binds directly to the neuronal SNARE complex. Proc Natl Acad Sci U S A *104*, 2697-2702. 10.1073/pnas.0611318104.

Falkowski, M.A., Thomas, D.D., and Groblewski, G.E. (2010). Complexin 2 modulates vesicle-associated membrane protein (VAMP) 2-regulated zymogen granule exocytosis in pancreatic acini. J Biol Chem *285*, 35558-35566. 10.1074/jbc.M110.146597.

Fasshauer, D. (2003). Structural insights into the SNARE mechanism. Biochim Biophys Acta *1641*, 87-97. 10.1016/s0167-4889(03)00090-9.

Fasshauer, D., Antonin, W., Subramaniam, V., and Jahn, R. (2002). SNARE assembly and disassembly exhibit a pronounced hysteresis. Nat Struct Biol *9*, 144-151. 10.1038/nsb750.

Fasshauer, D., Sutton, R.B., Brunger, A.T., and Jahn, R. (1998). Conserved structural features of the synaptic fusion complex: SNARE proteins reclassified as Q- and R-SNAREs. Proc Natl Acad Sci U S A *95*, 15781-15786. 10.1073/pnas.95.26.15781.

Fields, S., and Song, O. (1989). A novel genetic system to detect protein-protein interactions. Nature *340*, 245-246. 10.1038/340245a0.

Francis, A.A., Mehta, B., and Zenisek, D. (2011). Development of new peptide-based tools for studying synaptic ribbon function. J Neurophysiol *106*, 1028-1037. 10.1152/jn.00255.2011.

Galli, T., Chilcote, T., Mundigl, O., Binz, T., Niemann, H., and De Camilli, P. (1994). Tetanus toxin-mediated cleavage of cellubrevin impairs exocytosis of transferrin receptor-containing vesicles in CHO cells. J Cell Biol *125*, 1015-1024. 10.1083/jcb.125.5.1015.

Gee, H.Y., Tang, B.L., Kim, K.H., and Lee, M.G. (2010). Syntaxin 16 binds to cystic fibrosis transmembrane conductance regulator and regulates its membrane trafficking in epithelial cells. J Biol Chem *285*, 35519-35527. 10.1074/jbc.M110.162438.

Guan, R., Dai, H., and Rizo, J. (2008). Binding of the Munc13-1 MUN domain to membrane-anchored SNARE complexes. Biochemistry *47*, 1474-1481. 10.1021/bi702345m.

Gulyás-Kovács, A., de Wit, H., Milosevic, I., Kochubey, O., Toonen, R., Klingauf, J., Verhage, M., and Sørensen, J.B. (2007). Munc18-1: sequential interactions with the fusion machinery stimulate vesicle docking and priming. J Neurosci *27*, 8676-8686. 10.1523/jneurosci.0658-07.2007.

Gururaja, T.L., Li, W., Payan, D.G., and Anderson, D.C. (2003). Utility of peptide-protein affinity complexes in proteomics: identification of interaction partners of a tumor suppressor peptide. J Pept Res *61*, 163-176. 10.1034/j.1399-3011.2003.00044.x.

Hanson, P.I., Heuser, J.E., and Jahn, R. (1997). Neurotransmitter release - four years of SNARE complexes. Curr Opin Neurobiol *7*, 310-315. 10.1016/s0959-4388(97)80057-8.

Heidelberger, R., Heinemann, C., Neher, E., and Matthews, G. (1994). Calcium dependence of the rate of exocytosis in a synaptic terminal. Nature *371*. 10.1038/371513a0.

Hong, W. (2005). SNAREs and traffic. Biochim Biophys Acta *1744*, 120-144. 10.1016/j.bbamcr.2005.03.014.

Hong, W., and Lev, S. (2014). Tethering the assembly of SNARE complexes. Trends Cell Biol *24*, 35-43. 10.1016/j.tcb.2013.09.006.

Hoogenraad, C.C., Popa, I., Futai, K., Martinez-Sanchez, E., Wulf, P.S., van Vlijmen, T., Dortland, B.R., Oorschot, V., Govers, R., Monti, M., et al. (2010). Neuron specific Rab4 effector GRASP-1

coordinates membrane specialization and maturation of recycling endosomes. PLoS Biol *8*, e1000283. 10.1371/journal.pbio.1000283.

Hunt, J.M., Bommert, K., Charlton, M.P., Kistner, A., Habermann, E., Augustine, G.J., and Betz, H. (1994). A post-docking role for synaptobrevin in synaptic vesicle fusion. Neuron *12*, 1269-1279. 10.1016/0896-6273(94)90443-x.

Huntwork, S., and Littleton, J.T. (2007). A complexin fusion clamp regulates spontaneous neurotransmitter release and synaptic growth. Nat Neurosci *10*, 1235-1237. 10.1038/nn1980.

Ishizuka, T., Saisu, H., Suzuki, T., Kirino, Y., and Abe, T. (1997). Molecular cloning of synaphins/complexins, cytosolic proteins involved in transmitter release, in the electric organ of an electric ray (Narke japonica). Neurosci Lett *232*, 107-110. 10.1016/s0304-3940(97)00586-7.

Jackman, S.L., Choi, S.Y., Thoreson, W.B., Rabl, K., Bartoletti, T.M., and Kramer, R.H. (2009). Role of the synaptic ribbon in transmitting the cone light response. Nat Neurosci *12*, 303-310. 10.1038/nn.2267.

Jahn, R., and Scheller, R.H. (2006). SNAREs--engines for membrane fusion. Nat Rev Mol Cell Biol *7*, 631-643. 10.1038/nrm2002.

Kaeser-Woo, Y.J., Yang, X., and Südhof, T.C. (2012). C-terminal complexin sequence is selectively required for clamping and priming but not for Ca2+ triggering of synaptic exocytosis. J Neurosci *32*, 2877-2885. 10.1523/jneurosci.3360-11.2012.

Khanna, H. (2015). Photoreceptor Sensory Cilium: Traversing the Ciliary Gate. Cells *4*, 674-686. 10.3 0/cells4040674.

Koike, S., and Jahn, R. (2019). SNAREs define targeting specificity of trafficking vesicles by combinatorial interaction with tethering factors. Nat Commun *10*, 1608. 10.1038/s41467-019-09617-9.

Kreykenbohm, V., Wenzel, D., Antonin, W., Atlachkine, V., and von Mollard, G.F. (2002). The SNAREs vti1a and vti1b have distinct localization and SNARE complex partners. Eur J Cell Biol *81*, 273-280. 10.1078/0171-9335-00247.

Kuharev, J., Navarro, P., Distler, U., Jahn, O., and Tenzer, S. (2015). In-depth evaluation of software tools for data-independent acquisition based label-free quantification. Proteomics *15*, 3140-3151. 10.1002/pmic.201400396.

Laemmli, U.K. (1970). Cleavage of structural proteins during the assembly of the head of bacteriophage T4. Nature *227*, 680-685. 10.1038/227680a0.

Lagnado, L., and Schmitz, F. (2015). Ribbon Synapses and Visual Processing in the Retina. Annu Rev Vis Sci *1*, 235-262. 10.1146/annurev-vision-082114-035709.

Landgraf, I., Muhlhans, J., Dedek, K., Reim, K., Brandstatter, J.H., and Ammermuller, J. (2012). The absence of Complexin 3 and Complexin 4 differentially impacts the ON and OFF pathways in mouse retina. Eur J Neurosci *36*, 2470-2481. 10.1111/j.1460-9568.2012.08149.x.

Lee, S.H., Valtschanoff, J.G., Kharazia, V.N., Weinberg, R., and Sheng, M. (2001). Biochemical and morphological characterization of an intracellular membrane compartment containing AMPA receptors. Neuropharmacology *41*, 680-692. 10.1016/s0028-3908(01)00124-1.

Lin, R.C., and Scheller, R.H. (1997). Structural organization of the synaptic exocytosis core complex. Neuron *19*, 1087-1094. 10.1016/s0896-6273(00)80399-2.

Liu, X., Heidelberger, R., and Janz, R. (2014). Phosphorylation of syntaxin 3B by CaMKII regulates the formation of t-SNARE complexes. Mol Cell Neurosci *60*, 53-62. 10.1016/j.mcn.2014.03.002.

López-Murcia, F.J., Reim, K., Jahn, O., Taschenberger, H., and Brose, N. (2019). Acute Complexin Knockout Abates Spontaneous and Evoked Transmitter Release. Cell Rep *26*, 2521-2530.e2525. 10.1016/j.celrep.2019.02.030.

Luo, W., Ruba, A., Takao, D., Zweifel, L.P., Lim, R.Y.H., Verhey, K.J., and Yang, W. (2017). Axonemal Lumen Dominates Cytosolic Protein Diffusion inside the Primary Cilium. Sci Rep *7*, 15793. 10.1038/s41598-017-16103-z.

Lux, U.T., Ehrenberg, J., Joachimsthaler, A., Atorf, J., Pircher, B., Reim, K., Kremers, J., Gießl, A., and Brandstätter, J.H. (2021). Cell Types and Synapses Expressing the SNARE Complex Regulating Proteins Complexin 1 and Complexin 2 in Mammalian Retina. Int J Mol Sci *22*. 10.3390/ijms22158131.

Ma, L., Rebane, A.A., Yang, G., Xi, Z., Kang, Y., Gao, Y., and Zhang, Y. (2015). Munc18-1-regulated stage-wise SNARE assembly underlying synaptic exocytosis. Elife *4*. 10.7554/eLife.09580.

Magupalli, V.G., Schwarz, K., Alpadi, K., Natarajan, S., Seigel, G.M., and Schmitz, F. (2008). Multiple RIBEYE-RIBEYE interactions create a dynamic scaffold for the formation of synaptic ribbons. J Neurosci *28*, 7954-7967. 10.1523/JNEUROSCI.1964-08.2008.

Mallard, F., Tang, B.L., Galli, T., Tenza, D., Saint-Pol, A., Yue, X., Antony, C., Hong, W., Goud, B., and Johannes, L. (2002). Early/recycling endosomes-to-TGN transport involves two SNARE complexes and a Rab6 isoform. J Cell Biol *156*, 653-664. 10.1083/jcb.200110081.

Malsam, J., and Söllner, T.H. (2011). Organization of SNAREs within the Golgi stack. Cold Spring Harb Perspect Biol *3*, a005249. 10.1101/cshperspect.a005249.

Matsui, T., Jiang, P., Nakano, S., Sakamaki, Y., Yamamoto, H., and Mizushima, N. (2018). Autophagosomal YKT6 is required for fusion with lysosomes independently of syntaxin 17. J Cell Biol *217*, 2633-2645. 10.1083/jcb.201712058.

Matthews, G., and Fuchs, P. (2010). The diverse roles of ribbon synapses in sensory neurotransmission. Nat Rev Neurosci *11*, 812-822. 10.1038/nrn2924.

McBride, H.M., Rybin, V., Murphy, C., Giner, A., Teasdale, R., and Zerial, M. (1999). Oligomeric complexes link Rab5 effectors with NSF and drive membrane fusion via interactions between EEA1 and syntaxin 13. Cell *98*, 377-386. 10.1016/s0092-8674(00)81966-2.

McMahon, H.T., Missler, M., Li, C., and Südhof, T.C. (1995). Complexins: cytosolic proteins that regulate SNAP receptor function. Cell *83*, 111-119. 10.1016/0092-8674(95)90239-2.

McMahon, H.T., Ushkaryov, Y.A., Edelmann, L., Link, E., Binz, T., Niemann, H., Jahn, R., and Südhof, T.C. (1993). Cellubrevin is a ubiquitous tetanus-toxin substrate homologous to a putative synaptic vesicle fusion protein. Nature *364*, 346-349. 10.1038/364346a0.

Mortensen, L.S., Park, S.J.H., Ke, J.B., Cooper, B.H., Zhang, L., Imig, C., L√∂wel, S., Reim, K., Brose, N., Demb, J.B., et al. (2016). Complexin 3 Increases the Fidelity of Signaling in a Retinal Circuit by Regulating Exocytosis at Ribbon Synapses. Cell Rep *15*, 2239-2250. 10.1016/j.celrep.2016.05.012.

Moser, T., Brandt, A., and Lysakowski, A. (2006). Hair cell ribbon synapses. Cell Tissue Res *326*, 347-359. 10.1007/s00441-006-0276-3.

Pabst, S., Hazzard, J.W., Antonin, W., Südhof, T.C., Jahn, R., Rizo, J., and Fasshauer, D. (2000). Selective interaction of complexin with the neuronal SNARE complex. Determination of the binding regions. J Biol Chem *275*, 19808-19818. 10.1074/jbc.M002571200.

Pabst, S., Margittai, M., Vainius, D., Langen, R., Jahn, R., and Fasshauer, D. (2002). Rapid and selective binding to the synaptic SNARE complex suggests a modulatory role of complexins in neuroexocytosis. J Biol Chem *277*, 7838-7848. 10.1074/jbc.M109507200.

Parsons, T.D., and Sterling, P. (2003). Synaptic ribbon. Conveyor belt or safety belt? Neuron *37*, 379-382. 10.1016/s0896-6273(03)00062-x.

Prekeris, R., Klumperman, J., Chen, Y.A., and Scheller, R.H. (1998). Syntaxin 13 mediates cycling of plasma membrane proteins via tubulovesicular recycling endosomes. J Cell Biol *143*, 957-971. 10.1083/jcb.143.4.957.

Proctor, K.M., Miller, S.C., Bryant, N.J., and Gould, G.W. (2006). Syntaxin 16 controls the intracellular sequestration of GLUT4 in 3T3-L1 adipocytes. Biochem Biophys Res Commun *347*, 433-438. 10.1016/j.bbrc.2006.06.135.

Pryor, P.R., Mullock, B.M., Bright, N.A., Lindsay, M.R., Gray, S.R., Richardson, S.C., Stewart, A., James, D.E., Piper, R.C., and Luzio, J.P. (2004). Combinatorial SNARE complexes with VAMP7 or VAMP8 define different late endocytic fusion events. EMBO Rep *5*, 590-595. 10.1038/sj.embor.7400150.

Reim, K., Mansour, M., Varoqueaux, F., McMahon, H.T., Südhof, T.C., Brose, N., and Rosenmund, C. (2001). Complexins regulate a late step in Ca2+-dependent neurotransmitter release. Cell *104*, 71-81. 10.1016/s0092-8674(01)00192-1.

Reim, K., Regus-Leidig, H., Ammermöller, J., El-Kordi, A., Radyushkin, K., Ehrenreich, H., Brandstätter, J.H., and Brose, N. (2009). Aberrant function and structure of retinal ribbon synapses in the absence of complexin 3 and complexin 4. J Cell Sci *122*, 1352-1361. 10.1242/jcs.045401.

Reim, K., Wegmeyer, H., Brandstätter, J.H., Xue, M., Rosenmund, C., Dresbach, T., Hofmann, K., and Brose, N. (2005). Structurally and functionally unique complexins at retinal ribbon synapses. J Cell Biol *169*, 669-680. 10.1083/jcb.200502115.

Riggs, K.A., Hasan, N., Humphrey, D., Raleigh, C., Nevitt, C., Corbin, D., and Hu, C. (2012). Regulation of integrin endocytic recycling and chemotactic cell migration by syntaxin 6 and VAMP3 interaction. J Cell Sci *125*, 3827-3839. 10.1242/jcs.102566.

Rodkey, T.L., Liu, S., Barry, M., and McNew, J.A. (2008). Munc18a scaffolds SNARE assembly to promote membrane fusion. Mol Biol Cell *19*, 5422-5434. 10.1091/mbc.e08-05-0538.

Schaub, J.R., Lu, X., Doneske, B., Shin, Y.K., and McNew, J.A. (2006). Hemifusion arrest by complexin is relieved by Ca2+-synaptotagmin I. Nat Struct Mol Biol *13*, 748-750. 10.1038/nsmb1124.

Schiavo, G., Matteoli, M., and Montecucco, C. (2000). Neurotoxins affecting neuroexocytosis. Physiol Rev *80*, 717-766. 10.1152/physrev.2000.80.2.717.

Schindler, C., Chen, Y., Pu, J., Guo, X., and Bonifacino, J.S. (2015). EARP is a multisubunit tethering complex involved in endocytic recycling. Nat Cell Biol *17*, 639-650. 10.1038/ncb3129.

Schmitz, F., Königstorfer, A., and Südhof, T.C. (2000). RIBEYE, a component of synaptic ribbons: a protein's journey through evolution provides insight into synaptic ribbon function. Neuron *28*, 857-872. 10.1016/s0896-6273(00)00159-8.

Schoch, S., Deák, F., Königstorfer, A., Mozhayeva, M., Sara, Y., Südhof, T.C., and Kavalali, E.T. (2001). SNARE function analyzed in synaptobrevin/VAMP knockout mice. Science *294*, 1117-1122. 10.1126/science.1064335.

Scholz, N., Ehmann, N., Sachidanandan, D., Imig, C., Cooper, B.H., Jahn, O., Reim, K., Brose, N., Meyer, J., Lamberty, M., et al. (2019). Complexin cooperates with Bruchpilot to tether synaptic vesicles to the active zone cytomatrix. J Cell Biol *218*, 1011-1026. 10.1083/jcb.201806155.

Schulze, W.X., and Mann, M. (2004). A novel proteomic screen for peptide-protein interactions. J Biol Chem *279*, 10756-10764. 10.1074/jbc.M309909200.

Shen, J., Tareste, D.C., Paumet, F., Rothman, J.E., and Melia, T.J. (2007). Selective activation of cognate SNAREpins by Sec1/Munc18 proteins. Cell *128*, 183-195. 10.1016/j.cell.2006.12.016.

Shih, A.M., and Shin, O.H. (2011). Interactions among the SNARE proteins and complexin analyzed by a yeast four-hybrid assay. Anal Biochem *416*, 107-111. 10.1016/j.ab.2011.05.010.

Sigler, A., Oh, W.C., Imig, C., Altas, B., Kawabe, H., Cooper, B.H., Kwon, H.B., Rhee, J.S., and Brose, N. (2017). Formation and Maintenance of Functional Spines in the Absence of Presynaptic Glutamate Release. Neuron *94*, 304-311.e304. 10.1016/j.neuron.2017.03.029.

Silva, J.C., Gorenstein, M.V., Li, G.Z., Vissers, J.P., and Geromanos, S.J. (2006). Absolute quantification of proteins by LCMSE: a virtue of parallel MS acquisition. Mol Cell Proteomics *5*, 144-156. 10.1074/mcp.M500230-MCP200.

Solinger, J.A., Rashid, H.O., Prescianotto-Baschong, C., and Spang, A. (2020). FERARI is required for Rab11-dependent endocytic recycling. Nat Cell Biol *22*, 213-224. 10.1038/s41556-019-0456-5.

Sondermann, J.R., Barry, A.M., Jahn, O., Michel, N., Abdelaziz, R., Kügler, S., Gomez-Varela, D., and Schmidt, M. (2019). Vti1b promotes TRPV1 sensitization during inflammatory pain. Pain *160*, 508-527. 10.1097/j.pain.0000000000001418.

Stenmark, H. (2009). Rab GTPases as coordinators of vesicle traffic. Nat Rev Mol Cell Biol *10*, 513-525. 10.1038/nrm2728.

Sterling, P., and Matthews, G. (2005). Structure and function of ribbon synapses. Trends Neurosci *28*, 20-29. 10.1016/j.tins.2004.11.009.

Stevens, C.F., and Tsujimoto, T. (1995). Estimates for the pool size of releasable quanta at a single central synapse and for the time required to refill the pool. Proc Natl Acad Sci U S A *92*, 846-849. 10.1073/pnas.92.3.846.

Strenzke, N., Chanda, S., Kopp-Scheinpflug, C., Khimich, D., Reim, K., Bulankina, A.V., Neef, A., Wolf, F., Brose, N., Xu-Friedman, M.A., and Moser, T. (2009). Complexin-I is required for high-fidelity transmission at the endbulb of Held auditory synapse. J Neurosci *29*, 7991-8004. 10.1523/jneurosci.0632-09.2009.

Sudhof, T.C. (2004). The synaptic vesicle cycle. Annu Rev Neurosci *27*, 509-547. 10.1146/annurev.neuro.26.041002.131412.

Südhof, T.C. (2013). Neurotransmitter release: the last millisecond in the life of a synaptic vesicle. Neuron *80*, 675-690. 10.1016/j.neuron.2013.10.022.

Südhof, T.C., and Rizo, J. (2011). Synaptic vesicle exocytosis. Cold Spring Harb Perspect Biol *3*. 10.1101/cshperspect.a005637.

Südhof, T.C., and Rothman, J.E. (2009). Membrane fusion: grappling with SNARE and SM proteins. Science *323*, 474-477. 10.1126/science.1161748.

Sun, W., Yan, Q., Vida, T.A., and Bean, A.J. (2003). Hrs regulates early endosome fusion by inhibiting formation of an endosomal SNARE complex. J Cell Biol *162*, 125-137. 10.1083/jcb.200302083.

Tadokoro, S., Nakanishi, M., and Hirashima, N. (2005). Complexin II facilitates exocytotic release in mast cells by enhancing Ca2+ sensitivity of the fusion process. J Cell Sci *118*, 2239-2246. 10.1242/jcs.02338.

Tareste, D., Shen, J., Melia, T.J., and Rothman, J.E. (2008). SNAREpin/Munc18 promotes adhesion and fusion of large vesicles to giant membranes. Proc Natl Acad Sci U S A *105*, 2380-2385. 10.1073/pnas.0712125105.

Tiwari, A., Jung, J.J., Inamdar, S.M., Brown, C.O., Goel, A., and Choudhury, A. (2011). Endothelial cell migration on fibronectin is regulated by syntaxin 6-mediated alpha5beta1 integrin recycling. J Biol Chem *286*, 36749-36761. 10.1074/jbc.M111.260828.

tom Dieck, S., Altrock, W.D., Kessels, M.M., Qualmann, B., Regus, H., Brauner, D., Fejtova, A., Bracko, O., Gundelfinger, E.D., and Brandstatter, J.H. (2005). Molecular dissection of the photoreceptor ribbon synapse: physical interaction of Bassoon and RIBEYE is essential for the assembly of the ribbon complex. J Cell Biol *168*, 825-836. 10.1083/jcb.200408157.

tom Dieck, S., and Brandstätter, J.H. (2006). Ribbon synapses of the retina. Cell Tissue Res *326*, 339-346. 10.1007/s00441-006-0234-0.

Trimbuch, T., and Rosenmund, C. (2016). Should I stop or should I go? The role of complexin in neurotransmitter release. Nat Rev Neurosci *17*, 118-125. 10.1038/nrn.2015.16.

Trischler, M., Stoorvogel, W., and Ullrich, O. (1999). Biochemical analysis of distinct Rab5- and Rab11-positive endosomes along the transferrin pathway. J Cell Sci *112 (Pt 24)*, 4773-4783.

Vaithianathan, T., Henry, D., Akmentin, W., and Matthews, G. (2015). Functional roles of complexin in neurotransmitter release at ribbon synapses of mouse retinal bipolar neurons. J Neurosci *35*, 4065-4070. 10.1523/jneurosci.2703-14.2015.

Vaithianathan, T., Zanazzi, G., Henry, D., Akmentin, W., and Matthews, G. (2013). Stabilization of spontaneous neurotransmitter release at ribbon synapses by ribbon-specific subtypes of complexin. J Neurosci *33*, 8216-8226. 10.1523/jneurosci.1280-12.2013.

von Gersdorff, H., Vardi, E., Matthews, G., and Sterling, P. (1996). Evidence that vesicles on the synaptic ribbon of retinal bipolar neurons can be rapidly released. Neuron *16*, 1221-1227. 10.1016/s0896-6273(00)80148-8.

Wandinger-Ness, A., and Zerial, M. (2014). Rab proteins and the compartmentalization of the endosomal system. Cold Spring Harb Perspect Biol *6*, a022616. 10.1101/cshperspect.a022616.

Wang, C.C., Ng, C.P., Lu, L., Atlashkin, V., Zhang, W., Seet, L.F., and Hong, W. (2004). A role of VAMP8/endobrevin in regulated exocytosis of pancreatic acinar cells. Dev Cell *7*, 359-371. 10.1016/j.devcel.2004.08.002.

Watson, R.T., Hou, J.C., and Pessin, J.E. (2008). Recycling of IRAP from the plasma membrane back to the insulin-responsive compartment requires the Q-SNARE syntaxin 6 but not the GGA clathrin adaptors. J Cell Sci *121*, 1243-1251. 10.1242/jcs.017517.

Weninger, K., Bowen, M.E., Choi, U.B., Chu, S., and Brunger, A.T. (2008). Accessory proteins stabilize the acceptor complex for synaptobrevin, the 1:1 syntaxin/SNAP-25 complex. Structure *16*, 308-320. 10.1016/j.str.2007.12.010.

Xu, Y., Martin, S., James, D.E., and Hong, W. (2002). GS15 forms a SNARE complex with syntaxin 5, GS28, and Ykt6 and is implicated in traffic in the early cisternae of the Golgi apparatus. Mol Biol Cell *13*, 3493-3507. 10.1091/mbc.e02-01-0004.

Xue, M., Craig, T.K., Xu, J., Chao, H.T., Rizo, J., and Rosenmund, C. (2010). Binding of the complexin N terminus to the SNARE complex potentiates synaptic-vesicle fusogenicity. Nat Struct Mol Biol *17*, 568-575. 10.1038/nsmb.1791.

Xue, M., Reim, K., Chen, X., Chao, H.T., Deng, H., Rizo, J., Brose, N., and Rosenmund, C. (2007). Distinct domains of complexin I differentially regulate neurotransmitter release. Nat Struct Mol Biol *14*, 949-958. 10.1038/nsmb1292.

Xue, M., Stradomska, A., Chen, H., Brose, N., Zhang, W., Rosenmund, C., and Reim, K. (2008). Complexins facilitate neurotransmitter release at excitatory and inhibitory synapses in mammalian central nervous system. Proc Natl Acad Sci U S A *105*, 7875-7880. 10.1073/pnas.0803012105.

Yang, X., Pei, J., Kaeser-Woo, Y.J., Bacaj, T., Grishin, N.V., and Südhof, T.C. (2015). Evolutionary conservation of complexins: from choanoflagellates to mice. EMBO Rep *16*, 1308-1317. 10.15252/embr.201540305.

Yoon, E.J., Gerachshenko, T., Spiegelberg, B.D., Alford, S., and Hamm, H.E. (2007). Gbetagamma interferes with Ca2+-dependent binding of synaptotagmin to the soluble N-ethylmaleimide-sensitive factor attachment protein receptor (SNARE) complex. Mol Pharmacol *72*, 1210-1219. 10.1124/mol.107.039446.

Yoon, T.Y., Lu, X., Diao, J., Lee, S.M., Ha, T., and Shin, Y.K. (2008). Complexin and Ca2+ stimulate SNARE-mediated membrane fusion. Nat Struct Mol Biol *15*, 707-713. 10.1038/nsmb.1446.

Zenisek, D., Horst, N.K., Merrifield, C., Sterling, P., and Matthews, G. (2004). Visualizing synaptic ribbons in the living cell. J Neurosci *24*, 9752-9759. 10.1523/JNEUROSCI.2886-04.2004.

Zhang, T., and Hong, W. (2001). Ykt6 forms a SNARE complex with syntaxin 5, GS28, and Bet1 and participates in a late stage in endoplasmic reticulum-Golgi transport. J Biol Chem *276*, 27480-27487. 10.1074/jbc.M102786200.

Zhang, T., Wong, S.H., Tang, B.L., Xu, Y., and Hong, W. (1999). Morphological and functional association of Sec22b/ERS-24 with the pre-Golgi intermediate compartment. Mol Biol Cell *10*, 435-453. 10.1091/mbc.10.2.435.

Zhang, T., Wong, S.H., Tang, B.L., Xu, Y., Peter, F., Subramaniam, V.N., and Hong, W. (1997). The mammalian protein (rbet1) homologous to yeast Bet1p is primarily associated with the pre-Golgi intermediate compartment and is involved in vesicular transport from the endoplasmic reticulum to the Golgi apparatus. J Cell Biol *139*, 1157-1168. 10.1083/jcb.139.5.1157.

Zhao, L., Burkin, H.R., Shi, X., Li, L., Reim, K., and Miller, D.J. (2007). Complexin I is required for mammalian sperm acrosomal exocytosis. Dev Biol *309*, 236-244. 10.1016/j.ydbio.2007.07.009.

Zhao, L., Reim, K., and Miller, D.J. (2008). Complexin-I-deficient sperm are subfertile due to a defect in zona pellucida penetration. Reproduction *136*, 323-334. 10.1530/rep-07-0569.

Zilly, F.E., Sørensen, J.B., Jahn, R., and Lang, T. (2006). Munc18-bound syntaxin readily forms SNARE complexes with synaptobrevin in native plasma membranes. PLoS Biol *4*, e330. 10.1371/journal.pbio.0040330.

Zwilling, D., Cypionka, A., Pohl, W.H., Fasshauer, D., Walla, P.J., Wahl, M.C., and Jahn, R. (2007). Early endosomal SNAREs form a structurally conserved SNARE complex and fuse liposomes with multiple topologies. Embo j *26*, 9-18. 10.1038/sj.emboj.7601467.

Appendix

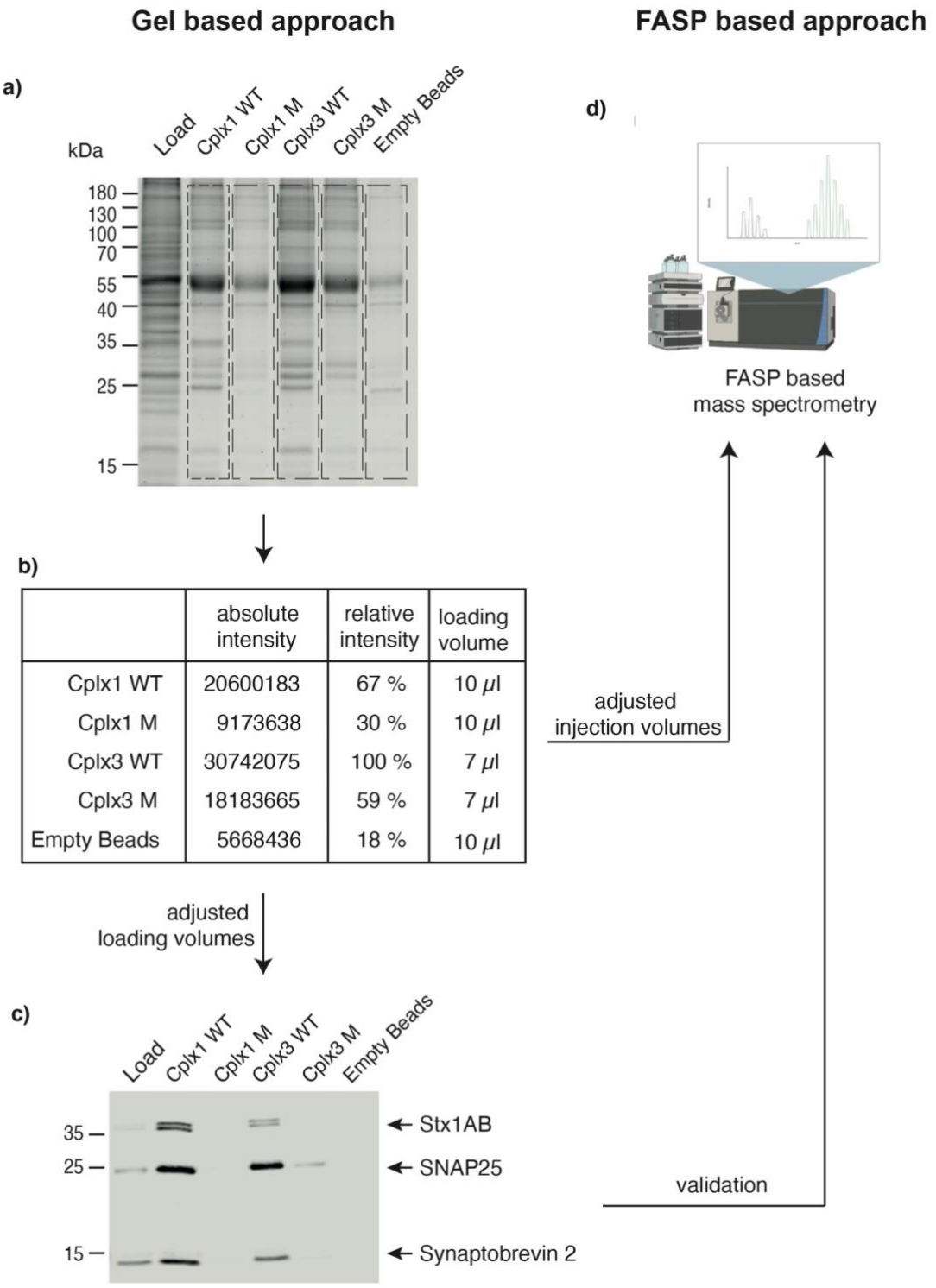

Figure 31: Loading volume adjustment for each screen
(a) By Coomassie staining the quality of each affinity purification screen was monitored. **(b)** Moreover, the gels were used for quantification of selected protein bands in order to adapt the amounts of samples for subsequent **(c)** WB and **(d)** MS analyses.

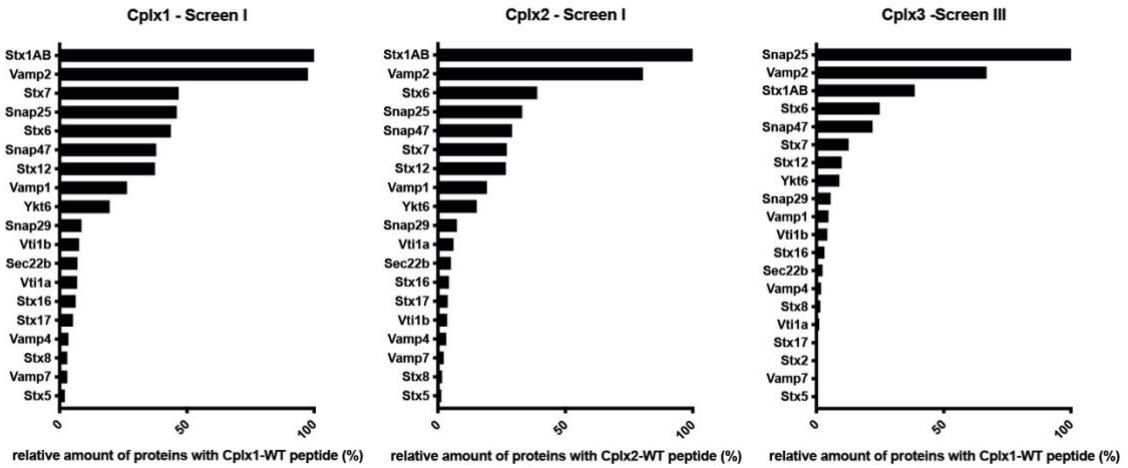

Figure 32: Relative amount of SNARE proteins analyzed via quantitative MS (second screen)
SNARE proteins binding to Cplx peptides were listed regarding their amounts and set in relation to the SNARE protein with the highest amount. For each isoform are two datasets available, one is shown here (Cplx1, screen I; Cplx2, screen I; Cplx3, screen III) and the other in the figure 14 (Cplx1, screen II; Cplx2, screen III; Cplx3, screen II).

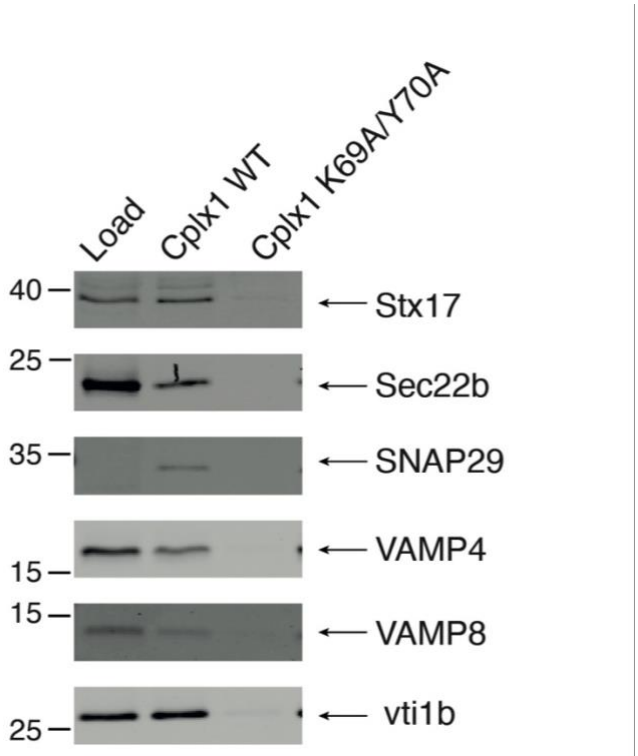

Figure 33: Additional non-neuronal SNARE proteins binding to Cplx1 peptide were verified by WB

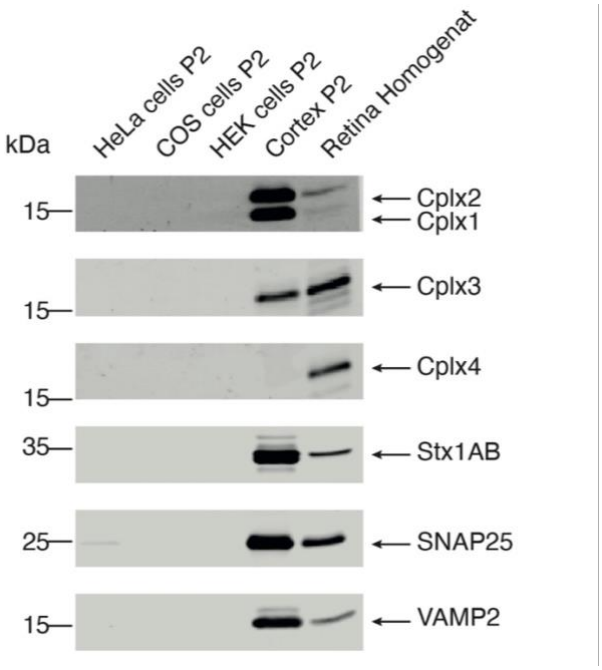

Figure 34: Lack of Cplxs and the neuronal SNARE proteins in HeLa cells, COS cells and HEK cells.
The lack of Cpxs and the neuronal SNARE proteins were shown in WBs for a variety of cell culture systems, like HeLa cells P2, COS cells P2 and HEK cells P2 with cortex and retina material as positive control.

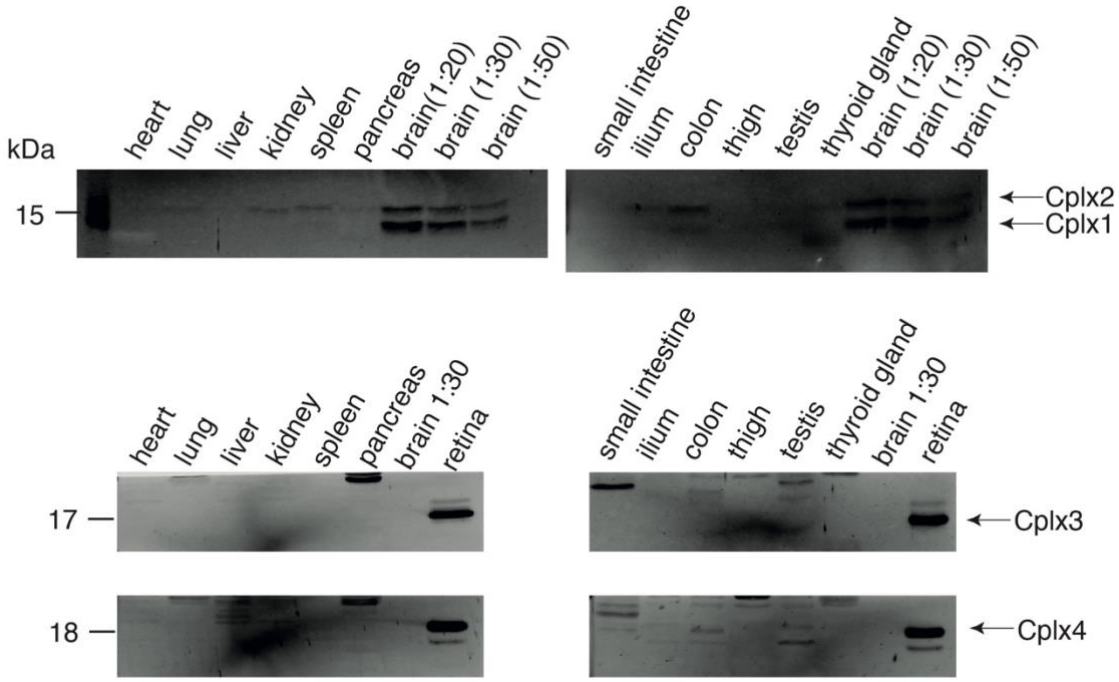

Figure 35: WB of Cplxs with organ samples of WT mouse.
Heart, lung, liver, kidney, spleen, pancreas, small intestine, ilium, colon, thigh, testis, thyroid gland, retina and brain of a WT mouse were homogenized, protein concentrations were measured and 20 µg of the sample were loaded for SDS-PAGE. The protein expression of Cplx1, Cplx2, Cplx3 and Cplx4 was checked by immunoblotting. Kidney, spleen, colon and brain of the WT mouse show Cplx2, whereas Cplx1 was just detected in the brain and Cplx3 and Cplx4 in the retina.

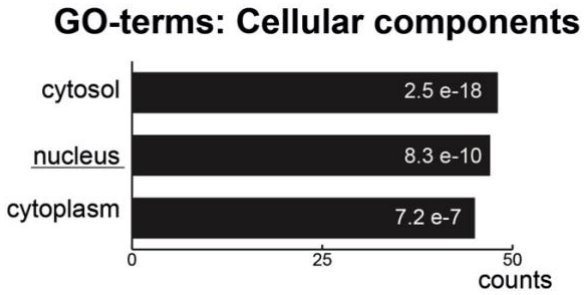

Figure 36: GO-term analysis of monomer RBP interactome.
71 proteins (RBP-WT/RBP-control >2), identified by MS were analyzed with the freely available bioinformatic database DAVID corresponding to the GO term *Cellular components*. The top three listed terms regarding to protein counts are displayed for each category. The p-values are given in the bars.

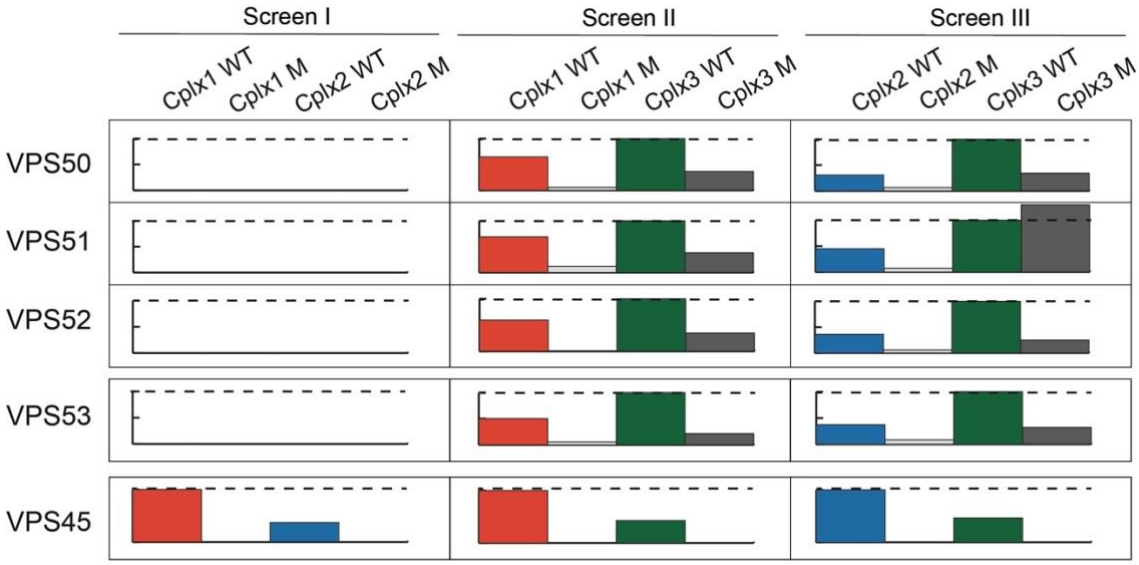

Figure 37: FASP-MS-based quantification of VPS proteins.
Visualization of the three FASP based screen data for VPS50, VPS51, VPS52, VPS53 and VPS45. Data are shown as relative amounts, whereas Cplx3 wildtype (WT) data were set as 100 % for VPS50, VPS51, VPS52 and VPS53 and Cplx1 wildtype (WT) data were set as 100 % for VPS45. The stitched line indicates 100%.

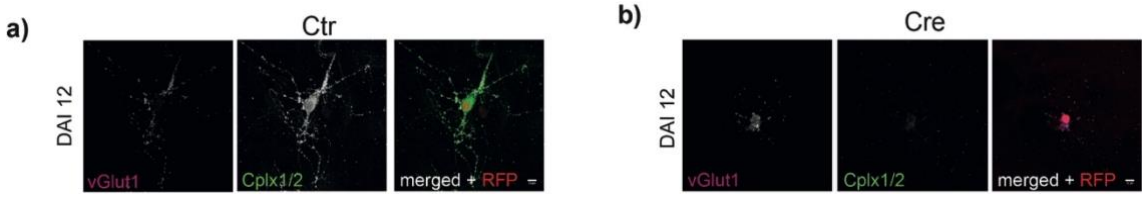

Figure 38: Cplx1 may affect neuronal health.
Cplx1flox/floxCplx2/3 DKO hippocampal mass cultures were infected at DIV 7 with (a) RFP virus or (b) Cre-RFP virus, fixated at DAI 12 and immunolabeled against Cplx1/Cplx2 and the presynaptic marker protein vGlut1.

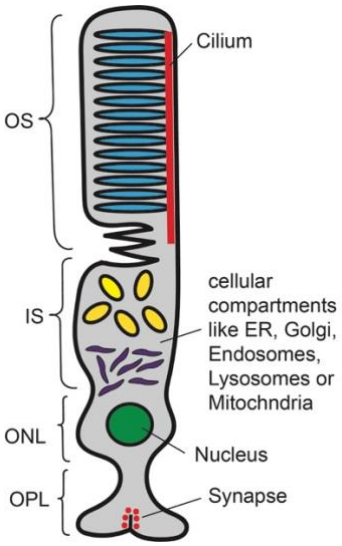

Figure 39: Schematic illustration of a rod photoreceptor cell with the cilium.
Abbreviations: OS: outer segment; IS: inner segment; ONL: outer nuclear layer; OPL: outer plexiform layer.

List of figures

List of tables

Acknowledgements

I am very grateful for all the help and support I have received in the last four years, both in and out of the lab.

In particular I would like to thank my supervisors Kerstin Reim and Olaf Jahn. They took me as master student and offered me to continue as PhD student. They teach me in the lab, gave me support and guidance, explained and discussed the data with me every Friday and trusted me.

I would also like to thank Prof. Nils Brose for giving me the opportunity to work in his lab. His feedback, advice and positive attitude helped me a lot.

Over the last years I got also additional advice in the TAC meetings with Prof. Dr. Reinhard Jahn and Prof. Dr. Blanche Schwappach. Thanks to their scientific feedback, the meetings were always very instructive and pointing me the way to my work.

A special thanks also to Prof. Dr. Outeiro, who took over the responsibility as second reviewer and the additional members of my examination board Prof. Dr. Wirths and Prof. Dr. Wichmann to take the time to evaluate my thesis.

I wish to thank Thea Hellman and Manuela Schwark for their technical support and their continuous helpfulness.

A special thanks to our collaboration partners of the Department of Biology of the Universität Erlangen, Prof. Brandstätter, Uwe Lux and Dr. Andreas Gießl for all the inspiring and enjoyable meetings.

I was lucky to work in an environment with many friendly and supportive colleagues in the department of Molecular Neurobiology. Especially I would like to thank my past or present PhD colleagues Ines, Aisha, Dragana, Sofia, Heba, Frederieke, Valentina and Lydia for all the shared moments inside and outside of the lab. And all the colleagues who made the life in the lab easier: Sally, Astrid, Sabine and Klaus.

Last, but not least, I would like to specially thank my family, partner and friends. Thank you for all your love and support throughout the years.